NASA CR-66903

Massachusetts Institute of Technology
Department of Aeronautics and Astronautics
Aerospace Research Division

Technical Report 136

DESIGN, CONSTRUCTION, AND EVALUATION OF A MAGNETIC SUSPENSION AND BALANCE SYSTEM FOR WIND TUNNELS

by

Timothy Stephens

November 1969

NASA, Langley Research Center
Contract No. NAS1-4421
MIT DSR No. 75396

FOREWORD

This work was performed at the Aerophysics Laboratory, Massachusetts Institute of Technology, Cambridge, Massachusetts. The work was sponsored by the Full-Scale Research Division, NASA Langley Research Center, Hampton, Virginia, under Contract NAS1-4421. This contract was monitored by Mr. Harleth Wiley, of the NASA Langley Vehicle Dynamics Section. Overall supervision of this study was provided by Professor Eugene E. Covert, of the M.I.T. Aerophysics Laboratory, in the capacity of Principal Investigator. This report covers work performed during the period from February, 1966 to November, 1969.

ABSTRACT

The basic design principles of a relatively interaction-free six component magnetic suspension and balance system are defined. The construction of a particular magnet configuration is described. The performance of the magnet configuration is evaluated. The evaluation is based upon parameters measured on the assembled and operating system. The evaluation is extended to a range of system sizes, by use of scaling laws. Design and construction of the required feedback compensation electronics system is described. Design of a five-component model position remote transducer is described. Magnet power supplies and control amplifiers are described, and the performance requirements are related to system size, model configuration, and test conditions.

TABLE OF CONTENTS

LIST OF ILLUSTRATIONS

Figure Page

Figure Page

LIST OF TABLES

LIST OF SYMBOLS

$\hat{a}$	model roll axis, principal magnetic axis
$\hat{b}$	model pitch axis
$\hat{c}$	model yaw axis
$\hat{x}$	wind axis
$\hat{y}$	horizontal axis (perpendicular to wind axis)
$\hat{z}$	vertical axis
$\overline{m}_{a,b,c}$	average magnetization in the "a","b", or "c" direction
$\overline{D}_{a,b,c}$	average demagnetizing factor in "a","b", or "c" direction
$\overline{B}_{a,b,c}$	average applied magnetic field intensity in the "a","b", or "c" direction
$\overline{T}$	magnetic torque on model
K_t	magnetic moment constant
v	volume of magnetic model core
$\vec{\overline{B}}_A$	applied magnetic field, averaged over model volume
p_{mt}, p_{tm}	transformation matrices or dyadics
p_{ax}, p_{xa}	coefficients of transformation dyadics
B_{xx}	average value of $\partial B_x/\partial x$ over model volumn
B_{xy}	average value of $\partial B_x/\partial y$ over model volumn (likewise for B_{xy}, B_{xz}, etc)
$\overline{B}_y^*$	defined as $B_x \tan \psi$
$\overline{B}_y(\omega), \overline{B}_z(\omega)$	alternating y and z field components used to control rolling moment

$(NI)_n$	ampere-turns of magnet coil "n"
D	characteristic linear dimension of the magnet system
$\vec{\nabla}$	field gradient operator
d	characteristic linear dimensions of a magnet coil
P_f	packing factor for magnet coil conductor
L	self-inductance of a magnet coil
Re	Reynolds number of wind tunnel air stream, per unit length
q	tunnel dynamic pressure
M	tunnel Mach number
T	tunnel static temperature (model absent)
T_t	tunnel total temperature
F_a	generalized aerodynamic forces on suspended model
T_a	generalized aerodynamic moments
d_m	characteristic linear dimension of suspended model
F_m	generalized magnetic forces
T_m	generalized magnetic moments
P_s	static electrical power
P_x	reactive electrical power
$K_{\omega r}$	reduced frequency parameter
z	translational oscillation amplitude
z^*	translational oscillation amplitude relative to magnet size

P_e	electrical power dissipation in magnet coils
P_r	power required to run refrigerator to cool magnet coil
I	current in magnet coil
R	resistance of magnet coil
R_o	resistance of magnet coil at room temperature
T	magnet coil temperature
T_o	room temperature
$T_{b.e.}$	"break-even" temperature
A	amperes
N_x	number of turns on magnetization coils
R_x	d.c. resistance of magnetizing coils
L_x	self inductance of combined magnetizing coils
I_x	magnetizing current
N_y'	total number of turns on inner saddle coils
$R_{y\ dc(ac)}'$	total d.c. (a.c.) resistance of inner saddle coils
L_y'	total self inductance of installed inner saddle coils
I_y'	inner saddle coil current
N_z'	total number of turns on outer saddle coils
$R_{y\ dc(ac)}'$	total d.c. (a.c.) resistance of outer saddle coils
L_y'	total self inductance of installed outer saddle coils
I_z'	outer saddle coil current

N_{xx}	total number of turns on drag coils
R_{xx}	total d.c. resistance of drag coils
L_{xx}	total self-inductance of installed drag coils
I_{xx}	"drag" current
N_{yx}	total number of turns on "side force" coils
R_{yx}	total d.c. resistance of side force coils
L_{yx}	total self inductance of installed side force coils
I_{yx}	"side-force" current
N_{zx}	total number of turns on "lift force" coils
R_{zx}	total d.c. resistance of lift force coils
L_{zx}	total self inductance of installed lift force coils
I_{zx}	"lift force" current
B_{pt}	magnetic field strength at magnet pole tip
W	weight of model
z_c	compensation system zeros
P_c	compensation system poles
$K_{PA/C}$	d.c. gain of power amplifier/coil combination, amperes/volt
$P_{PA/C}$	poles (or lags) in power amplifier - coil combination
M	model mass
S	Laplace transform operator
K_{EPS}	electromagnetic position sensor system gain
$V_{in(out)}$	voltage in (out)

ℓ/d	length/diameter of model core
$\dot{x}$	first time derivative of x-motion (x-velocity)
$\ddot{x}$	second time derivative of x-motion (x-acceleration)
D	inside clear dimension of completed suspension system
Q	coolant flow rate
θ	pitch angle
ψ	yaw angle
ϕ	roll angle
$\overline{\chi}_m$	average magnetic susceptibility of the model
ρ	resistivity of magnet coil conductor
γ	ratio of specific heat, C_p/C_v, for tunnel gas
Φ_{hm}	magnetization tensor
ω	angular frequency of forced oscillation
η	refrigerator thermal efficiency relative to Carnot cycle coefficient of performance
σ	real part of Laplace transfer operator
$j\omega$	imaginary part of Laplace transform operator

CHAPTER I

INTRODUCTION

1:1:1 CONTENTS OF REPORT

This report describes the design, development, and construction of a working prototype model of a six-component magnetic suspension and balance system for use in wind tunnels. The performance requirements of such a system are defined, and the particular design solution which evolved is described in detail. Performance parameters determined by experiment from the prototype system, and the relations required to extend the design to larger (or smaller) sizes are presented.

1:1:2 MAGNETIC BALANCE DEVELOPMENT AT M.I.T.

Development of magnetic suspension and balance systems for wind tunnels was begun at M.I.T. in 1957, shortly after publication of the work of Tournier and Laurenceau (1). Chrisinger (13), Tilton and Schwartz (14), and Tilton and Baron (15) were responsible for the first work on the problem done at M.I.T. This initial work was in the form of student theses, and was sponsored internally by M.I.T. The design approach used by Tournier and Laurenceau was considered to be particularly attractive, since five components could be controlled (roll component free). The basic magnet configuration described in (1) was adopted, and the design and development of the M.I.T. Aerophysics Laboratory Systems started from this point.

Since the further development of the system appeared to require and warrant greater support than could be expected from academic funds, outside support for the project was solicited. In 1960, support was obtained from the Aerospace Research Laboratories (ARL), Wright-Patterson Air Force Base,

to continue the development. (Part of the mission of ARL is the development of ground-based aerodynamic test facilities). Support from ARL continued from 1960 to 1969, under Contracts AF 33(616)-7023, and AF 33(615)-1470. Many improvements in the design were made, and usable wind tunnel results were obtained with the "first generation" suspension system. This system is still in use, and is extensively documented (2,3,4, 5,6). In the course of the initial development work, the limitations of the basic configuration became more apparent, and the areas in which further development and innovation were required became more clearly defined.

At this time (1963), personnel of the NASA Langley Research Center became interested in the M.I.T. development work. Support was obtained from NASA under Contract NAS1-4421 to proceed with a second development phase, to result in construction of a "second-generation" suspension system which incorporated all the design innovations, developed to a suitable level of performance. This report describes this "second-generation" suspension system.

In addition to development of hardware design, development of operating procedures was called for. As a consequence of operational experience with the working "second-generation" system, many areas in the hardware design were improved, and greater confidence can be placed in the usefulness of the system as it has now developed, and is described here.

1:1:3 DESIGN APPROACH: EXPERIENCE FROM EARLIER STUDIES

Early in the development of magnetic suspensions suitable for use with wind tunnels, it became apparent that certain approaches held greater promise than others. An important decision involves the basic method of support. One possible approach could use the interaction between alternating magnetic fields and the eddy currents which would be induced in an electrically conducting body immersed in the magnetic field. Such a scheme is feasible from a stability standpoint, since the magnetic fields can conceivably be arranged in space to provide a "potential well" in which the body (that is, the wind tunnel model) could be contained, free of any mechanical support, and

without any external means of providing stability. This approach immediately runs into such serious problems, however, when realistic physical values are considered for model material, force ranges, and power requirements, that it appears generally impractical. The main problem is the excessive heating of the model which would occur, even with small aerodynamic loads. Since this basic approach (7) has been used with success for a number of years for induction melting of metals with simultaneous levitation, the heating problem in the wind tunnel case can be appreciated. Consequently, an alternative approach was indicated.

A practical alternative to the induction method of magnetic levitation uses the interaction of a quasi-steady magnetic field with a ferromagnetic body. In this case some external means of stabilization is required. This implies that a feedback control system is needed to maintain the suspended body in the desired position. This requirement results from an extension of Earnshaw's Theorem of classical electrodynamics, which dictates that a "potential well" cannot be produced by a system of ferromagnetic material and steady magnetic fields. Since the equivalent of a potential well is required to stably support a ferromagnetic body, then this must be created artificially by control of the system of magnetic fields. The most practical method of controlling the magnetic field system appears to be by control of the currents in a rigid and stationary array of magnet coils. Stabilization of the model at some equilibrium position in the magnetic field requires a continuous measure of any departures from this equilibrium position, coupled with a means of adjusting the magnetic field properties which in turn provide restoring forces to maintain the equilibrium. The suspension system is thus a position control loop, with the aerodynamic forces and gravity acting as disturbance inputs, which must be countered by sufficiently large and fast-responding magnetic forces. Implicit in this is the need for a sensing system to determine the position of the suspended model, a "compensation" system to provide

the required loop dynamics, and a power amplification system to control the currents in the magnet coils.

The basic system is shown in functional block diagram form in Figure 1.1. As it is shown, the suspension system is a position control servo, designed to maintain the suspended model at some commanded position within the suspension magnet structure, according to the model position input signals. The position of the model is translated into electrical signals by means of a position sensing device, and these signals are compared with the position input signals. The resulting "position error" signals are modified in passing through a set of feedback compensation circuits to provide proportional, rate, acceleration, and integral functions of the error signals. The compensated error signals are then amplified and applied to the suspension system magnet coils. The magnetic fields produced by the suspension magnets produce magnetic forces on the

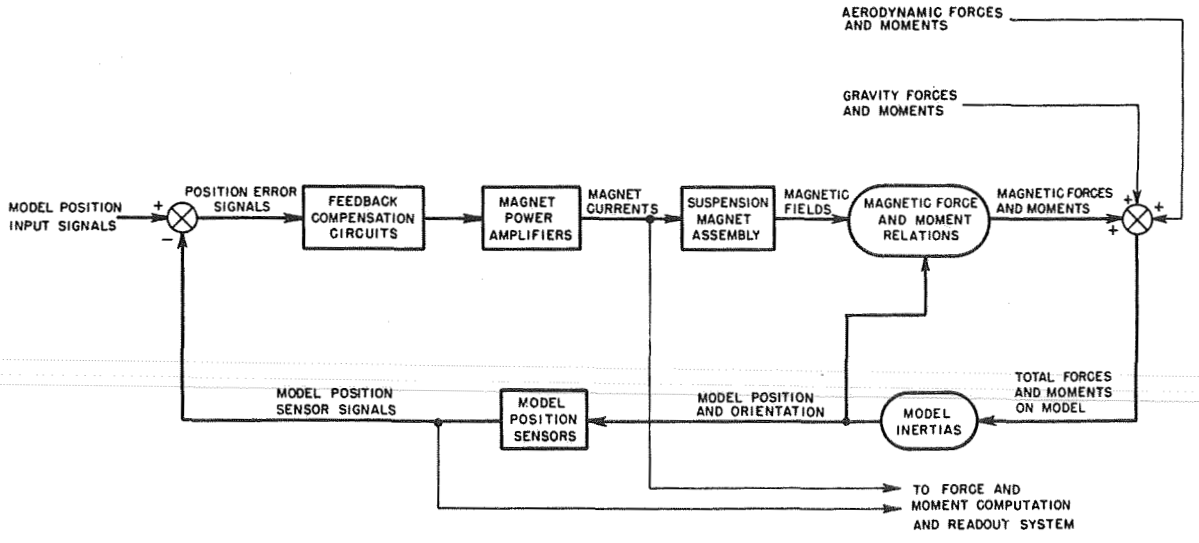

Figure 1.1. Functional block diagram of magnetic suspension and balance system

suspended model according to the "magnetic force and moment relations" which are functions of the model position and orientation, as indicated by the internal feedback path of Figure 1. The magnetic forces and moments add to the aerodynamic and gravity forces and moments, and the resultant forces and moments act through the model inertias to cause changes in the position and orientation of the model. These changes are in turn sensed by the position sensor system, and so the servo loop is closed. The function of the servo loop is to minimize the position error, by continuously counteracting the aerodynamic and gravity loads.

Suspension of the wind tunnel model is part of the problem; the remaining part of the problem is the determination of the laods acting on the suspended model. This requires that the variables that can be easily measured, such as the magnet coil currents and model position signals, are related unambiguously, to the forces and moments applied to the suspended model. With careful design, this requirement can be satisfied, and apparently within the accuracy generally required of a wind tunnel balance system.

The magnetic suspension system can be seen to consist of the following subsystems: a magnet coil assembly, a model position sensor system, a compensation system, and a power amplifier system. To provide the "balance", or load-measurement function, additional instruments are required. These are in part off-the-shelf items, and partly specially designed hardware for the calibration function. The design of each of the component subsystems outlined above must be based on the total system environment; thus, there is typically extensive interaction between design decisions. An additional consideration of course is the design of the wind tunnel system, which may or may not be established before the suspension system design is started.

The discussion which follows consists of a description of the basic building blocks of the system taken in turn, as follows:

a) Magnet system

b) Position sensor system

c) Compensation system

d) Power amplifier system.

CHAPTER II

DESIGN OF THE SUSPENSION MAGNET SYSTEM

2:1:1 PURPOSE OF PROTOTYPE DESIGN

The usefulness of a working prototype suspension system is based on the operational experience which can be gained, and on the quantitative information which can be applied to scaled versions of the prototype. Exact scaling laws are applicable to magnet systems of this type, and as a result, a family of magnet systems with accurately known performance can be based on the prototype. Thus, design tradeoffs can be evaluated quantitatively on the basis of the size of the suspension system and wind tunnel.

The prototype design is based upon a particular approach. The six translational and rotational degrees of freedom are to be controlled, and the controlling variables must be related in a simple way to the magnetic forces and moments. Certain magnetic field variables have been found which provide the required control and simplicity. Generation of these field variables can be accomplished in a variety of ways. Search for the "most suitable" way is of course the object of the design, but the many uncertainties inherent in the design of a system as complicated as this imply that improvements will be inevitable if design and development is carried further. The prototype design must be based on the careful application of the information that is currently available; and once the design is "frozen" and construction begins, the performance of the whole design family is established.

The prototype magnet system design was "frozen" in June, 1966, and construction completed in June, 1967. A few electrical modifications, mainly related to compatibility with the position sensor system, were found to be required.

The rational design of a suspension system such as this might possibly proceed from a set of performance specifications. These specifications presumably would be based on the "typical" test models to be suspended, the "typical" Mach numbers and Reynold's numbers, and the expected ranges of aerodynamic loads to be expected under these conditions. In practice, to provide as many options as possible, the design procedure resolves itself into the problem of producing the largest magnetic forces and moments possible, while maintaining acceptable measurement accuracy, again for "typical" test models. Probably the most reasonable approach is to define a range of model slenderness ratios, and a range of model sizes based on the size of the wind tunnel to be accommodated by the suspension system. These parameters can then be related to the magnetic properties (demagnetizing factors) of the model, and to the size of the syspension system (scale effects).

2:2:1 DESIGN PROCEDURE

The layout and detailed design of the suspension magnet system proceeds from the force and moment relations defined below, and from the scaling laws which apply to magnet design. The design approach consists of the following steps:

1) Definition of the physical constraints imposed on the magnet configuration by the requirements of the wind tunnel to be used with the system.

2) Identification of the magnetic field variables which provide control of each force and moment component.

3) Estimation of the maximum levels within which the field properties found in Step 2 must be controlled, to provide maximum forces and moments, without saturation of the model.

4) Identification of all the relevant scaling laws.

5) Tentative choice of the basic magnet coil construction.

6) Layout of the magnet system design, according to Steps 1 to 5.

7) Detailed analysis of the design, to identify possible areas for improvement, or to determine the necessity of a small-scale model study, if the theoretical analysis is not sufficiently conclusive.

8) Construction and test of small-scale test model, if found to be necessary.

9) Layout of final design based on preliminary layout, with the improvements indicated by Steps 7 and 8.

10) Detailed design of the prototype, using off-the-shelf materials and components, and calling for standard manufacturing processes if possible.

2:3:1 DESIGN CONSTRAINTS DUE TO TUNNEL

Constraints are placed on the design of the suspension system by the requirements of the wind tunnel design. For the purposes of making the prototype suspension system design as flexible and useful as possible, certain features must be included in the design.

Geometrical - Operational Constraints

i) Tunnel test section must be provided. This implies an unobstructed cylindrical volume passing through the complete suspension structure, large enough to accommodate the tunnel test section, including the walls of the test section if a closed jet, and also including the plenum volume if a transonic test section. If the test section is of the open-jet supersonic type, the diffuser inlet diameter will govern the size.

ii) Convenient access must be provided to the test section, either from the sides, top, bottom, upstream, or doenstream of the test section. The access areas should be large enough to allow installation of the largest model, calibration, installation and adjustment of probes, etc.

iii) Viewing ports must be provided. These will be unobstructed cylindrical passages through the complete suspension system, perpendicular to, and passing through the wind axis at the point of model suspension. There will be one horizontal and one vertical. These viewing ports will be used for general viewing, schlieren, and other optical applications.

iv) The suspension system will be compact, and will be suitably covered with appropriate shrouding to prevent accidents, both to the suspension system itself, and to operating personnel. (Foreign objects such as tools can be attracted into the magnet system if such shrouding is not provided, and can possibly cause short-circuiting of the magnet coils. Exposed electrical terminals can cause electric shock, if shrouds are not provided.)

2:4:1 MAGNETIC FORCES AND MOMENTS

The basic design problem lies in the generation of magnetic forces and moments. The design of a suitable magnet system can best proceed only when the relationship between fields and forces is quantitatively defined. These relations are explained in detail in Reference 8, and are summarized here.

2:4:2 MAGNETIZATION IN UNIFORM FIELDS

In general, the wind tunnel model can be considered to be a three-dimensional, non-axisymmetric shape, with principal magnetic axes "a", "b", and "c". The wind tunnel axes are defined as the "x", "y", "z" axes. In general, the a,b,c-axes will be at angles of "θ", "ψ", "ϕ", with the x,y,z-axes, as shown in Figure 2.1.

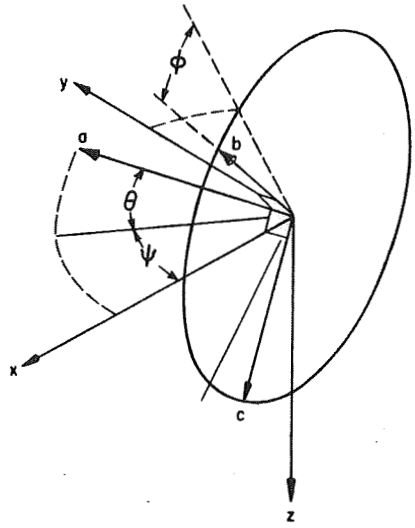

Figure 2.1. Model and wind tunnel axis system

The "average magnetization" components in the a,b,c-directions are given by the following equations:

$$\bar{m}_a \simeq \left[\frac{\bar{X}_m}{1 + \bar{X}_m \bar{D}_a}\right] \bar{B}_a \qquad \text{(II-1)}$$

$$\bar{m}_b \simeq \left[\frac{\bar{X}_m}{1 + \bar{X}_m \bar{D}_b}\right] \bar{B}_b \qquad \text{(II-2)}$$

$$\bar{m}_c \simeq \left[\frac{\bar{X}_m}{1 + \bar{X}_m \bar{D}_c}\right] \bar{B}_c \qquad \text{(II-3)}$$

The factor "$\bar{X}_m$" is the magnetic susceptibility of the model material, and the three factors $\bar{D}_a$, $\bar{D}_b$ and $\bar{D}_c$ are the average demagnetizing factors in the a,b,c-directions respectively, as

defined in Reference 8. The factors $\bar{B}_a$, $\bar{B}_b$, $\bar{B}_c$ represent the average applied magnetic field strengths in the a,b,c-directions. The demagnetizing factors are related to each other as follows:

$$\bar{D}_a + \bar{D}_b + \bar{D}_c = 1 \qquad \text{(II-4)}$$

Equations II-1, -2, -3 can be expanded as follows:

$$\bar{m}_a = \frac{\bar{B}_a}{\bar{D}_a}\left(1 - \frac{1}{(\bar{X}_m \bar{D}_a)} + \frac{1}{(\bar{X}_m \bar{D}_a)^2} - \frac{1}{(\bar{X}_m \bar{D}_a)^3} + \cdots\cdots\right) \qquad \text{(II-5)}$$

Thus, if the factor $1/D_a X_m$ is small relative to unity, then II-5 reduces to the approximate form:

$$\bar{m}_a \doteq \frac{\bar{B}_a}{\bar{D}_a}, \qquad \text{if} \quad \frac{1}{(\bar{X}_m \bar{D}_a)} \ll 1 \qquad \text{(II-6)}$$

For soft iron at magnetic induction levels below saturation, the value of X_m is typically in the range of 10^4 to 10^5, and the demagnetizing factors for typical models are usually in the range from .01 for slender models to .2 for relatively blunt models. Thus the difference between the exact form of II-5 and the approximate II-6 will be typically no greater than 1 percent. Since the demagnetizing factor is a function only of the shape of the model and X_m is a material property, then II-6 indicates that the material properties play only a small part in the relation between magnetization and applied field, below saturation. This can be seen in Fig. 2.1a which shows a typical magnetizing curve for iron. The rightward sloping lines are solutions to II-6 for several values of demagnetizing factor, and the curved contours indicate the degree of departure from II-6 due to the material properties.

2:4:3 MAGNETIC MOMENT OF THE MODEL

The actual magnetic moments or torques that can be applied to the model are defined by the following:

$$\vec{T} \simeq k_t v \, \vec{\bar{m}} \times \vec{\bar{B}}_A \text{ in.lb} \qquad \text{(II-7)}$$

where k_t = magnetic moment constant
$= 1.14$ (in.lb)/(in.)^3 (kilogauss)^2

$v \doteq$ model core volume, (in)^3

$\vec{\bar{m}}$ = kilograms

$\bar{B}_A$ = kilograms

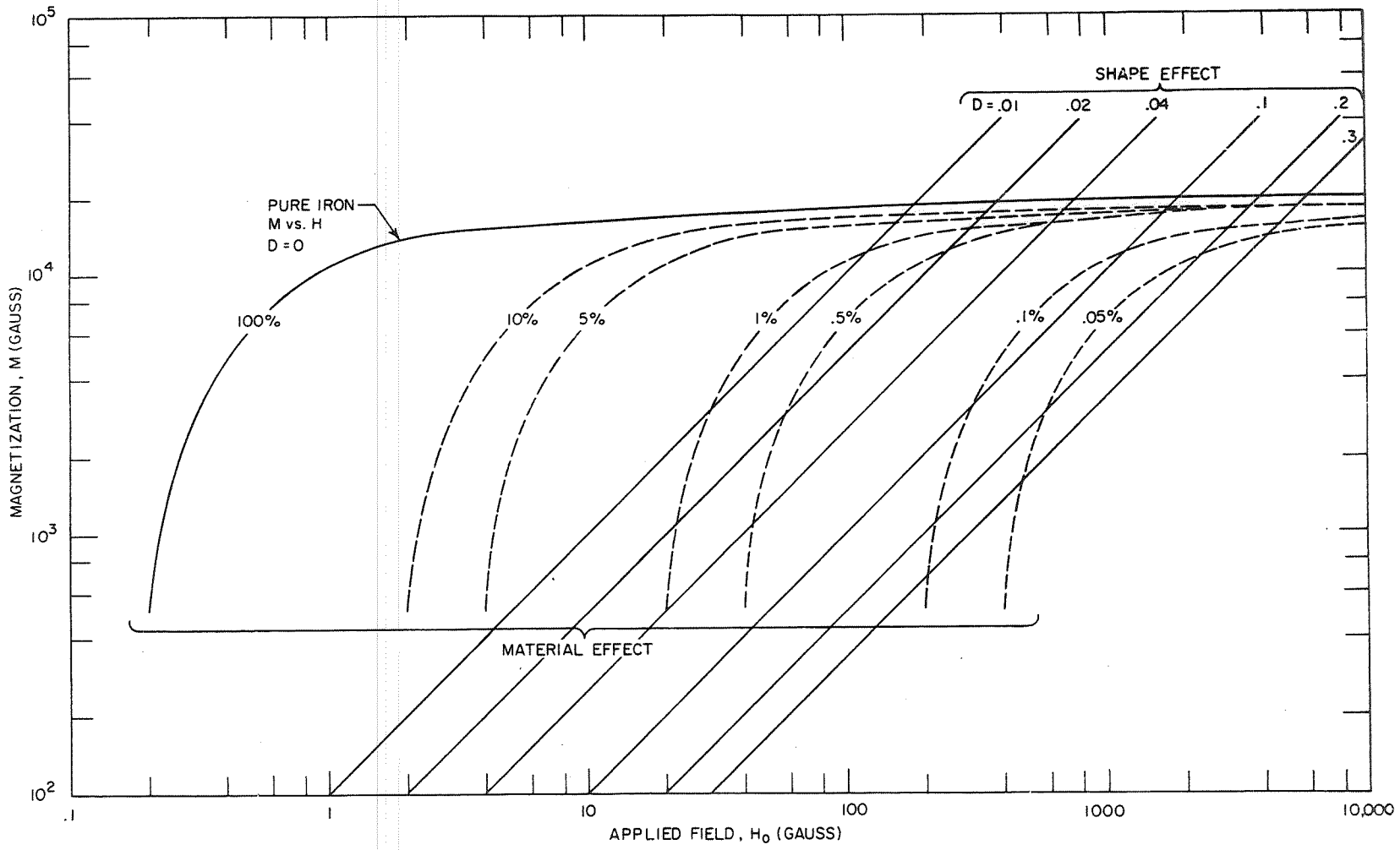

Figure 2.1a. Typical model magnetizing curves for iron showing effects of material (curved lines) and effect of model shape (or demagnetizing factor)

The magnetization "m" has been defined in terms of the three principal axis components by (II-1, -2, -3) and by (II-6). Expanding II-7 gives:

$$\bar{T} = k_t v \left[\hat{a} \bar{B}_b \bar{B}_c \left[\frac{1}{\bar{D}_b} - \frac{1}{\bar{D}_c} \right] + \hat{b} \bar{B}_a \bar{B}_c \left[\frac{1}{\bar{D}_c} - \frac{1}{\bar{D}_a} \right] + \hat{c} \bar{B}_a \bar{B}_b \left[\frac{1}{\bar{D}_a} - \frac{1}{\bar{D}_b} \right] \right] \qquad \text{(II-8)}$$

where $\hat{a}, \hat{b}, \hat{c}$ = unit vectors in a,b,c axis directions
= principal magnetic axes

Thus the magnetic torque vanishes for total applied fields parallel to any of the principal magnetic axes, and also for the case of equal demagnetizing factors (e.g. for a sphere). Also, for an axisymmetric model, two of the demagnetizing factors will be equal, and the torque about the axis of symmetry will be zero. If the roll, pitch and yawing moments are defined about the a,b,c-axes, they are as follows:

Rolling moment: $$T_a = k_t v \bar{B}_b \bar{B}_c \left[\frac{1}{\bar{D}_b} - \frac{1}{\bar{D}_c} \right] \qquad \text{(II-9)}$$

Pitching moment: $$T_b = k_t v \bar{B}_a \bar{B}_c \left[\frac{1}{\bar{D}_c} - \frac{1}{\bar{D}_a} \right] \qquad \text{(II-10)}$$

Yawing moment: $$T_c = k_t v \bar{B}_a \bar{B}_b \left[\frac{1}{\bar{D}_a} - \frac{1}{\bar{D}_b} \right] \qquad \text{(II-11)}$$

The model axis system can be transformed into the wind tunnel axis with a pair of transformation dyadics as follows:

$$\begin{vmatrix} \hat{a} \\ \hat{b} \\ \hat{c} \end{vmatrix} = \begin{vmatrix} p_{mt} \end{vmatrix} \cdot \begin{vmatrix} \hat{x} \\ \hat{y} \\ \hat{z} \end{vmatrix} \qquad \text{(II-12)}$$

$$\begin{vmatrix} \hat{x} \\ \hat{y} \\ \hat{z} \end{vmatrix} = \begin{vmatrix} p_{tm} \end{vmatrix} \cdot \begin{vmatrix} \hat{a} \\ \hat{b} \\ \hat{c} \end{vmatrix} \qquad \text{(II-13)}$$

The dyadics are defined as follows:

$$p_{mt} = \begin{vmatrix} p_{ax}(\hat{a}\hat{x}) & p_{ay}(\hat{a}\hat{y}) & p_{az}(\hat{a}\hat{z}) \\ p_{bx}(\hat{b}\hat{x}) & p_{by}(\hat{b}\hat{y}) & p_{bz}(\hat{b}\hat{z}) \\ p_{cx}(\hat{c}\hat{x}) & p_{cy}(\hat{c}\hat{y}) & p_{cz}(\hat{c}\hat{z}) \end{vmatrix} \qquad \text{(II-14)}$$

$$p_{tm} = \begin{vmatrix} p_{xa}(\hat{x}\hat{a}) & p_{xb}(\hat{x}\hat{b}) & p_{xc}(\hat{x}\hat{c}) \\ p_{ya}(\hat{y}\hat{a}) & p_{yb}(\hat{y}\hat{b}) & p_{yc}(\hat{y}\hat{c}) \\ p_{za}(\hat{z}\hat{a}) & p_{zb}(\hat{z}\hat{b}) & p_{zc}(\hat{z}\hat{c}) \end{vmatrix} \qquad \text{(II-15)}$$

For the rotation angles shown in Figure 2.1 the elements of these dyadics are as follows:

$$p_{mt} \begin{cases} p_{ax} = \cos\psi\cos\theta \\ p_{ay} = \sin\psi\ \cos\theta \\ p_{az} = \sin\theta \\ p_{bx} = -\cos\psi\sin\theta\sin\phi - \sin\psi\cos\phi \\ p_{by} = \cos\psi\cos\phi + \sin\psi\sin\theta\sin\phi \\ p_{bz} = \cos\theta\sin\phi \\ p_{cx} = \sin\psi\sin\phi + \cos\psi\sin\theta\cos\phi \\ p_{cy} = \sin\psi\sin\theta\cos\phi - \cos\psi\sin\phi \\ p_{cz} = \cos\theta\cos\phi \end{cases} \qquad \text{(II-16)}$$

$$p_{tm} = \begin{cases} p_{xa} = \cos\psi\cos\theta \\ p_{xb} = -\sin\psi\sin\phi - \cos\psi\sin\theta\sin\phi \\ p_{xc} = \sin\psi\sin\phi + \cos\psi\sin\theta\cos\phi \\ p_{ya} = \sin\psi\cos\theta \\ p_{yb} = \cos\psi\cos\phi + \sin\psi\sin\theta\sin\phi \\ p_{yc} = \sin\psi\sin\theta\cos\phi - \cos\psi\sin\phi \\ p_{za} = \sin\theta \\ p_{zb} = \cos\theta\sin\phi \\ p_{zc} = \cos\theta\cos\phi \end{cases} \qquad \text{(II-17)}$$

Note that $P_{ax} = P_{xa}$, etc. The three moments T_a, T_b, and T_c can now be written in terms of the applied field components parallel to the wind tunnel axes; namely H_x, H_y, and H_z.

$$T_a = k_f v\left[\frac{1}{\bar{D}_b}-\frac{1}{\bar{D}_c}\right]\left[p_{bx}p_{cx}\bar{B}_x^2+p_{by}p_{cy}\bar{B}_y^2+p_{bz}p_{cz}\bar{B}_z^2 + (p_{bx}p_{cy}+p_{by}p_{cx})\bar{B}_x\bar{B}_y\right.$$
$$\left. + (p_{bx}p_{cz}+p_{bz}p_{cx})\bar{B}_x\bar{B}_z + (p_{by}p_{cz}+p_{bz}p_{cy})\bar{B}_y\bar{B}_z\right] \qquad \text{(II-18)}$$

$$T_b = k_f v\left[\frac{1}{\bar{D}_c}-\frac{1}{\bar{D}_a}\right]\left[p_{ax}p_{cx}\bar{B}_x^2+p_{ay}p_{cy}\bar{B}_y^2+p_{az}p_{cz}\bar{B}_z^2 + (p_{ax}p_{cy}+p_{ay}p_{cx})\bar{B}_x\bar{B}_y\right.$$
$$\left. + (p_{ax}p_{cz}+p_{az}p_{cx})\bar{B}_x\bar{B}_z + (p_{ay}p_{cz}+p_{az}p_{cy})\bar{B}_y\bar{B}_z\right] \qquad \text{(II-19)}$$

$$T_c = k_f v\left[\frac{1}{\bar{D}_a}-\frac{1}{\bar{D}_b}\right]\left[p_{ax}p_{bx}\bar{B}_x^2+p_{ay}p_{by}\bar{B}_y^2+p_{az}p_{bz}\bar{B}_z^2 + (p_{ax}p_{by}+p_{ay}p_{bx})\bar{B}_x\bar{B}_y\right.$$
$$\left. + (p_{ax}p_{bz}+p_{az}p_{bx})\bar{B}_x\bar{B}_z + (p_{ay}p_{bz}+p_{az}p_{by})\bar{B}_y\bar{B}_z\right] \qquad \text{(II-20)}$$

If an axisymmetric model is considered, with the axis of symmetry the roll or a-axis, and with $\bar{D}_a$ less than $\bar{D}_b$ and $\bar{D}_c$, and with $\bar{B}_x$ greater than $\bar{B}_y$ and $\bar{B}_z$, the picture is somewhat simplified. If $\bar{B}_y$ and ψ are zero, in addition, then it follows that:

$$\bar{D}_b = \bar{D}_c > \bar{D}_a, \quad \bar{B}_y = 0, \quad \psi = 0$$

$$T_a = 0$$

$$T_c = 0$$

$$T_b = \frac{k_f v}{\bar{D}_a}\left[1-\frac{\bar{D}_a}{\bar{D}_b}\right]\bar{B}_x^2\left[\left(1-\frac{\bar{B}_z^2}{\bar{B}_x^2}\right)\frac{\sin 2\theta}{2} - \frac{\bar{B}_z}{\bar{B}_x}\cos 2\theta\right] \qquad \text{(II-21)}$$

also, $T_b = 0$, for $\dfrac{\bar{B}_z}{\bar{B}_x} = \tan\theta$

Equation (II-21) indicates that the model experiences a "restoring moment", which tends to align the roll axis with the wind, or x-axis, if $\bar{B}_z$ is zero. Also, the model will align itself with the local resultant field, whose direction is controlled by the ratio $\bar{B}_z/\bar{B}_x$.

In practice, in the prototype suspension system, the field component $\bar{B}_x$ is set at some constant value, and the component $\bar{B}_z$ is controlled to provide pitch attitude control. Yawing moment and yaw attitude is controlled by the $\bar{B}_y$ component, which is independently variable.

2:4:4 MAGNETIC FORCES

Magnetic forces are applied to the magnetized model by means of a set of controlled gradients in the magnetic fields. The general equation describing these magnetic forces is as follows:

$$\vec{F} \simeq k_f v \quad \bar{\bar{m}} \cdot \vec{\nabla} \vec{B} \tag{II-22}$$

This can be expanded as follows[a]:

$$F_x \simeq k_f v \quad (\bar{m}_x \bar{B}_{xx} + \bar{m}_y \bar{B}_{yx} + \bar{m}_z \bar{B}_{zx}) \tag{II-23}$$

$$F_y \simeq k_f v \quad (\bar{m}_x \bar{B}_{xy} + \bar{m}_y \bar{B}_{yy} + \bar{m}_z \bar{B}_{zy}) \tag{II-24}$$

$$F_z \simeq k_f v \quad (\bar{m}_x \bar{B}_{xz} + \bar{m}_y \bar{B}_{yz} + \bar{m}_z \bar{B}_{zz}) \tag{II-25}$$

If the a-axis of the model is aligned with the x-axis, and $\bar{B}_y$ and $\bar{B}_z$ are zero (no pitching or yawing moments), then

---

[a] $\bar{B}_{xx}$ = average value of $\partial B_x/\partial x$ over model volume
$\bar{B}_{yx}$ = average value of $\partial B_y/\partial x$, over model volume
Subscripts can be inverted eg. xy for yx (see Eq. II-30)

$m_x = m_a$, and $m_y = m_z = 0$. Consequently, the three forces reduce to the following:

$$F_x \simeq k_f v \; \bar{m}_x \bar{B}_{xx} \qquad \text{(II-26)}$$

$$F_y \simeq k_f v \; \bar{m}_x \bar{B}_{xy} \qquad \text{(II-27)}$$

$$F_z \simeq k_f v \; \bar{m}_x \bar{B}_{xz} \qquad \text{(II-28)}$$

Thus, according to (II-26, -27, -28), the three forces can be controlled independently, provided m_x is somehow fixed, and the three gradient components can be controlled independently. This is the approach that has been taken in the prototype system in fact. It is possible to provide independent control of the three gradient components and at the same time maintain the magnetizing field in the vicinity of the model approximately constant. That is, at a point, it is possible to provide independent control of $\bar{B}_x$, $\bar{B}_y$, $\bar{B}_z$, B_{xx}, B_{yx}, and B_{xx}. In general of course the forces and moments on the suspended model will be coupled. However, the degree of coupling will be substantially reduced if these field properties are manipulated in the above manner.

The field gradient components are related to each other through Maxwell's Equations as follows:

$$B_{xx} + B_{yy} + B_{zz} = 0 \qquad \text{(II-29)}$$

and,

$$B_{xy} = B_{yx}, \; B_{xz} = B_{zx}, \; B_{yz} = B_{zy} \qquad \text{(II-30)}$$

If attention is confined to "Drag" and "Side Force", i.e. F_x and F_y, and setting $m_z = 0$, then a simpler picture of the coupling between forces emerges, as follows:

$$F_x \simeq k_f v \left[\left[\bar{B}_x \left(\frac{\cos^2\psi}{\bar{D}_a} + \frac{\sin^2\psi}{\bar{D}_b} \right) + \bar{B}_y \sin\psi\cos\psi \left(\frac{1}{\bar{D}_a} - \frac{1}{\bar{D}_b} \right) \right] \bar{B}_{xx} \right. \tag{II-31}$$
$$\left. + \left[\bar{B}_x \sin\psi\cos\psi \left(\frac{1}{\bar{D}_a} - \frac{1}{\bar{D}_b} \right) + \bar{B}_y \left(\frac{\cos^2\psi}{\bar{D}_b} + \frac{\sin^2\psi}{\bar{D}_a} \right) \right] \bar{B}_{xy} \right]$$

$$F_y \simeq k_f v \left[\left[\bar{B}_x \left(\frac{\cos^2\psi}{\bar{D}_a} + \frac{\sin^2\psi}{\bar{D}_b} \right) + \bar{B}_y \sin\psi\cos\psi \left(\frac{1}{\bar{D}_a} - \frac{1}{\bar{D}_b} \right) \right] \bar{B}_{xy} \right. \tag{II-32}$$
$$\left. + \left[\bar{B}_x \sin\psi\cos\psi \left(\frac{1}{\bar{D}_a} - \frac{1}{\bar{D}_b} \right) + \bar{B}_y \left(\frac{\cos^2\psi}{\bar{D}_b} + \frac{\sin^2\psi}{\bar{D}_a} \right) \right] \bar{B}_{yy} \right]$$

If the yawing moment is assumed to be zero, then:

$(T_z = 0)$

$$\bar{B}_y = \bar{B}_x \tan\psi$$

and

$$F_x \simeq k_f v \frac{\bar{B}_x}{\bar{D}_a} \left(\bar{B}_{xx} + \bar{B}_{xy} \tan\psi \right) \tag{II-33}$$

$$F_y \simeq k_f v \frac{\bar{B}_x}{\bar{D}_a} \left(\bar{B}_{xy} + \bar{B}_{yy} \tan\psi \right) \tag{II-34}$$

If the gradient $\bar{B}_{xx}$ is produced by a system of coils having principal axis of symmetry aligned with the x-axis, then it follows from II-29 that

$$B_{yy} = B_{zz} = -\frac{1}{2} B_{xx} \tag{II-35}$$

This result can be introduced into II-34 thereby reducing the number of variables in the two equations, II-33 and II-34. The second term in brackets in each of these equations can be considered the "interaction" terms, since they vanish at zero

yaw angle. The first term in brackets is the controlling variable in each case. The "magnetizing field", $\bar{B}_x$ is common to both force equations.

2:4:5 MOMENT - FORCE INTERACTIONS

Equations II-33 and II-34 can be expanded to include the effect of yawing moment.

$$\text{Define} \qquad \bar{B}_y^* = \bar{B}_x \tan\psi \tag{II-36}$$

Then,

$$T_z \simeq k_t v \frac{\bar{B}_x}{\bar{D}_a}\left(1 - \frac{\bar{D}_a}{\bar{D}_a}\right)(\bar{B}_y - \bar{B}_y^*)\left[1 + \left(\frac{\bar{B}_y - \bar{B}_y^*}{\bar{B}_x}\right)\sin\psi\cos\psi\right] \tag{II-37}$$

The variable of interest here is $(\bar{B}_y - \bar{B}_y{}^*)$. This variable can be introduced into (II-31) and II-32) as follows:

$$F_x \simeq k_t v \frac{\bar{B}_x}{\bar{D}_a}\left[(\bar{B}_{xx} + \bar{B}_{xy}\tan\psi) + \frac{(\bar{B}_y - \bar{B}_y^*)}{\bar{B}_x}\left[\left(1 - \frac{\bar{D}_a}{\bar{D}_b}\right)\sin\psi\cos\psi\,\bar{B}_{xx} + \left(1 - \left(1 - \frac{\bar{D}_a}{\bar{D}_b}\right)\cos^2\psi\right)\bar{B}_{xy}\right]\right] \tag{II-38}$$

$$F_y \simeq k_t v \frac{\bar{B}_x}{\bar{D}_a}\left[(\bar{B}_{xy} + \bar{B}_{yy}\tan\psi) + \frac{(\bar{B}_y - \bar{B}_y^*)}{\bar{B}_x}\left[\left(1 - \frac{\bar{D}_a}{\bar{D}_b}\right)\sin\psi\cos\psi\,\bar{B}_{xy} + \left(1 - \left(1 - \frac{\bar{D}_a}{\bar{D}_b}\right)\cos^2\psi\right)\bar{B}_{yy}\right]\right] \tag{II-39}$$

Again, if the gradient $\bar{B}_{xx}$ is axisymmetric, then $\bar{B}_{yy} = -\frac{1}{2}\bar{B}_{xx}$, which can be substituted in (II-38, -39).

From II-37 it can be seen that the yawing moment T_z is approximately a linear function of the variable $(\bar{B}_y - \bar{B}_y{}^*)$. Assuming then that the other variables in (II-37) can be measured, this primary variable provides the measure of yawing moment. The interaction of this variable with F_x and F_y

is typically relatively small, and is defined quantitatively in II-38, -39.

2:4:6 ROLLING MOMENTS*

Rolling moments can be produced by steady fields, according to II-18. However, it is impractical in general to separate the rolling moment from pitch and yawing moments. Also, it is necessary that the iron core of the model be non-axisymmetric ($\bar{D}_b \neq \bar{D}_c$). As a result, the production of rolling moments requires control of additional independent magnetic field variables. This independent variable can be some spatial, or some temporal property of the magnetic fields. It has been found possible to control rolling moments by modifying the electrical properties of the model, and applying audio frequency average field components $B_y(\omega)$ and $B_z(\omega)$. This method is described in detail in References 3 and 9, and is summarized here. Two basic methods are actually possible, based on time-varying transverse field components $B_y(\omega)$ and $B_z(\omega)$. In the first approach, the resistivity of the model is made to be anisotropic, with high resistivity in the "b" or "c" direction, whichever has the smaller demagnetizing factor. The resistivity in the other two directions is made as small as possible. This can be achieved by constructing the model of alternate laminations of copper and iron, insulated from one another, and with the planes of the laminations parallel to the axis of the smaller demagnetizing factor ("b" or "c" axes only). An alternative method of producing anisotropic resistivity, which was proposed originally, employs a conducting loop in a solid iron model, with the loop serving the same purpose as the laminations.

The reason that roll control can be separated from pitch and yaw control in this way, is that the two demagnetizing factors $\bar{D}_b$ and $\bar{D}_c$ are frequency dependent, and this frequency dependence has been enhanced to a greater degree for one axis than for the other, by the process described in the preceding

*The material in this section is primarily from Ref. 9. It is included here for completeness and clarity.

paragraph. Thus, for an axisymmetric model, for example, the effective demagnetizing factors transverse to the axis of symmetry will not be equal, for audio-frequency fields, and rolling moments can be produced by the $\bar{B}_y(\omega)$, $\bar{B}_z(\omega)$ components, but not by the steady B_y and B_z components, which are used to control pitch and yaw.

The actual frequency dependence of the demagnetizing factors is a complicated problem in general, and in practice test models must be made. The important design variables which must be determined are the amplitude and carrier frequency of $\bar{B}_y(\omega)$ and $\bar{B}_z(\omega)$, for typical models and required rolling moments. These design variables have been tentatively established and the coil and power supply design appears to be straightforward.

An alternative roll control method, also based upon time-varying transverse field components $\bar{B}_y(\omega)$, $\bar{B}_z(\omega)$ may be used although the rolling moments which may be produced are generally less than those in the method described above. The principle of operation is that of a two-phase hysteresis-synchronous motor. The components $\bar{B}_y(\omega)$ and $\bar{B}_z(\omega)$ are varied sinusoidally at the same frequency and amplitude and in time-quadrature, thereby producing a transverse field which rotates in the y,z plane at the roll power frequency. The test model is constructed of a medium-carbon steel heat treated to increase magnetic hysteresis. The rotating transverse field produces a corresponding rotating transverse magnetization of the model, which lags the field, due to the hysteresis. The space lag, or angle between the field and the magnetization produces a net average rolling moment in the direction of the rotating field. The direction and strength of the rotating field and hence the rolling moment can be controlled by variation of the relative phase and amplitude of $\bar{B}_y(\omega)$ and $\bar{B}_z(\omega)$. This approach is attractive since the model construction is relatively simple, and high roll rates can be obtained easily (maximum roll rate equals the roll field frequency.

The roll control variables, $\bar{B}_b(\omega)$ and $\bar{B}_c(\omega)$, produce spurious pitch and yawing moments. These spurious moments are caused by modulation products of the pitch, yaw and roll frequencies, with the roll carrier frequency. There is a d.c. low frequency interaction due to the audiofrequency field alone, and interactions at the roll carrier frequency due to interaction with the pitch and yaw fields, and an interaction at twice the roll carrier frequency, due to the roll field alone. The roll carrier frequency will typically be sufficiently high that the higher frequency interactions will result in negligible model motion. The d.c. or low frequency interactions will result in negligible model motion. Since these interactions will be counteracted by the pitch and yaw control fields, $\bar{B}_b$ and $\bar{B}_c$.

Passive Roll Control (Roll Stiffness)

Roll "stiffness" may be introduced by cambering the model core. The core is bent, and the convex part of the core tends to align with the direction of the resultant of the gravitational and aerodynamic normal forces.(Reference 9). This approach is quite simple, and some range of roll attitude may be accommodated (in discrete steps) by changing the orientation of the cambered core within the model.

2:4:7 CONTROLLED FIELD VARIABLES: SUMMARY

The magnetic field variables which are designed to provide control of each force and moment component are summarized here. The material of (2:4:1) to (2:4:6) forms the background for the choice of controlled field variables. The coordinate frame is a right-handed x,y,z wind tunnel axis system. The x-axis is aligned with the wind axis, pointing upstream, the y-axis is horizontal, and the z-axis is vertical, pointing down.

The synthesis of the magnet design begins with a consideration of the typical model which will be used in the suspension

system. The typical model will accommodate a "slender" core. That is, the iron core can generally be longer in the roll axis direction than in the other directions. A "slender" core will tend to align itself with a uniform magnetic field. Models are usually tested at angles of attack no greater than 45°. Thus, a conceivable method of controlling pitch and yaw attitude is to provide a steady, uniform field component $\bar{B}_x$ to provide alignment of the model with the wind axis, and also provide controlled field components $\bar{B}_y$ and $\bar{B}_z$ to change direction of the aligning field. That is, the model roll axis tends to align with the resultant field direction, which can be controlled by $\bar{B}_y$ and $\bar{B}_z$.

At zero angle of attack, the model, which is magnetically polarized by the resultant field composed of the vector sum of $\bar{B}_x$, $\bar{B}_y$, and $\bar{B}_z$, can be forced in the "drag", or x-direction, by the gradient component $\bar{B}_{xx}$. This gradient component can be controlled <u>at a point</u> independently of $\bar{B}_x$, $\bar{B}_y$ and $\bar{B}_z$.

Similarly, at zero angle of attack, "lift" and "side force" can be controlled independently, by control of the gradient components B_{zx} and B_{yx}. These gradient components can also be controlled independently <u>at a point</u>.

Rolling moments can be controlled by the field variables, $\bar{B}_y(\omega)$ and $\bar{B}_z(\omega)$, which are sinusoidally varying at some carrier frequency, and modulated by a control signal.

These controlled field variables are summarized in the list below.

	<u>To control</u>:	<u>Vary</u>:
1)	MAGNETIZATION (BIAS) FIELD	- $\bar{B}_x$
2)	ROLLING MOMENT - T_a	- $\bar{B}_y(\omega)$, $\bar{B}_z(\omega)$
3)	YAWING MOMENT - T_b	- $\bar{B}_y$
4)	PITCHING MOMENT - T_c	- $\bar{B}_z$
5)	DRAG FORCE - F_x	- $\bar{B}_{xx}$
6)	SIDE FORCE - F_y	- $\bar{B}_{yx}$
7)	LIFT FORCE - F_z	- $\bar{B}_{zx}$

A magnet system which provides control of these field variables will thus afford the forces and moments required of a six-component model suspension system. The magnet design therefore proceeds with the aim of producing these field variables independently of one another, at a central point.

2:5:1 MAXIMUM CONTROLLED FIELD LEVELS BASED ON MODEL SATURATION

It is required that the iron model not be magnetically saturated at any point within it, since this condition compromises the accuracy with which the forces and moments may be related to the controlled field variables. Consequently, the applied magnetic fields will be expected to be limited to a greater or lesser extent depending upon the size and shape of the model to be suspended and the alloy used in the core.

The magnetization of ellipsoidal models in uniform applied fields is known in detail (Sec. 2:4:2); however, analysis of the magnetization of bodies of other than ellipsoidal shape, in non-uniform applied fields, is a far more complicated problem.

Since magnetic forces are proportional to the product of the magnetization and the field gradient, then it is of interest to estimate the combination of average applied field and field gradient which will produce the largest forces without saturating the model. For simple symmetrical shapes such as the ellipsoid, the magnetization will be composed of a uniform part due to the average part of the applied field and a non-uniform part due to the gradient. The problem then is to relate the non-uniform magnetization to the gradient.

It can be shown for a sphere that the local magnetization due to the gradient field reaches a maximum of 2 1/2 times the local applied field. This occurs on the axis at the surface. If the applied field is assumed to consist of a uniform component $\bar{B}_x$ and an axial gradient component $\bar{B}_{xx}$, the resultant

peak magnetization is as follows:

$$\left(\text{Applied field } H_{x_A} = B_x + (\bar{B}_{xx})x\right)$$

$$\text{Peak Magnetization, } M_{max} = 3\bar{B}_x + \frac{5}{2}\bar{B}_{xx}\, r < M_{saturation} \qquad \text{(II-40)}$$

Equation II-40 indicates that the uniform field and the gradient field are mutually constrained due to the saturation constraint, M_{sat}. For small sphere models ($r \to 0$), the limit on the uniform part of the field defined by Eq. II-40 is as follows:

$$r \to 0$$
$$H_{xo} \to \frac{M}{3}sat$$

The magnetization and the gradient field are related through the magnetic force. The maximum magnetic force is also related to the saturation limit. The axial force due to the axial gradient is:

$$F_x = k_f v\, \bar{m}_x \bar{B}_{xx} = k\left(\frac{4}{3}\pi r^3\right)\bar{m}_x \bar{B}_{xx}$$

This can be combined with Eq. II-40 to give:

For sphere: $$F_{x(max)} = \frac{2}{15}(\pi r^2) k_f \bar{m}^2_{sat} \qquad \text{(II-41)}$$

The maximum value of the gradient, corresponding to the maximum force of Eq. II-41, is as follows:

For sphere: $$\bar{B}_{xx(max)} = \frac{m_{sat}}{5r} \qquad \text{(II-42)}$$

(essentially unlimited, for small models)

For model shapes with slenderness ratio greater than unity, the limits on $\bar{B}_x$ will be lower than for the sphere.

2:6:1 GENERAL SCALING LAWS

The magnetic performance and electrical requirements of a particular magnet system are related to several factors, one of these being the size of the system. This introduces the question of scaling laws; that is, the laws that relate performance to size, for a particular system configuration. These laws are of particular interest in the study of the magnetic balance system, since they can be used to predict the behavior of large systems on the basis of measurements made on a small-scale prototype.

The scaling laws can be summarized as follows:

(a) Magnet Scaling Laws: Fields and Gradients

(i) The components of the static (low frequency) magnetic field at any point* in a system of media of constant permeability and of a given configuration having a characteristic linear dimension "D" are linear functions of the applied ampere-turns (NI), $(NI)_2, \ldots (NI)_n$, and are inversely proportional to the linear dimension "D".

i.e. $$\vec{B}(x/D, y/D, z/D) = \frac{1}{D} \sum_{n=1}^{N} \vec{B}_n(x/D, y/D, z/D)(NI)_n \qquad \text{(II-43)}$$

(ii) The components of the static magnetic field gradient tensor (B) at any point* in a system of media of constant permeability and of a given configuration and having a characteristic linear dimension "D" are linear functions of the applied ampere-turns $(NI)_1$, $(NI)_2, \ldots (NI)_n$ and are inversely proportional to the square of the linear dimension "D".

i.e. $$\vec{\nabla}\vec{B}(x/D, y/D, z/D) = \frac{1}{D^2} \sum_{n=1}^{N} \vec{\nabla}\vec{B}_n(x/D, y/D, z/D)(NI)_n \qquad \text{(II-44)}$$

*"At any given point" refers to geometrically similar points, or coordinates relative to the magnet system normalized with respect to "D", i.e. x/D, y"D, z/D.

(b) Electrical Scaling Laws: Magnet Coils

(i) The low frequency resistance R_{dc} of a magnet coil of a given configuration having a characteristic linear dimension "d" and composed of "n" turns of uniform size, of which the conductive portion accounts for a proportion "P_f" (packing factor) of the total cross-section of the coil, and of resistivity "ρ", will be proportional to "ρ", "n" squared, and inversely proportional to the linear dimension "d", and the packing factor "P_f".

i.e. $$R_{d.c.} \propto \frac{\rho n^2}{d P_f} \qquad \text{(II-45)}$$

(ii) The self-inductance "L" of a magnet coil of a given configuration having a characteristic linear dimension "d" and composed of "n" turns of uniform conductor, is proportional to the number of turns squared, and the linear dimension.

i.e. $$L \propto n^2 d \qquad \text{(II-46)}$$

(iii) The voltage/current time-constant, L/R_{dc}, of a magnet coil of given configuration is proportional to the linear dimension "d" squared and the packing factor, and is inversely proportional to the resistivity (i&ii).

i.e. $$L/R_{d.c.} \propto \frac{d^2 P_f}{\rho} \qquad \text{(II-47)}$$

(c) Aerodynamic Scaling Laws

It is of interest here to introduce the relevant aerodynamic parameters which influence the choice of aerodynamic test conditions and which will influence the design of the magnet system. The important quantities are related to the loads which must be accommodated. Simulation of free flight in a wind tunnel usually calls for duplication of Mach number, and Reynolds number if possible. In addition, simulation of time-varying aerodynamic phenomena usually requires duplication in the tunnel of the reduced frequency parameter.

These factors influence to a large extent the power requirements and the size of the magnet system, and also the power, size,

and complexity of the wind tunnel itself.

(i) The Reynolds number "Re" can be related approximately to the dynamic pressure "q", the Mach number "M", and the static temperature "T" (or the stagnation temperature "T_t") for a wind tunnel model of characteristic linear dimension "d_m", as follows:

(for air, T ranging from 300°R to 900°R)

$$\frac{R_e}{d_m} \simeq (1.84 \times 10^9) \frac{q}{T^{1.26} M} \qquad \text{(II-48)}$$

or,

$$\frac{R_e}{d_m} \simeq (1.84 \times 10^9) \frac{q}{T_t^{1.26}} \frac{\left[1 + (\frac{\gamma-1}{2}) M^2\right]^{1.26}}{M} \qquad \text{(II-49)}$$

where: d_m = ft. $\qquad \gamma = 1.4$ for air

q = psi

T, T_t = deg. R

(ii) Aerodynamic forces "F_a" on a particular model configuration at a given Mach number, Reynolds number, and flight attitude are proportional to the dynamic pressure "q", and the linear dimension "d_m" squared.

(Configuration, M, Re, fixed)

$$F_a \propto q\, d_m^2 \qquad \text{(II-50)}$$

(iii) Aerodynamic moments "T_a" on a particular model configuration at a given Mach number, Reynolds number, and flight attitude are proportional to the dynamic pressure "q", and the linear dimension "d_m" cubed.

(Configuration, M, Re, fixed)

$$T_a \propto q\, d_m^3 \qquad \text{(II-51)}$$

(iv) For a given M, Re, test model, and tunnel configuration, aerodynamic considerations usually dictate the size of the model "d_m" relative to the characteristic inner dimension "d_t" of the wind tunnel test section. The test section size in turn will generally be proportional to the characteristic linear dimension "D" of the magnet system.

(Model & tunnel configuration, M, Re, fixed)

$$d_m \propto d_t \propto D \qquad \text{(II-52)}$$

(d) Magnetic Forces and Moments

(i) Magnetic forces "F_m" on a given test model of linear dimension "d_m" and at a given attitude, are proportional to the uniform part of the applied field "H_a", the gradient of the applied field "H_a", and the volume of the model, "d_m^3".

(Model configuration and attitude fixed)

$$\vec{F}_m \propto \vec{B}_A \cdot \vec{\vec{\Phi}}_{hm} \cdot \vec{\nabla} \vec{B}_A \, d_m^3 \qquad \text{(II-53)}$$

where: $\vec{\vec{\Phi}}_{hm}$ = magnetization tensor

(ii) Magnetic moments "T_m" on a given test model of linear dimension "d_m" and at a given attitude, are proportional to the uniform part of the field "H_a" squared, and the volume of the model "d_m^3".

(Model configuration and attitude fixed)

$$\vec{T}_m \propto \vec{B}_A \cdot \vec{\vec{\Phi}}_{hm} \times \vec{B}_A \, d_m^3 \qquad \text{(II-54)}$$

(e) Limits Due to Saturation

It was shown in Sec. 3:2:4 that magnetic forces will be limited if saturation of the model is to be avoided. Similarly, if the magnet system is partly composed of iron, additional limits will thus be dictated partly by the model saturation, and partly by saturation in the magnet system. Saturation in either the model or the magnet system has generally the same effect on the maximum forces as a function of the size of the model and magnet system.

(i) For a given model configuration, and magnet which may contain iron cores, the magnetic force limits imposed by saturation are proportional to the characteristic

dimension squared, that is, "d_m^2" or "D^2", depending on the model configuration.

(Model, magnet configuration - fixed)

$$\max F_m \propto d_m^2 \propto D^2 \qquad \text{(II-55)}$$

(f) Reynolds Number Limits

The magnetic force limits are related to the maximum Reynolds number which can be achieved, for a given model and suspension configuration. The Reynolds number was seen to be inversely related to the temperature (Eqs. 47, 48). Thus lower temperature would result in higher Reynolds number, other factors remaining the same. However, the static temperature can only be lowered so far before condensation and other non-ideal gas effects come into prominence. The Reynolds number is proportional to the dynamic pressure (fixed T,M). The dynamic pressure is limited by the performance of the magnetic suspension: the peak aerodynamic forces must not exceed the maximum magnetic forces. From these constraints can be established the general form of the relation for the minimum size of model and suspension system for a given Mach number, Reynolds number, model configuration, and suspension system configuration, as follows:

$$d_{m(min)} \propto D_{(min)} \propto R_e T_{min}^{1.26} M \qquad \text{(II-56)}$$

(g) Static Power Limits

(i) The static electrical power "P_s (max)" required to reach the static saturation limits is proportional to the size of the magnet system, for a given configuration, packing factor, and conductivity.

(Configuration, packing factor, conductivity - fixed)

$$P_{s(max)} \propto D \qquad \text{(II-57)}$$

(ii) The static electrical power density (dissipation), "$P_{s\,(max)}/D^3$" is related to the problem of cooling the magnets. This problem is diminished for larger magnet systems, because:

$$\frac{P_{s(max)}}{D^3} \propto \frac{1}{D^2} \qquad \text{(II-58)}$$

(h) Dynamic Power Limits

The magnetic suspension can be used to measure aerodynamic forces arising from unsteady motion of the test model. Since the suspension system provides a continuous record of the model position and aerodynamic forces, correlation of these records will provide the aerodynamic "transfer functions" for the particular test model and flight conditions. These transfer functions may be interpreted in terms of the usual static and dynamic aerodynamic coefficients, or may be used in some other way. Frequency-dependent parameters can be included in the measurements if the model is forced to oscillate. Forced oscillation of the magnetically suspended model will generally require more electrical power than is required for support of the static loads, unless elaborate electrical and mechanical resonance[11] techniques are used.

A basic limitation is imposed on the acceleration of the model by the saturation limit.

(i) For a given magnet configuration containing iron cores, or for a given air-core magnet system with a particular model configuration, the saturation-limited reactive electrical power "P_x (max) required for forced oscillation of the (rigid) model is proportional to the oscillation frequency "ω", and the volume of the magnet system "D^3".

$$\text{(sat. limit)}\ P_{x(max)} \propto \omega D^3 \qquad \text{(II-59)}$$

(ii) The "Reduced Frequency Parameter, $K_{\omega r}$", is related to the peak reactive power as follows:

Define: $$K_{\omega r} \propto \frac{\omega D}{M\sqrt{T}} \qquad \text{(II-60)}$$

From II-57,-58:

$$P_{x(max)} \propto D^2 K_{\omega r} M\sqrt{T} \qquad \text{(II-61)}$$

(Amplitude constraint, see below)

(iii) At peak saturation limited power, the amplitude of oscillation "z" of a given model configuration varies inversely with the size of the magnet system, and hence the amplitude relative to the model size, "z*", varies inversely with the square of the size (d_m/D fixed).

I.e., at $P_x(max)$,

$$z \propto \frac{1}{D} \qquad \text{(II-62)}$$

(or, $$(\text{or, } z^* \propto \frac{z}{d_m} \propto \frac{1}{D^2}) \qquad \text{(II-63)}$$

(iv) Below the saturation limit, the power required for forced oscillation is related to the amplitude "z", the relative amplitude, "z*", the forcing frequency, "ω", and the size of the system. The reduced frequency parameter can also be related.

($\omega L/R > 1$)

$$P_x \propto z^2 \omega^5 D^3 \qquad \text{(II-64)}$$

or, $$P_x \propto z^{*2} \omega^5 D^5 \qquad \text{(II-65)}$$

or, $$P_x \propto z^{*2} (K_{\omega r} M\sqrt{T})^5 \qquad \text{(II-66)}$$

2:7:1 MAGNET CONSTRUCTION: DESIGN CHOICES

Several approaches can be taken in the design of a magnet system having the basic specifications outlined in Sections 3:2:2

and 3:2:3. The basic design alternatives are tabulated below.

TABLE 2.1

DESIGN ALTERNATIVES FOR MAGNET CONSTRUCTION

COIL OPERATING TEMPERATURE	COIL MATERIAL	COIL COOLANT	COOLING METHOD	FLUX RETURN PATH
"Room" temperature	Copper Aluminum	Air(Gas) Water(Liquid)	Bath	Air
Cryogenic	Copper Aluminum	Liquid nitrogen Liquid helium	Hollow conductor	Iron
Cryogenic	Superconducting and composites of various elements			

There is a total of 36 different alternatives suggested by this table. The particular approach that is chosen for a magnetic suspension system will be governed by a multitude of compromises, and by the current state of the art.

(a) Room-Temperature vs. Cryogenic Magnets

The most significant decision is based upon evaluation of the relative advantages and disadvantages of room-temperature magnets versus low temperature, or cryogenic, magnets.

There are apparent advantages to using cryogenic techniques. The main benefit comes in the reduction in conductor volume, and the extreme reduction in the static electrical power required for given field levels. The size reduction advantage will be offset

to some degree by the additional volume required for the elaborate thermal insulation jacket. In addition is the problem of coolant supply, and the generally higher costs of material and construction.

When reactive electrical power is considered, the relative advantages of the cryogenic magnet tend to disappear. The reactive power is related to the rate of storage of magnetic energy in the fields, and is independent of the resistance of the conductor. That is, the inductive reactance of the magnet tends to predominate, above the "corner-frequency" of the coil ($\omega L/R > 1$). Since the corner frequency of room-temperature coils varies inversely with the square of the size, then for a given bandwidth the advantage might go to the room temperature coil, in large sizes.

(b) Conductor Material

(i) Room-temperature coils

The most common material for magnet coils has been copper, since it has the highest conductivity at room temperature (next to silver). Copper is easy to fabricate, can be hard- or soft-soldered easily, and has excellent corrosion resistance. Copper, however, is in relatively short supply, and efforts have been made to substitute aluminum. The electrical conductivity of aluminum is approximately 60% that of copper, at room temperature, but is 1/3 of the density. Methods have been developed for soldering and brazing aluminum, and corrosion resistance of some alloys would make it suitable for use in water-cooled coil designs.

(ii) Cryogenic Coils

As the temperature is lowered, the electrical resistivity

of copper and aluminum decreases. The resistivity of aluminum decreases more rapidly than for copper, and at cryogenic temperatures the resistivities are approximately the same. It might appear that a reduction in static power could be achieved by reducing the resistivity by lowering the temperature. It must be remembered, however, that the power required to remove the dissipated power by refrigeration increases with decreasing temperature. It is of interest to compare the overall power required for refrigeration and ohmic losses in the cryogenic system, with the power required for the same coil at room temperature. Assuming a constant value for the thermal coefficient of resistance "α" for the coil, and a constant refrigeration plant efficiency "η" relative to the Carnot cycle coefficient of performance, the "break-even" temperature can be found at which the total power consumed by the refrigerator and coil power amplifiers is equal to the power consumed by the power amplifiers alone, at room temperature.

Power Diss. in Coil $$P_e = I^2R = I^2R_0(1 + \alpha(T - T_0)) \qquad \text{(II-67)}$$

Refrigerator Power $$P_r = I^2R\frac{1}{\eta}\left(\frac{T_0}{T} - 1\right) \qquad \text{(II-68)}$$

Total Power $$P_e + P_r = I^2R_0\left[\left[1 + \alpha(T - T_0)\right]\left[1 + \frac{1}{\eta}\left(\frac{T_0}{T} - 1\right)\right]\right] \qquad \text{(II-69)}$$

At "break-even" point, $P_e + P_r = I^2R_0$

Break-even Temperature $$T_{b.e.} = \frac{\left(T_0 - \frac{1}{\alpha}\right)}{\left(1 - \frac{1}{\eta}\right)} \qquad \text{(II-70)}$$

As an example, assume: $T_0 = 300$ K
$\alpha = 0.004$ per K (typical for copper)
$\eta = 0.35$

Then $T_{b.e.}$ = 77 K (approximately liquid nitrogen temp, at atmospheric pressure)

Thus, without changing the geometry of the magnet coils, it typically requires as much power to run the coils in liquid nitrogen as it takes at room temperature. Any power benefit from refrigeration must be found below the break-even point. For an estimate of the installed cost break-even temperature, the refrigerator efficiency "η" can be multiplied by the ratio of the installed cost per watt of power amplifier to the installed cost per watt of the refrigerator system. Since it will be most likely that this ratio will be less than unity, on a cost basis the break-even temperature will be even lower than liquid nitrogen. Liquid helium is the only practical choice here, and the temperature at atmospheric pressure is 4.2 K. The resistivity of copper at this temperature is not zero, but is approximately 0.5% of the room temperature value. In this case, the total power (dissipation plus refrigeration) is thus: (Cu at 4.2 K)

$$P_e + P_r \approx I^2 R_0 (0.5\%)\left(1 + \frac{1}{\eta}\left(\frac{300}{4.2} - 1\right)\right)$$

$$\approx I^2 R_0 \qquad (\eta = 0.35)$$

Thus, roughly the same total power is required for copper at liquid helium temperature as at room temperature, and higher costs, both in capital outlay and in operating convenience are involved.

The preceding discussion is based on the assumption that the magnet system and the refrigeration system would be in continuous operation, with no provision for storage of the vapor phase of the refrigerant.

(iii) Superconducting Coils

To gain any real benefit from low temperature

operation, superconducting coils must be used. In this case, the static power will be very small and the refrigeration system is of reasonable size. Liquid helium is used as the refrigerant.

The conducting material used in superconducting magnets must generally be provided with an additional parallel electrical path, in intimate electrical and thermal contact with the superconductor. This is known as "stabilizing" the superconductor. Copper appears to be the currently favored material for stabilization. The copper volume must be sufficient to absorb any transient quenching of the superconducting state, by channeling the current, and allowing the temperature of the superconductor to drop back below the critical point. The additional conducting material required for stabilization contributes significantly to the volume of the windings. When the volume required for the flow of liquid helium between the windings is considered, the winding overall volume is many times the volume of actual superconducting material. Typical current densities (for the overall coil cross-section) run in the range 6,000A/sq.in. to 30,000A/sq.in. This does not include the volume of the necessary thermal insulation, however.

(c) Cooling Methods

The coil conductor can be cooled by natural or forced convection of air or some other gas, or can be cooled by natural or forced convection of a liquid either through or around the conductor windings. Air or gas cooling is a relatively ineffective method, and for high current density, is generally impractical. It has the advantage that the cooling medium is readily available, and easily disposed of. Water cooling is quite common, and here the advantage goes clearly to forced convection, and the choice must be made between hollow conductor and spaced

solid conductor in a cooling bath. From the point of view of structural rigidity, hollow conductor is generally favored. Generally, however, with hollow conductor the hydraulic impedance to coolant flow is much greater than in the case of bath cooling. Hollow conductor allows winding of complicated shapes, with favorable packing factors. Generally, with water cooling, boiling heat transfer is avoided if possible, since the cooling passages can become vapor-bound, resulting in overheating or burnout.

Bath cooling is generally preferred for cryogenic applications, and nucleate boiling heat transfer is the usual mode of heat removal. Careful design is required in the layout of the coolant paths in this case to avoid vapor binding, or traps for coolant vapor.

(d) Flux-Return Path

The magnetic fields required in the test region can be produced with greater efficiency if suitable ferromagnetic flux return paths (iron cores) are provided. Iron cores provide additional design flexibility, since the actual coil windings can be located at relatively large distances from the center of the test region, and can be relatively small. Since the "air gaps" in this application are quite large, the effective permeability of the cores will be quite constant up to the saturation limit. However, core saturation imposes an upper limit on the usable field levels in the test region, both due to force limitation and to degradation in force measurement accuracy.

2:8:1 THE PROTOTYPE MAGNET DESIGN

Since the design of a new machine calls for the integration of many factors which often cannot be practically analyzed in the beginning, a "pre-prototype", or a series of "pre-prototype" models is usually required. In this case, where the model size can be tailored to reasonable cost, and is only required to provide limited information, there is more scope for innovation. Then, as improvements are indicated by measurements made on the small-scale model, the final prototype design will develop, and greater confidence can be placed in the anticipated performance.

This process was followed in the design of the prototype magnetic balance system. An additional influence was of course the extensive past experience gained in the design, construction, and operation of other magnetic balance systems, in particular the system described in Refs. 1, 2 and 3.

The design which evolved consisted of "room-temperature" copper coils cooled by forced convection of water, and employing square cross-section, hollow conductor. Laminated silicon steel cores were used for flux return paths. The design went through several preliminary design study stages, described in Ref. 8, and the configuration which was later chosen for construction is shown in Figs. 2.2-2.7.

2:8:2 FUNCTIONAL DESCRIPTION OF THE MAGNET DESIGN

The magnet structure is designed with several planes of symmetry all passing through the geometric center of the structure. Components are arranged in symmetrical subassemblies. Symmetrical groups of subassemblies produce the required magnetic field properties at the center of symmetry by variation of the currents in the several independent coil systems. The subassembly groups can be classified and discussed separately as follows:

(a) Helmholtz-coil System (controls $\bar{B}_x$, $\bar{B}_{xx}$)

(b) Saddle-coil System (controls $\bar{B}_y$, $\bar{B}_z$)

(c) Side and Lift System (controls $\bar{B}_{yx}$, $\bar{B}_{zx}$

(a) Helmholtz-Coil System ($\bar{B}_x$, $\bar{B}_{xx}$ Control)

The main axial magnetizing, or "bias" field, "$\bar{B}_x$", and the axial gradient of the axial field "$\bar{B}_{xx}$" used to control drag forces, are produced by a pair of identical circular solenoid coils arranged as shown in Fig. 2.2. Each coil is wound in three sections. The inner and outer sections are connected in series, such that the current passes through both sections in the same sense. Two electrical terminals (A and B) are provided for the combined windings. The middle section is separated from the inner and outer sections by extra layers of insulating material, and separate terminals (C and D) are provided for this section.

Both coils are assembled "back-to-back". The middle section windings of one coil are connected in series with the middle section windings of the other coil, such that the current passes in the same sense through both coils. The coils are assembled such that the axial spacing between the coil cross-section centroids is equal to the radius to the centroids. The middle section windings thus form a "Helmholtz-Pair", and provide uniform field "$\bar{B}_x$" over an appreciable volume of the central region, proportional to the coil current "I_x" provided by the "Magnetizing Power Supply", as shown.

The inner and outer winding sections of the coil are connected to the inner and outer sections of the other coil such that the current circulates in the opposite sense in both coils. This produces the field profile indicated in Fig. 2.2. At the center of symmetry, the axial field strength is zero, and the B_x component varies symmetrically such that an approximately uniform gradient "$\bar{B}_{xx}$" is produced over an appreciable volume

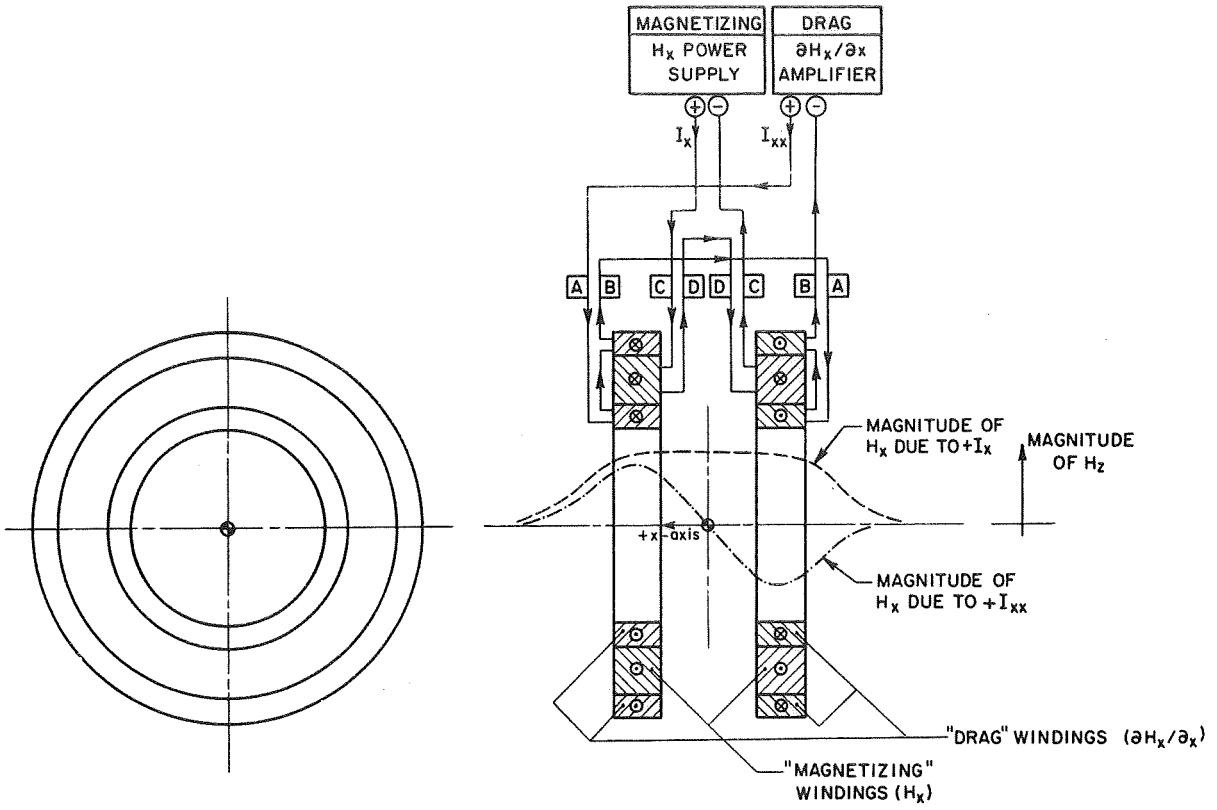

Figure 2.2. Helmholtz coil system

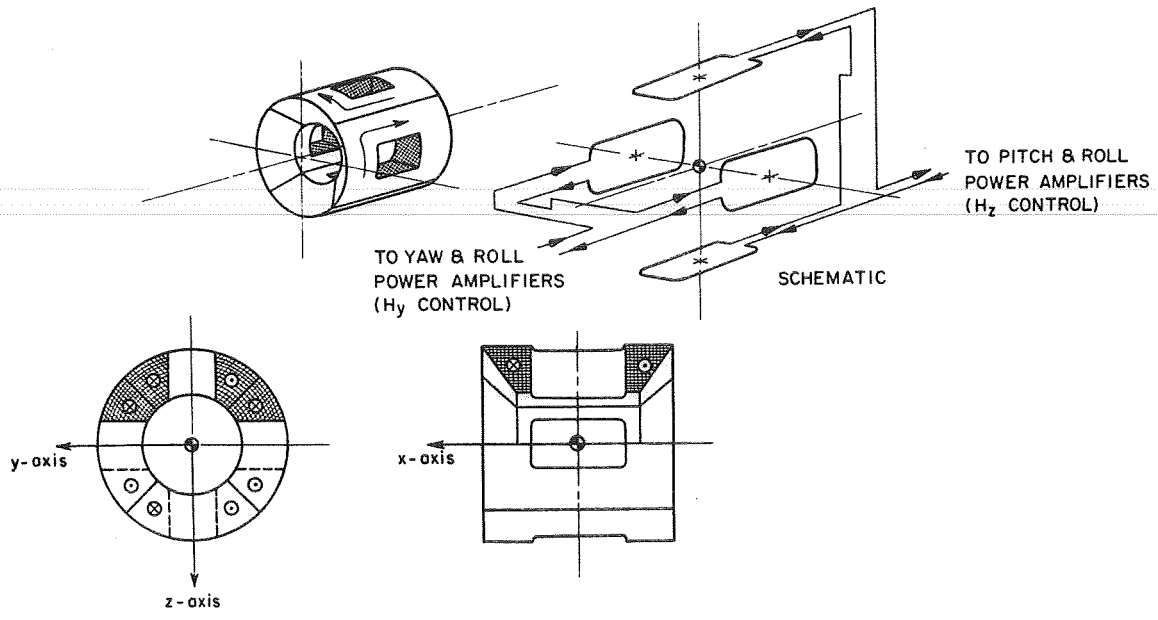

Figure 2.3. Simplified saddle coil arrangement

of the central region, which is proportional to the current "$\bar{I}_{xx}$" provided by the "drag power amplifier", as shown.

(b) Saddle Coil System ($\bar{B}_y$, $\bar{B}_z$ Control)

The transverse field components $\bar{B}_y$ and $\bar{B}_z$ are generated by two pairs of "saddle-coils" arranged symmetrically about the x-axis. The simplest arrangement consists of four identical saddle coils as shown in Fig. 2.3. In this arrangement, the coil axes are aligned with the "y" and "z" axes, and variation of the current in a pair of coils produces a corresponding variation in the field component along the coil axis. Vertical and horizontal windows are provided in the coil assembly for access and viewing.

An alternate arrangement is shown in Fig. 2.4, in which the transverse fields in the "y" and "z" directions are produced by vector addition of field components produced at 45° to the "y" and "z" axes. This arrangement is more complex, from several standpoints, but provides improved homogeneity of the $\bar{B}_y$ and $\bar{B}_z$ fields in the central region. (This design was chosen for the prototype.) However, the disadvantages of this configuration, arising from the sacrifice of symmetry, proved to offset the advantages due to the improved field homogeneity. These factors are discussed in Appendix A.

The saddle coil system is mounted inside the Helmholtz-coil pair as shown in the assembly drawing, Fig. 2.7.

(c) Side and Lift Force System (Control of $\bar{B}_{yx}$, $\bar{B}_{zx}$)

The axial gradients of the transverse fields, $\bar{B}_{yx}$ and $\bar{B}_{zx}$, are produced by a pair of iron-cored coil assemblies as shown in Figs. 2.5, 2.6. The core assembly consists of a laminated silicon steel ring, with four inward-pointing and axially canted poles, and with four exciting coils mounted

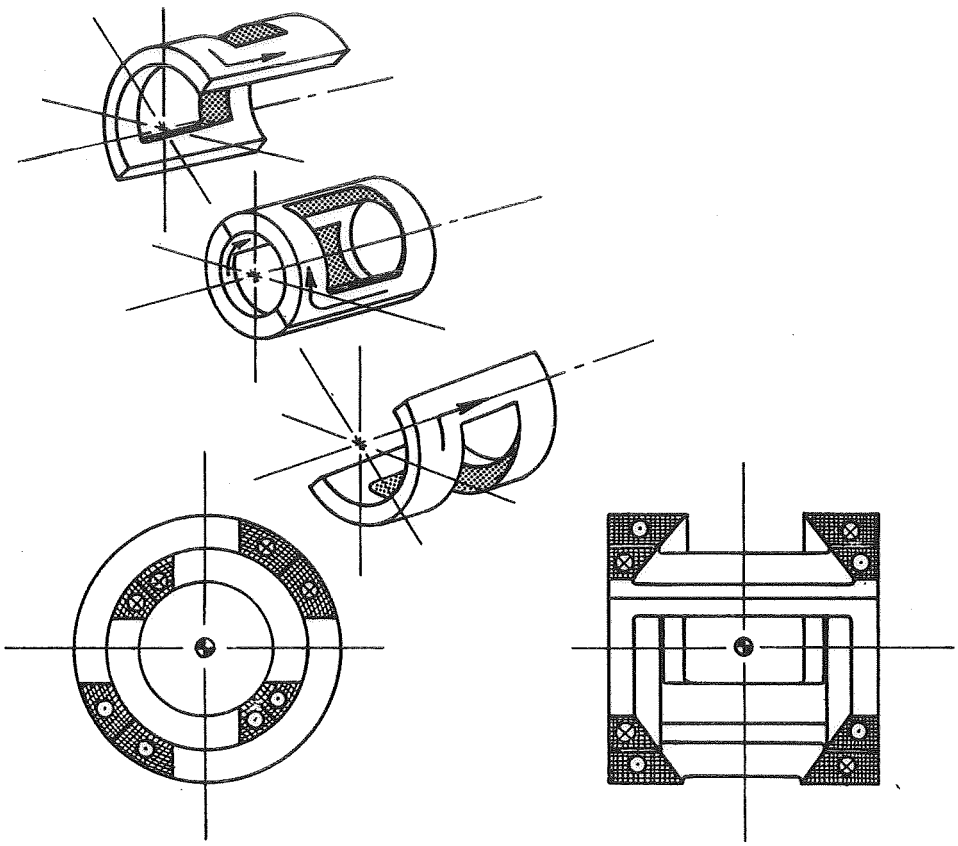

Figure 2.4. Nested saddle coil arrangement

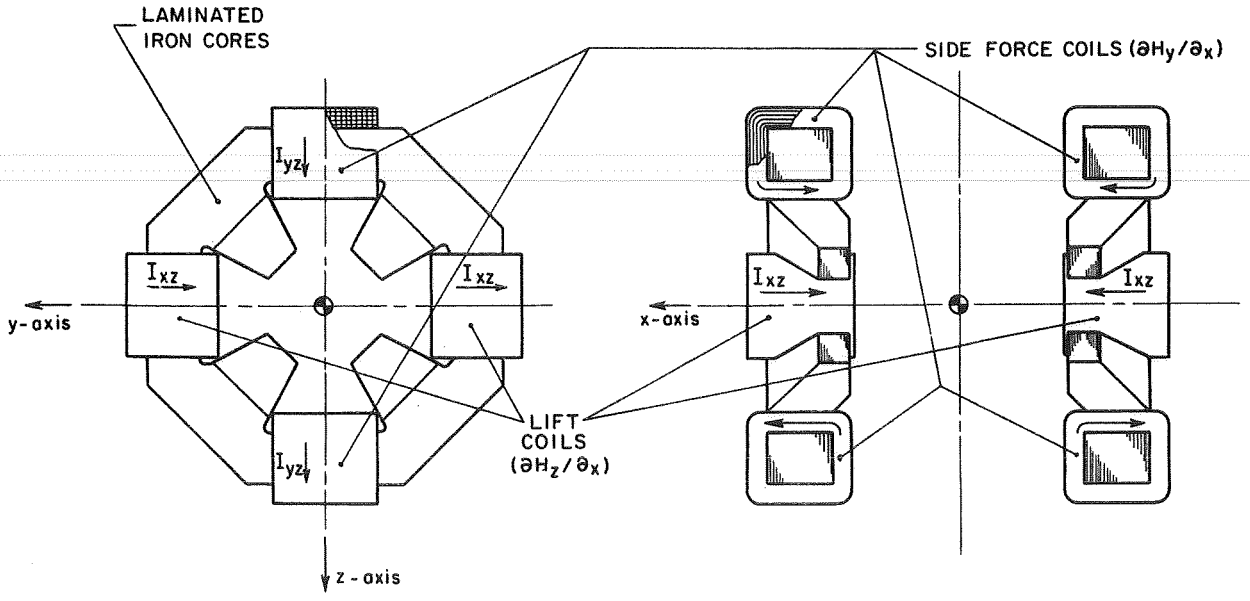

Figure 2.5. Side and lift force system

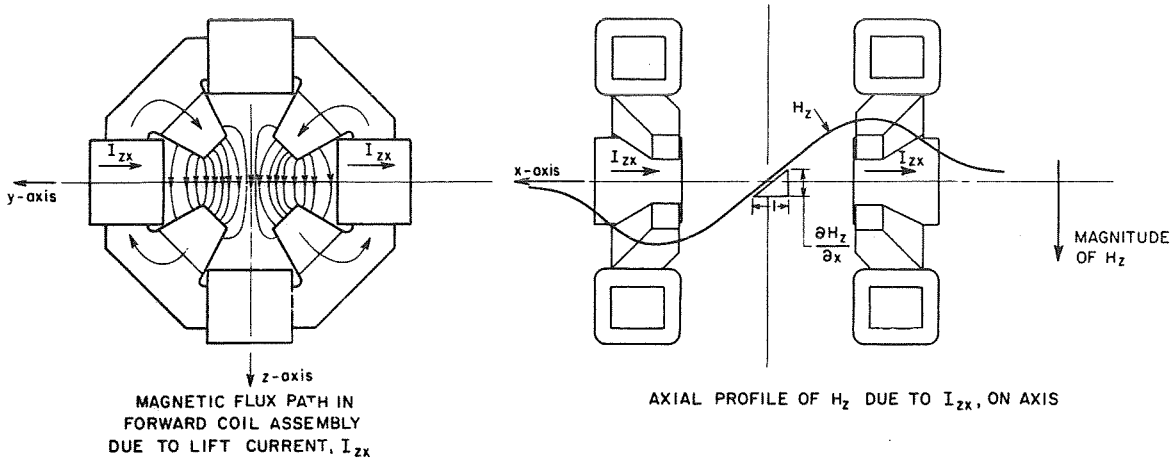

Figure 2.6. Flux paths in side and lift force system

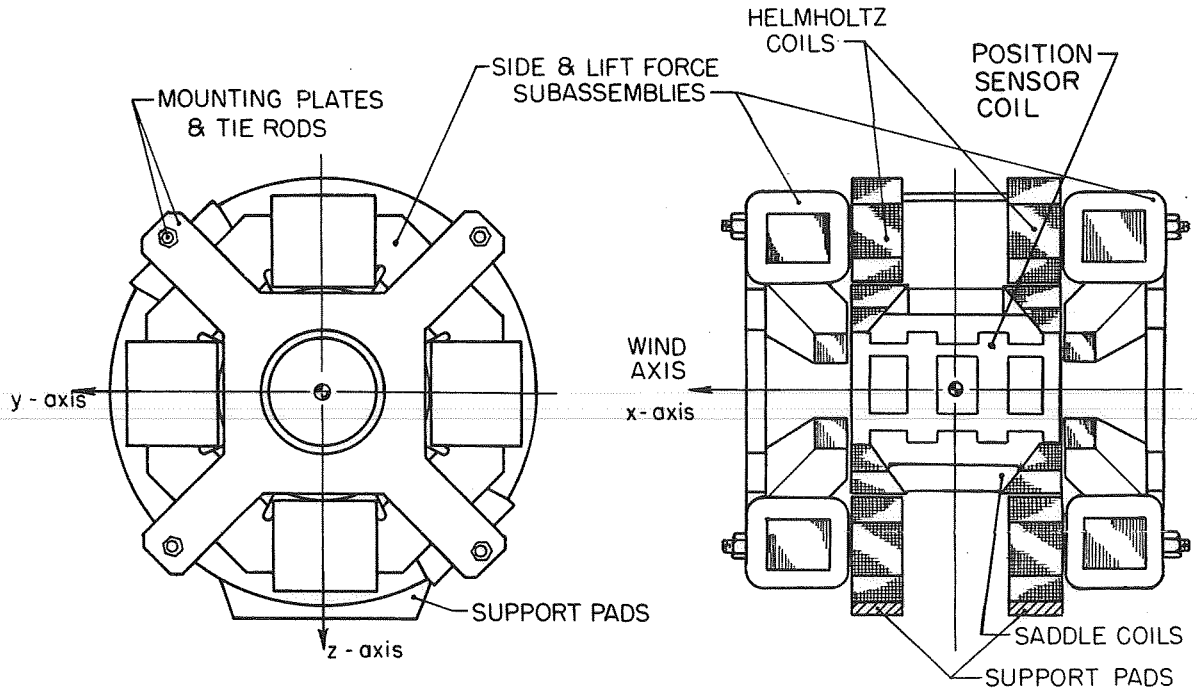

Figure 2.7. Assembly of magnet system

on the ring between the poles. The two assemblies are assembled "face-to-face" as shown, and the coils are connected in series in two sets of four. The four coils in the vertical plane control the axial gradient of the lateral field B_{yx} and the four coils in the horizontal plane control the axial gradient of the vertical field, $\overline{B}_{zx}$.

2:8:3 MECHANICAL SUPPORT OF COIL SYSTEM

The three magnetic subassemblies discussed above are assembled in a "sandwich" structure between two cruciform end plates, held together by axial tie rods. The Helmholtz coils are separated by integral pads on the inner faces of the coils, which also contain the cooling and electrical terminations. The basic overall structure is shown in the assembly drawing, Fig.2.7.

2:8:4 CONSTRUCTION DETAILS

The details involved in the construction of the magnet system are described further in Appendix B.

CHAPTER III

PROTOTYPE MAGNET SYSTEM

3:1:1 MEASURED PERFORMANCE OF MAGNET SYSTEM

The performance of the magnetic suspension system can be judged by analysis of the characteristics of the individual magnetic subsystem. These characteristics are estimated in the design phase but may be measured precisely once the prototype is assembled. The estimation analysis procedure and results are described in Appendix A.

The following is an analysis of the performance of the prototype suspension system based on the measured characteristics of the completely assembled prototype. These characteristics are summarized below. All electrical quantities are referred to the terminals of the individual coil systems, and apply to operation of the system within the range of linear relationship between currents and fields; that is, below saturation of the iron cores. The constraints due to saturation are described separately in Section 3:1:2.

(i) Bx Axial magnetizing bias field ("magnetization")
Helmholtz coils
Coil geometry - Fig. 2.2
Total turns. N_x = 800 (400 turns/coil)
Total resistance R_x = 2.0 ohms
Total inductance L_x = 0.36 henries
Magnetic performance $B_x = 20\ I_x$ gauss
or: $B_x = 0.025\ N_x I_x$ gauss
(I_x = "magnetizing" current)

(ii) B_y, B_z Traverse fields ("pitch, yaw, roll")
Overall geometry - Fig. 2.4

a) Inner saddle coils - B_y' (see Fig. 2.4)

Total turns. $N_y' = 176$ (88 turns/coil)

Total resistance (d.c.) $R_{y_{d.c.}}' = 0.24$ ohm

(a.c.) $R_{y_{a.c.}}' = 0.5$ ohm

(@ 400 Hz)

Total inductance $L_y' = 8$ millihenry

Magnetic performance $B_y' = 3.8\ I_y'$ gauss

or: $B_y' = 0.0216\ N_y' I_y'$

(I_y' = Inner saddle - coil current).

b) Outer saddle coils - B_z' (see Fig. 2.4)

Total turns. $N_z' = 266$ (133 turns/coil)

Total resistance (d.c.) $R_{z_{d.c.}}' = 0.44$ ohm

(a.c.) $R_{z_{a.c.}}' = 0.9$ ohm

(400 Hz)

Total inductance $L_z' = 17$ millihenry

Magnetic performance $B_z' = 3.5\ I_z'$ gauss

or: $B_z' = 0.0135\ N_z' I_z'$

(I_z' = outer saddle - coil current).

(iii) B_{xx} Axial gradient of axial field ("drag")
Helmholtz coils - Fig. 2.2.
Total turns. $N_{xx} = 800$ (400 turns/coil)

Total resistance $R_{xx} = 2.0$ ohm

Total inductance $L_{xx} = 0.16$ henry

Magnetic performance $\bar{B}_{xx} = 1.7\ I_{xx}$ gauss/in

or: $\bar{B}_{xx} = 4.3 \times 10^{-3}\ N_{xx} I_{xx}$ gauss/in

(I_{xx} = "drag" current).

(iv) B_{yx} Axial gradient of lateral field ("side force")
Side and lift magnet assemblies - Figs. 2.5, 2.6.
(Four coils in vertical plane)
Total turns $N_{yx} = 1{,}160$ turns (290 turns/coil)

Total resistance R_{yx} = 1.0 ohm

Total inductance L_{yx} = 0.40 henry

Magnetic performance $\bar{B}_{yx} = 1.4\ I_{yx}$ gauss/in

or: $\bar{B}_{yx} = 1.2 \times 10^{-3}\ N_{yx} I_{yx}$ gauss/in

(I_{yx} = "side-force" current).

(v) B_{zx} (Same as above, change y to z)

3:1:2 PERFORMANCE LIMITS DUE TO SATURATION OF THE IRON MAGNET CORES

The performance parameters listed above do not imply any bounds on the magnetic performance of the system. However, due to the saturation characteristics of the steel magnet cores, limits do exist. The steel cores are magnetized to a greater or lesser degree by all coil systems, and therefore a combination of magnet currents at some level is capable of saturating the cores at some point.

The most likely point at which saturation would occur in this geometry is at the pole tips. The flux density at the surface of the pole tips is made up of the applied field from the coils, and the magnetization of the cores. In general, the magnetization component will predominate, and hence can be assumed to be approximately equal to the measured flux density at the surface of the pole tips. The pole tip flux density is linearly related to all the magnet currents, at low current levels, and the relation can be easily found by successively energizing each coil system with low d.c. currents, and measuring the pole tip flux density with a gaussmeter. It is desirable that the magnetization level of the pole tips remain below the saturation level. For the material used in the cores, this level is approximately 15 kilogauss, at the lowest. This will consequently provide the constraint on the

performance of the magnet system. The pole tip flux density, "$B_{p.t.}$", was found to be a function of the coil currents as follows:

$$B_{pt} = 33I_x \pm 41I_y \pm 61I_z \pm 25I_{xx} \pm 39I_{xy} \pm 39I_{xz} < 15{,}000 \qquad \text{(III-1)}$$

This equation applies to the worst-case pole tip when all terms are of the same sign.

It will be useful to relate the actual field variables to the pole tip flux density. Using the magnetic performance parameters of 3:1:1, this relation follows:

$$B_{pt} = \pm 1.6B_x \pm 1.05B_y \pm 1.7B_z \pm 147B_{xx} \pm 28B_{xy} \pm 28B_{xz} < 15{,}000 \qquad \text{(III-2)}$$

3:2:1 SOME FORCE LIMITS FOR TYPICAL TEST MODELS

The parameters and constraints listed above can be used to determine some typical force limits. Several of these are computed in the examples below.

3:2:2 SIMPLIFIED MAGNETIC FORCE RELATIONS

Magnetic forces on the wind tunnel test model can be determined from a knowledge of the magnetic field strengths and the gradients in field strength, in addition to the magnetic properties of the test model geometry and material. These relationships have been worked out in some detail in Ref. 8. If certain simplifying conditions are imposed, these relations provide a convenient means of estimating the performance of

the suspension system.

The relations used here are as follows:

(a) Axial force per pound of iron in model, with model at zero angle of attack and zero pitching and yawing moments

$$F_x/W = 4.7 \times 10^{-6} \frac{\bar{B}_x}{\bar{D}_a} \bar{B}_{xx} \text{ "g's"} \qquad \text{(III-3)}$$

where D_a = demagnetizing factor of iron part of test model, in axial direction.

(b) Vertical force per pound of iron in model, with model at zero angle of attack and zero pitching and yawing moments.

$$F_z/W = 4.7 \times 10^{-6} \frac{\bar{B}_x}{\bar{D}_a} \bar{B}_{xz} \text{ "g's"} \qquad \text{(III-4)}$$

Since only axial and vertical forces are considered here, Eq. III-2 can be simplified as follows:

$$\text{(worst-case) } B_{pf} = 1.6|\bar{B}_x| + 14.7|\bar{B}_{xx}| + 28|\bar{B}_{xz}| < 15{,}000 \qquad \text{(III-5)}$$

Substituting Eqs. III-3 and III-4 into III-5,

$$|F_x/W| + 1.9|F_z/W| < 4.25 \times 10^{-3} \frac{|\bar{B}_x|}{\bar{D}_a}(1 - 1.09 \times 10^{-4}|B_x|) \qquad \text{(III-6)}$$

For maximum right-hand side of III-6, and for a range of the demagnetizing factor, D_a, the optimum value of B_x is

Optimum B_x = 4,600 gauss

(Condition: incipient saturation of magnet pole tips, and $.3 < D_a < 1.0$. See 3:2:3, Saturation Limits.

and $$|F_x/W| + |F_z/W| < \frac{9.7}{\bar{D}_a} \qquad (III\text{-}7)$$

$(D > 0.3$, see below)

3:2:3 SATURATION LIMITS

It is necessary to maintain the level of magnetization of the test model below saturation; i.e., below 15,000 gauss. This condition is expressed below.

$$\bar{m}_a = \frac{\bar{B}_x}{\bar{D}_a} < 15{,}000 \text{ gauss} \qquad (III\text{-}8)$$

Using the optimum value of B_x = 4,600 gauss, found from Eq. III-6, the limit of validity of Eq. III-7 in terms of D_a is found.

i.e. Eq. III-7 is valid if, $(\bar{D}_a) > \frac{2250}{15{,}000} = 0.3 \qquad (III\text{-}9)$

The consequences of test model demagnetizing factors less than 0.30 are as follows:

From Eqs. III-8 and III-9,

$$|F_x/W| + 1.9|F_z/W| < 64(1 - 1.7\bar{D}_a) \qquad (III\text{-}10)$$

$(\bar{D}_a < 0.3)$

The force limits defined by the relations III-7 and III-10 can be shown in graphical form as in Fig. 3.1 on the following page.

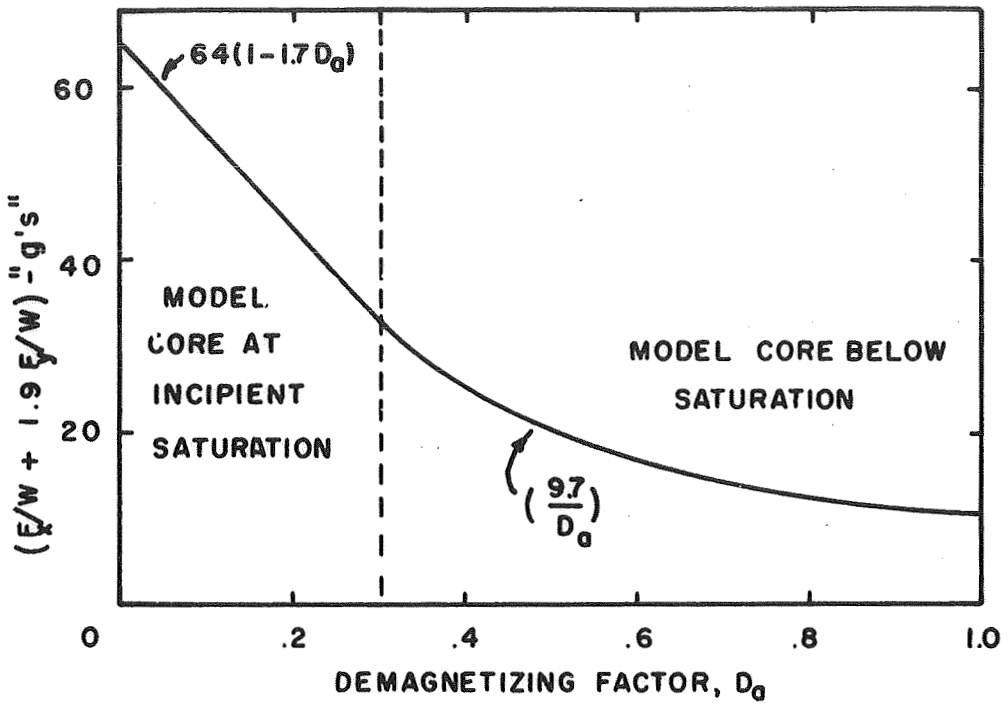

Figure 3.1. Axial and vertical force limits vs. demagnetizing factor ($B_y, B_z, B_{yx} = 0$)

3:2:4 PERFORMANCE OF TYPICAL MODEL CONFIGURATIONS

The demagnetizing factor D_a can be related to the geometry of the test model (Ref. 8). Values of D_a are tabulated below for a variety of configurations.

TABLE 3.1

AXIAL DEMAGNETIZING FACTORS FOR SEVERAL MODEL GEOMETRIES

Model Shape	Demagnetizing Factor D_a
1. Sphere	0.333
2. Cone - included angle = 10°	0.0259
3. " " " 30°	0.105
4. " " " 50°	0.281
5. " " " 90°	0.680

The limits on the axial and vertical forces, for the models of Table 3.1, for zero angle of attack, zero side force, and zero pitch, yaw, and roll moment, are shown graphically below, in Fig. 3.2.

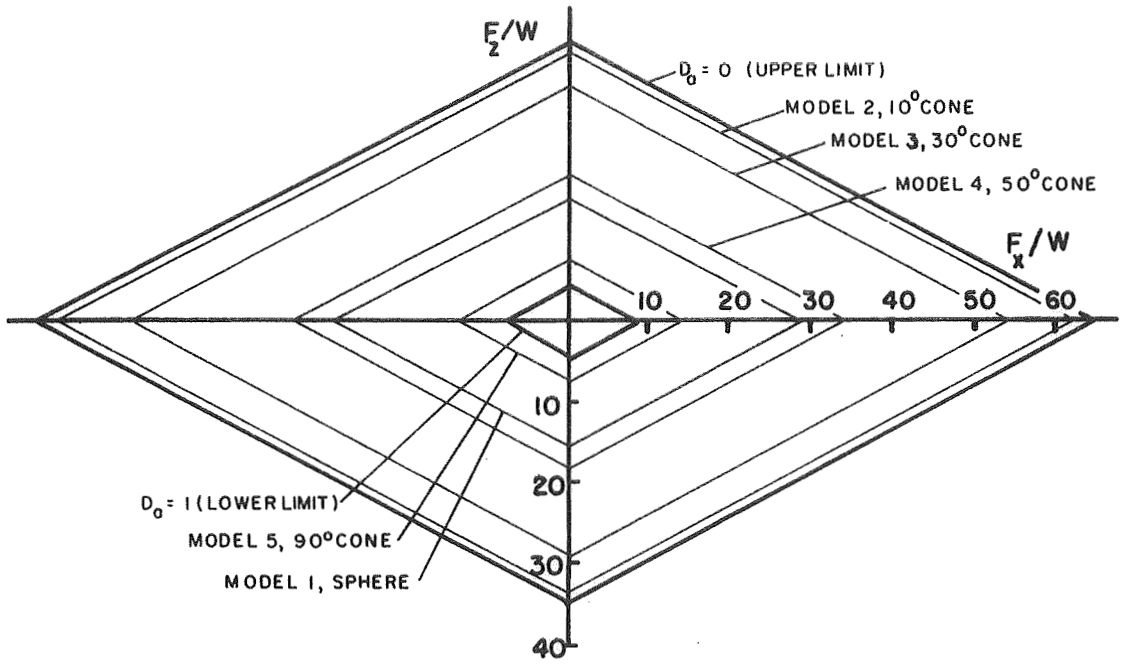

Figure 3.2. Magnetic limits of axial and vertical forces for various model shapes. (Zero angle of attack; zero yaw, pitch, roll moments, zero side force)

3:3:1 POWER REQUIREMENTS FOR PROTOTYPE (STEADY STATE)

The magnetic field properties are controlled by power amplifiers. The specifications of the performance of each power amplifier can be based on current limits derived from the relations in 3:2:3 and the magnetic performance parameters of 3:1:1. A detailed discussion of power supplies is given in Chapter VI.

(a) B_x Power Supply

It was found as a consequence of Eq. III-6 that an

optimum peak level of B_x existed, for models having demagnetizing factors "D_a" greater than 0.30. This will thus serve as the specification for the peak current for the B_x supply. Thus,

Field: $B_x = 0 \rightarrow 4{,}600$ gauss

Current: $I_x(\max) = \left(\frac{I_x}{B_x}\right) B_x(\max) = \left(\frac{1}{20}\right) (4600) = 230$ amps.

Voltage: $V_x(\max) = I_x R_x = (230)\ (2.0) = 460$ volts

Power: $I_x V_x(\max) = (225)\ (460) \simeq 100$ kilowatts

(b) B_{xx} Power Supply

A limit on $\partial B_x/\partial x$ and the corresponding limit on I_{xx} can be found from Eq. III-2 and Eq. III-3, respectively. If it is assumed that B_x, B_y', B_z', B_{yx} and B_{zx} are essentially zero, then from III-2,

Gradient: $B_{xx}(\max) = (15{,}000)/14.7 \simeq 1000$ gauss/in

Current: $I_{xx}(\max) = \left(\frac{I_{xx}}{B_{xx}}\right) (B_{xx}\ \max) = \left(\frac{1}{1.7}\right) 1000$

$= 590$ amperes

Voltage: $V_{xx}(\text{max d.c.}) = I_{xx} R_{xx} = (590)\ (2.0)$

$= 1{,}180$ volts

D.C. Power: $I_{xx} V_{xx} = (590)\ (1180) = 700$ kilowatts

This represents the steady state power limit imposed by the saturation characteristics of the magnet system.

(c) B_{zx} Power Supply

The maximum current limit for the B_{zx} power supply can be found from III-1 and III-2 assuming B_x, B_y, B_z', B_{xx}, B_{yx} are essentially zero.

i.e. Gradient: $B_{zx}(max) = 535$ gauss/in.

Current: $I_{zx}(max) = 385$ amperes

D.C. Voltage: $V_{zx}(max) = I_{zx}R_{zx} = (385)\ (1.0) = 385$ volts

D.C. Power $I_{zx}V_{zx}(max) = (385)\ (385) = 150$ kilowatts

These voltages and power limits apply only for the steady current (d.c.) case.

3:3:2 STEADY STATE PERFORMANCE LIMITS VERSUS D.C. POWER LIMITS

The performance limits of the balance system can be plotted as a function of the power supply capabilities, on a graph similar to Fig. 3.2. Contours of constant d.c. power level are superimposed upon the plot of magnetic limits, as shown in Fig. 3.3.

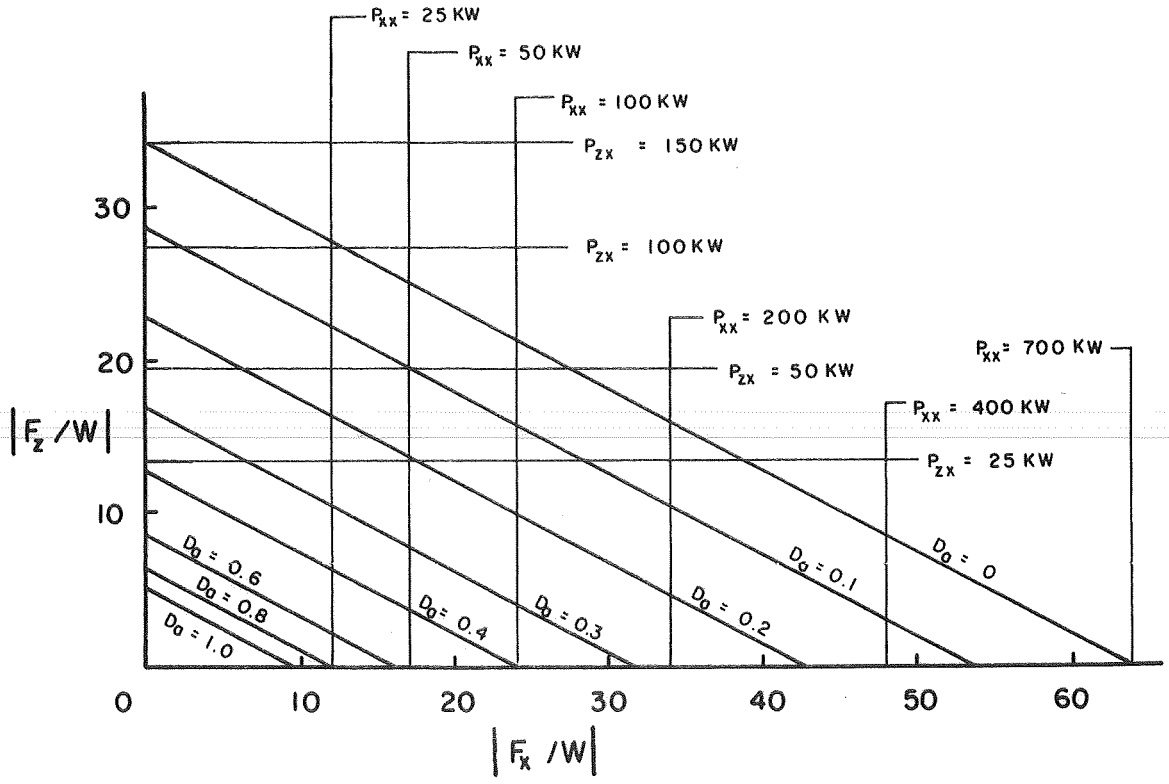

Figure 3.3. Limits on steady-state vertical and axial forces due to demagnetizing factor and d.c. amplifier power level limits. (Extrapolated from measurements made on prototype)

Figure 3.3 is interpreted as follows. The combined axial force capability falls in an area bounded by the F_x/w and F_z/w axes, and by the power level capability lines P_{xx} and P_{zx}. A further constraint is placed by the contour of constant demagnetizing factor, D_a. Take for example the case of P_{xx} = 50 kw, and P_{zx} = 50 kw. These two boundaries intersect at D_a = 0.1. Thus, the forces available for models with D_a < 0.1 will lie within this rectangular area. For D_a > 0.1, the rectangular boundary will be reduced by the D_a contour. This is illustrated in Fig. 3.4 below.

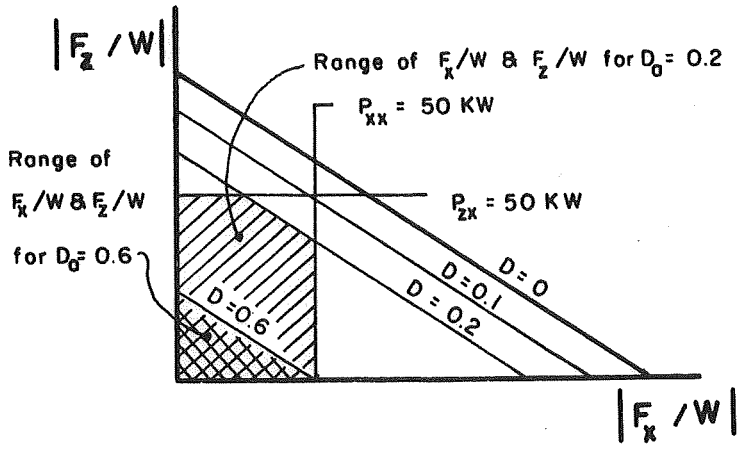

Figure 3.4. Dependence of force range upon power limits and demagnetizing factor

3:4:1 FREQUENCY DEPENDENCE OF VOLTAGE REQUIREMENTS

One of the important applications of the magnetic suspension and balance system will be in the field of dynamic stability testing. One of the techniques which will be used will involve oscillation of the test model in one or more degrees of freedom. To accomplish this, the model must be forced by the magnet system to perform the oscillatory motion. Since relations have been developed describing the magnetic body forces on the model as functions of the magnet currents, these can be used to find the power requirements for forced

oscillation of the test model.

As an example, consider the performance of the "LIFT" system; that is, the $\partial B_z/\partial x$ magnet system. For solid iron models magnetized to incipient saturation, ($D_a < .30$), the vertical acceleration, z, is given by Eq. III-4 as a function of B_{zx}.

$$\frac{\ddot{z}}{g} = F_z/W = 0.063\,\bar{B}_{xz} \qquad \text{(III-11)}$$

or, from 3:1:1(v),

$$\frac{\ddot{z}}{g} = 0.0875\,I_{xz} \qquad \text{(III-12)}$$

The amplitude "z" of vertical oscillation, as a function of voltage and frequency can be found.

$$z = \frac{\ddot{z}}{\omega^2} \qquad \text{(III-13)}$$

and

$$I_{xz} = \frac{V_{xz}}{R_{xz}}\left(\frac{1}{1 + j\omega\frac{L_{xz}}{R_{xz}}}\right) \text{ Amps.} \qquad \text{(III-14)}$$

$$z = (0.0875)\,g\left(\frac{1}{\omega^2}\right)\frac{V_{xz}}{R_{xz}}\left(\frac{1}{1 + j\omega\frac{L_{xz}}{R_{xz}}}\right) \qquad \text{(III-15)}$$

The power, $I_{zx}V_{zx}$, can be found as a function of z and ω.

A.C. Power:

$$P_{xz} = \frac{z^2\omega^4 R_{xz}}{(0.0875)g^2}\left(1 + j\omega\frac{L_{xz}}{R_{xz}}\right) \text{ Volt.amps} \qquad \text{(III-16)}$$

From Eq. III-16, it is seen that the a.c. power required varies as the square of the amplitude, and the fifth power of the frequency (above the corner frequency, R/L, of the coil system).

Substituting values in Eq. III-16,

$$P_{kz} = 8.75 \times 10^{-4}\, z^2 \omega^4 (1 + 0.4 j\omega) \quad \text{Volt.amps}$$

where z = inches

ω = radians/sec

or, at high frequencies,

$$P_{kz} = 3.4\, z^2 f^5 \text{ volt.amps}$$

where f = frequency in Hertz

z = inches

Page intentionally left blank

CHAPTER IV

MODEL POSITION SENSING SYSTEM

4:1:1 GENERAL REQUIREMENTS

It was pointed out in Chapter 1 that a model position sensing system was required for stabilization when the basic support mechanism was the interaction of quasi-steady magnetic fields with a ferromagnetic model. Continuous measurement of model position is also needed as an input for the computation of aerodynamic forces and moments. The characteristics of a suitable position sensing system can be set forth as follows:

a) No mechanical contact is made with the model

b) Translational displacements parallel to the (orthogonal tunnel axes will be transformed into three independent high level electrical signals proportional to the translational displacements, over a suitable range.

c) Rotational displacements of the model roll axis about the tunnel pitch and yaw axes ("y" and "z" axes) will be transformed into two independent, high level electrical signals proportional to the angular displacements, over a suitable range.

d) Rotational displacement of the model about the roll axis will be transformed into an independent, high level electrical signal proportional to the angular displacement over a suitable range.

e) Resolution, repeatability, and frequency response must be compatible with desired accuracy of static and dynamic wind tunnel test results.

f) The system must be easily adaptable to a broad range of model geometry.

g) The system must be compact, and must not interfere with access to the test section or prevent visual contact with the model from the top, bottom, or sides.

h) The system must operate without interference from the magnetic fields used to support the model.

j) Mechanical adjustments within the tunnel test section should be kept to a minimum.

4:2:1 DESIGN ALTERNATIVES

Visible-light optical devices were used to detect model position in the first magnetic suspension systems. Adaptation of these systems to complicated model geometries was found to be difficult, and so other alternatives were sought. Optical systems based on radioactive sources or X-rays are feasible, but may be undesirable due to the attendant health hazards.

A relatively simple electromagnetic position sensor (EPS) system based on differential transformer action has been proposed (Ref. 8) and extensively developed. The EPS is capable of indicating model position in five components, and offers the possibility of extension to the sixth component (roll angle). This system also appears to meet all the requirements of 4:1:1. It was chosen for use with the prototype suspension system, and is described below.

4:3:1 ELECTROMAGNETIC POSITION SENSOR (EPS) SYSTEM

The EPS system is shown schematically in Fig. 4.1. The heart of the system is the transducer coil assembly. This is basically a multi-component differential transformer, with the model forming the core. Movement of the model varies the coupling between the excitation windings and the pickup windings. The excitation windings are powered by a constant audio frequency voltage. The pickup coil voltages are filtered, amplified, added together, demodulated by a reference signal derived from the excitation signal, and are further filtered and amplified to high level. The output indications and signals are approximately proportional to the displacements of the model relative to the axes of the transducer assembly.

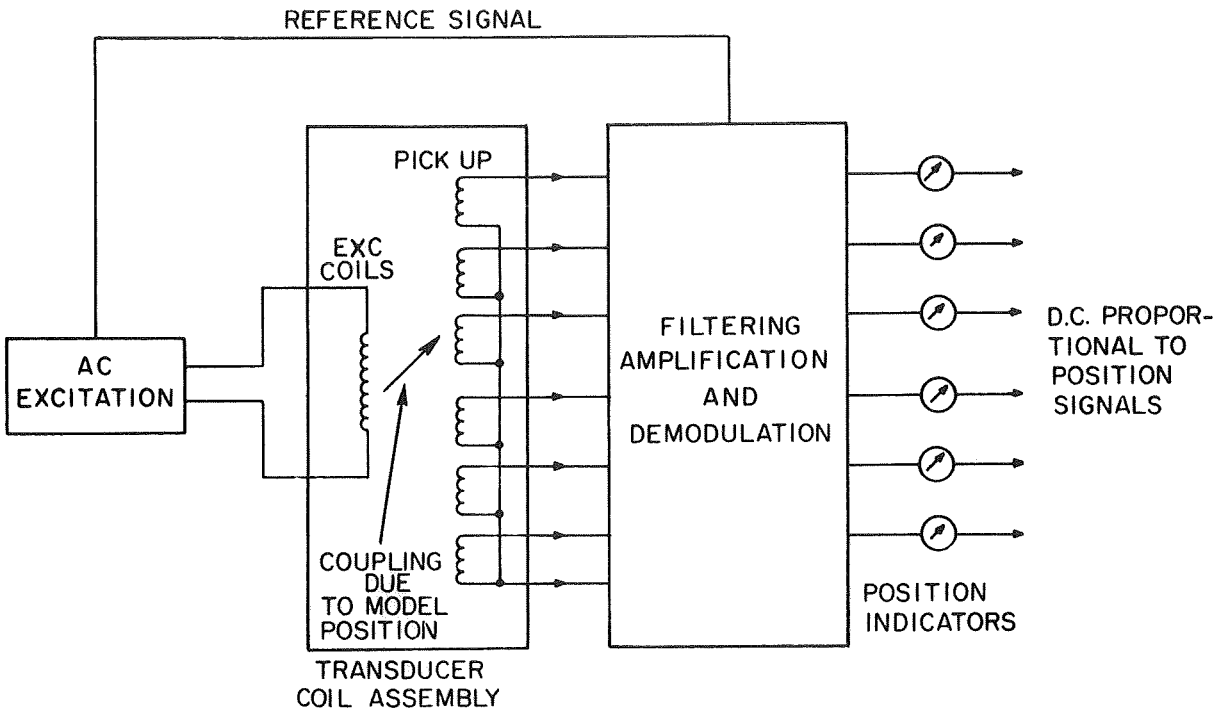

Figure 4.1. Electromagnetic position sensor (E.P.S.) system: simplified schematic

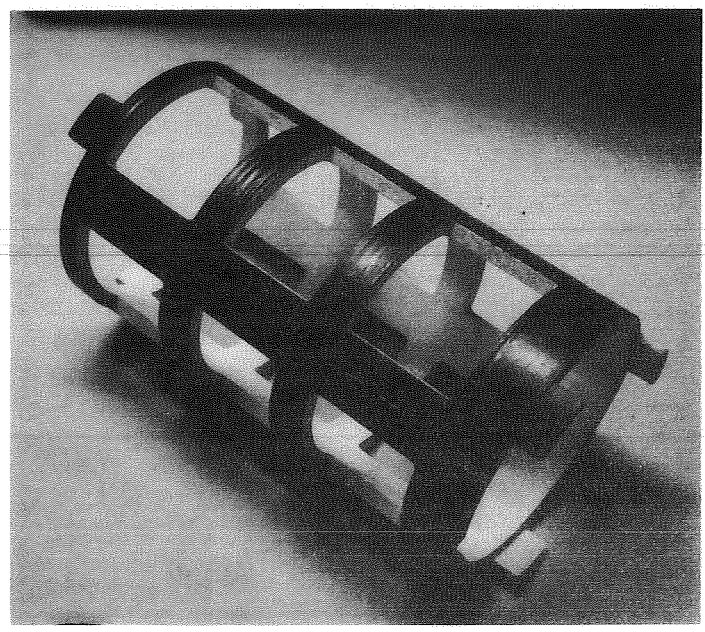

Figure 4.2. Prototype E.P.S. system transducer coil assembly

4:3:2 TRANSDUCER COIL DESIGN FOR FIVE-COMPONENT E.P.S.

The prototype transducer coil assembly is shown in Fig. 4.2 (photograph). The assembly consists of a cylindrical phenolic tube, 7 1/2" diameter, 8 1/2 " diameter, with azimuthal and longitudinal grooves cut into the outside. The excitation and pickup coils are used in the grooves, and the coils are connected to multiple-pin electrical connector sockets built into the end of the assembly. The windings are potted with epoxy for mechanical strength. Windows are provided for viewing from the top, bottom, and sides. The assembly is painted black on the outside, and flat white on the inside to enhance visibility of the model within the assembly during operation.

The windings are shown in more detail in Figures 4.3, 4.4, 4.5. The excitation windings consist of a pair of Litz-wire Helmholtz coils (equal turns) which are terminated at the end of the structure at a 2-pin socket. The pickup coils consist of a total of seven pairs of teflon-covered stranded small gage wire. One side of each coil pair is connected to a common ground wire; and the signal ends are terminated at a multiple-pin socket at the end of the structure. One of the pickup coil pairs is wound as a Helmholtz pair (equal turns), and is located adjacent to the excitation coils. These coils are connected in opposition such that the combination of excitation and pickup coils comprises what is commonly known as a linear variable differential transformer (or LVDT). The remaining pickup coil pairs are in the row of saddle coils, and lie along the same cylindrical surface as the excitation coils. The coils of each pair oppose each other diametrically, and are connected electrically in the same sense. All coils have an equal number of turns.

The pickup coil pairs are inherently magnetically uncoupled from the excitation coils in the absence of a model due to the simple symmetrical geometry. A generally shaped small body of ferromagnetic and/or electrically conducting material can be positioned and oriented within the transducer coil assembly such that there is no net coupling between the excitation and

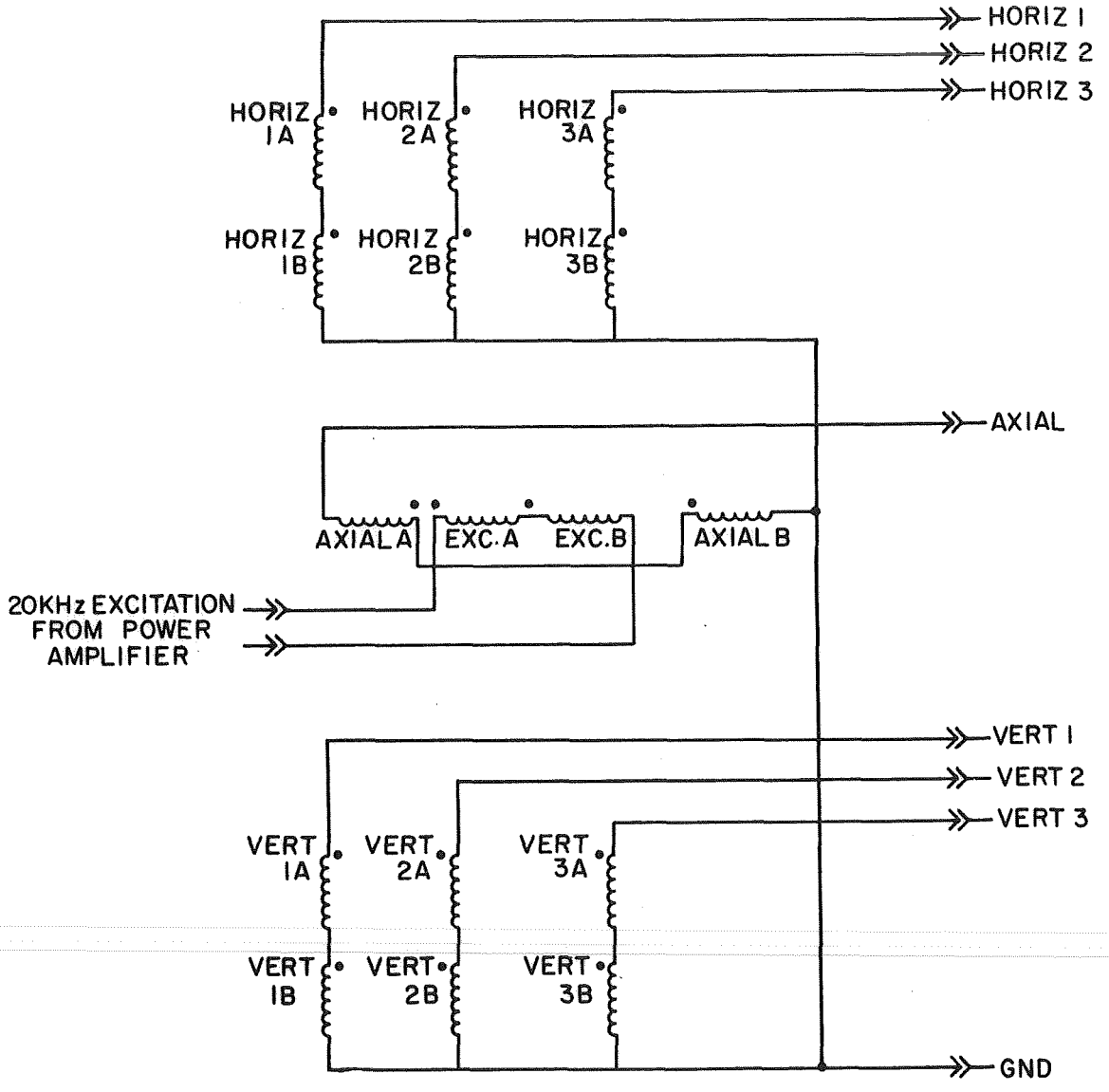

Figure 4.3. Schematic of E.P.S. transducer coils

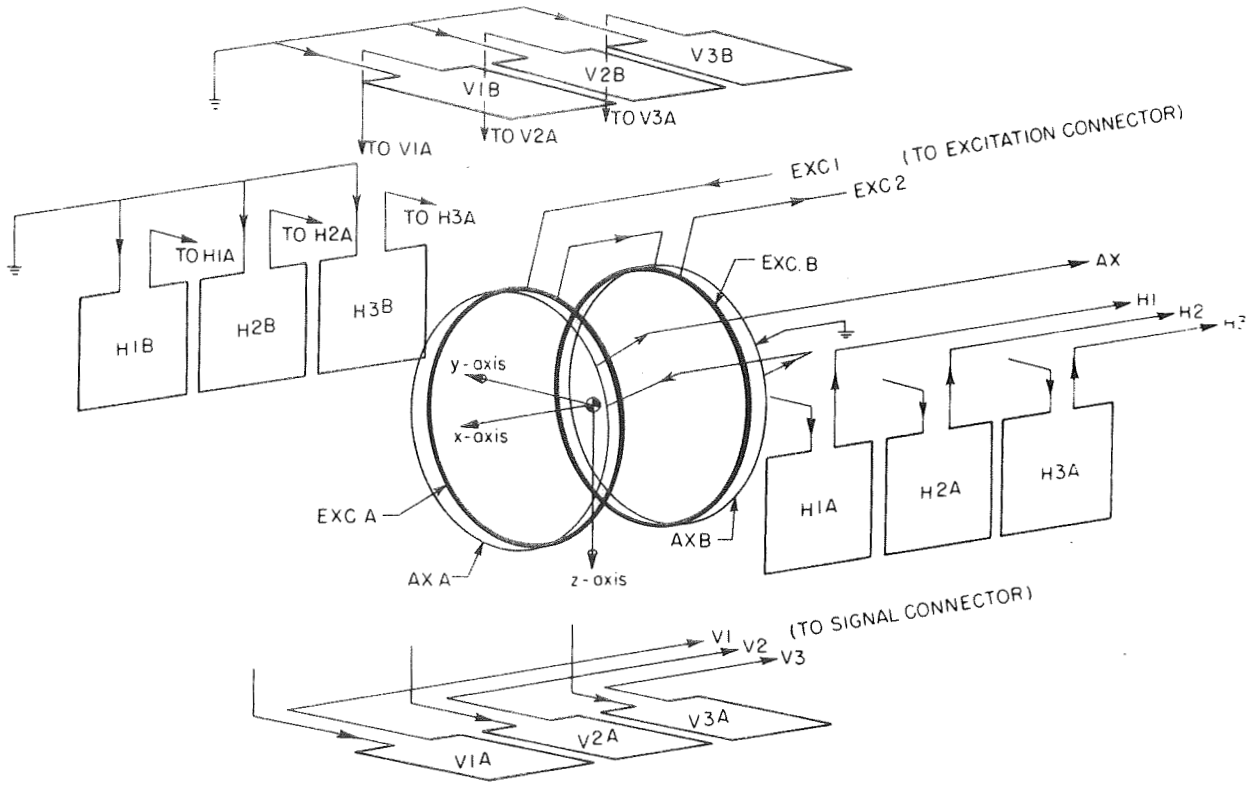

Figure 4.4. Pictorial of E.P.S. transducer coil windings

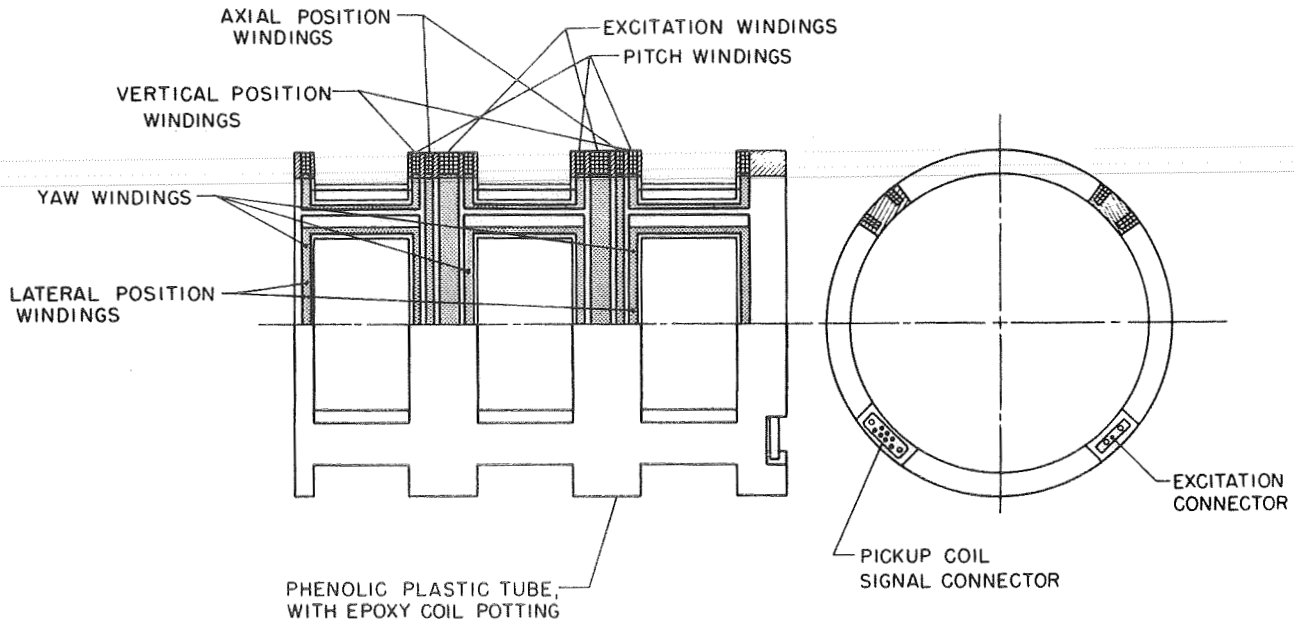

Figure 4.5. Sectional view of transducer coil

pickup coils and hence no output signal voltages. However, angular or translational displacements will result in coupling; that is, voltages will be produced at the pickup coil pair terminals, depending upon the position and orientation of the body relative to its zero output position and orientation.

4:3:3 THEORY OF OPERATION OF E.P.S. TRANSDUCER COIL SYSTEM

The operation of the system is described qualitatively as follows:

(a) Excitation of Model

The excitation Helmholtz coils produce an oscillating axial magnetic field which is quite uniform over a region surrounding the center of symmetry. If a ferromagnetic and/or electrically conducting body is placed in this field, it will be periodically magnetized, at the excitation frequency. At a given frequency, the strength, phase, and direction of the fluctuation magnetization will depend upon the size, material, shape, and orientation of the body. Demagnetizing factors can be defined for the alternating field case in a manner analogous to the steady-field case with phase as an additional term in each factor.

For the case of an axisymmetric, slender, ferromagnetic body of low electrical conductivity (typical of wind-tunnel test model cases), the situation is simplified. With the body centralized and aligned with the axis of the coil assembly, the magnetization vector is aligned with the coil axis. If the body is angulated, a transverse magnetization component is produced, approximately proportional to the sine of twice the deflection angle, and in the plane of the deflection. The axial component varies approximately as the square of the cosine of the deflection angle.

(b) Detection of Axial Position (LVDT Action)

Since the body is magnetized in a fluctuating manner, the far field due to the magnetization also fluctuates. This fluctuating field component can be detected by an electrical coil. In the case of the EPS system (as with LVDT's) the axial sensing channel has a null-center. The operation of the axial channel is shown diagramatically in Fig. 4-6(a) and (b). Figure 4.6(a) shows the effect of axial displacement. More flux couples with the forward pickup coil, and less flux couples with the aft coil. The net result is an output voltage which varies approximately proportionally to the axial displacement. The phase of the output voltage indicates the direction of displacement: zero degrees phase corresponds to forward motion, 180 degrees phase corresponds to aftward motion.

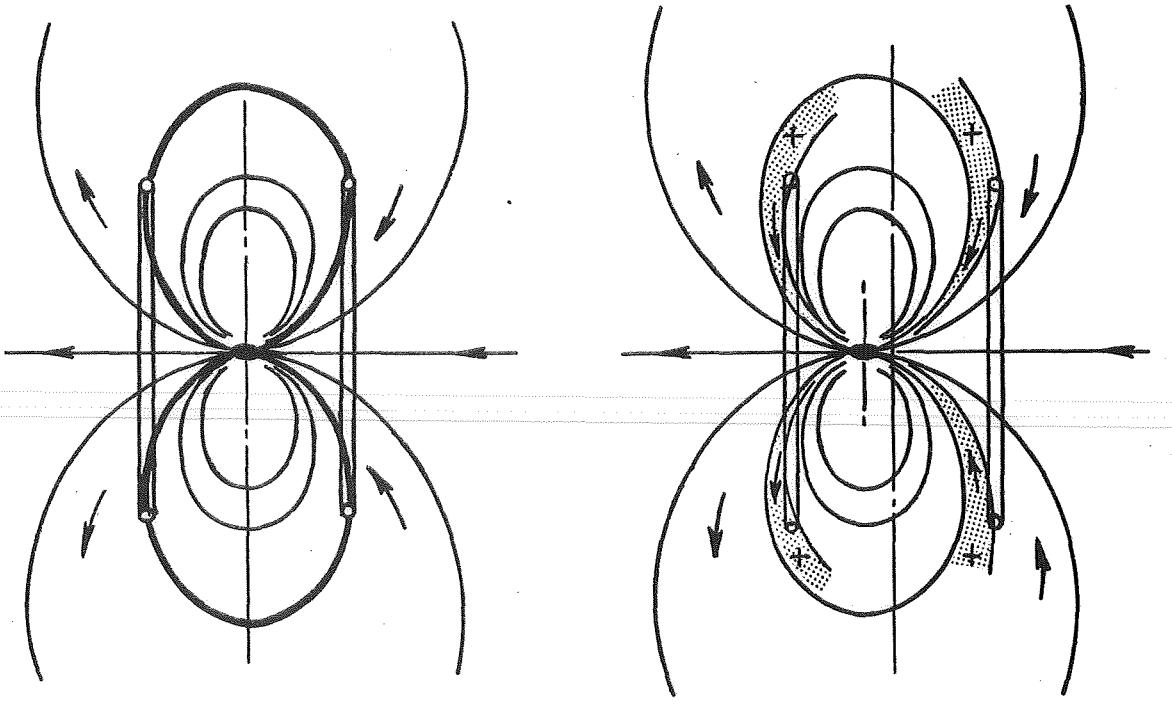

Figure 4.6. E.P.S. transducer coupling variation with axial position of model

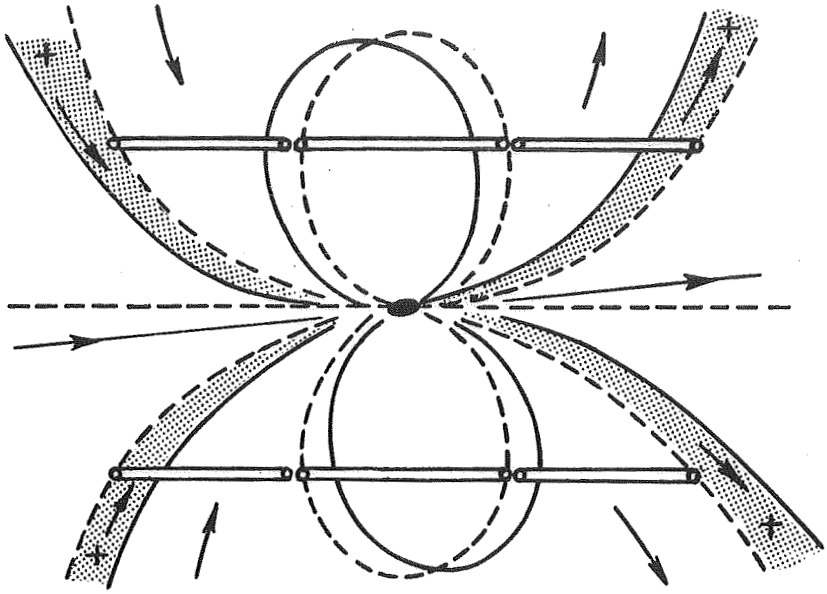

Figure 4.7. E.P.S. transducer coupling variation with pitch angle of model

(c) Detection of Pitch and Yaw Angles

It was pointed out in (a) that transverse magnetization components are introduced when the body is angulated. The existence of transverse magnetization can be detected by pickup coils transverse to the excitation axis. Figure 4.7 shows the manner in which the transverse magnetization flow field flux couples with the transverse coils in one plane (pitch or yaw plane). If the three coil pair output voltages are added together, the sum is approximately the same as the output of one large pair of coils in the same location, with the same number of turns as each of the small coil pairs. The output voltage is a strong function of the transverse magnetization, and hence of the angulation of the body in the plane of the coils. The output, however, is only weakly related to translations of the body and rotation out of the plane (no first-order coupling).

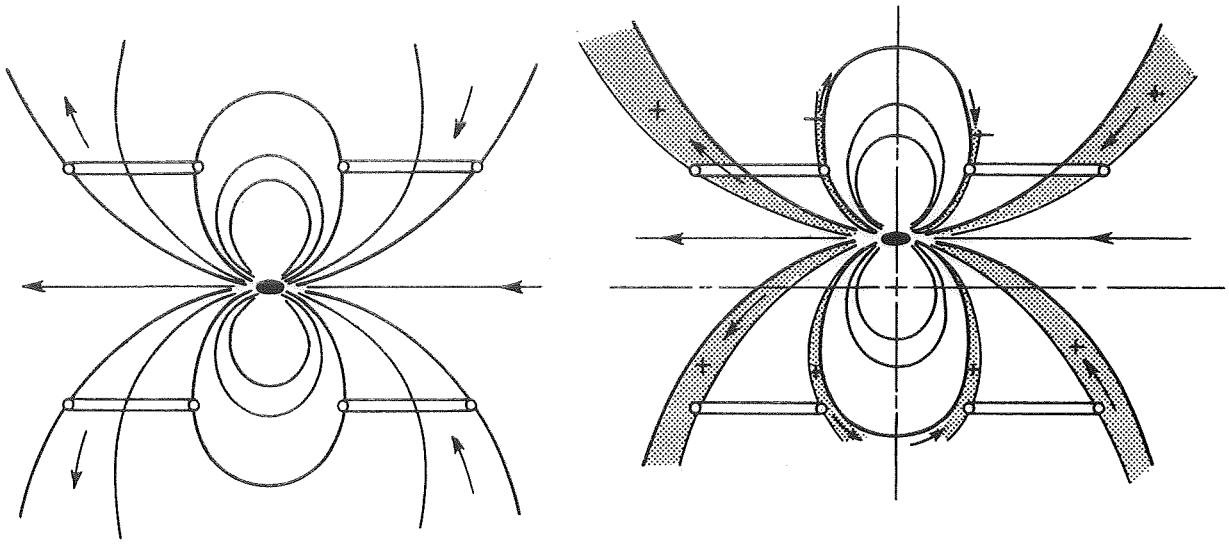

(a) (b)

Figure 4.8. E.P.S. transducer coupling variation with vertical displacement of model

(d) Detection of Lateral and Vertical Displacement

Lateral and vertical translation of the axial magnetization component of the body results in differential coupling between the fore and aft transverse coil pairs. Figure 4.8(a) shows the variation in coupling with motion in the plane of the transverse coil axes. Signal voltages approximately proportional to transverse displacement from the excitation coil axis, in the pickup-coil axis plane, are obtained by taking the difference between the forward and aft transverse coil-pair output signals. (This difference signal also contains a component proportional to the product of in-plane angulation and axial displacement. This is the most important cross-coupling effect.)

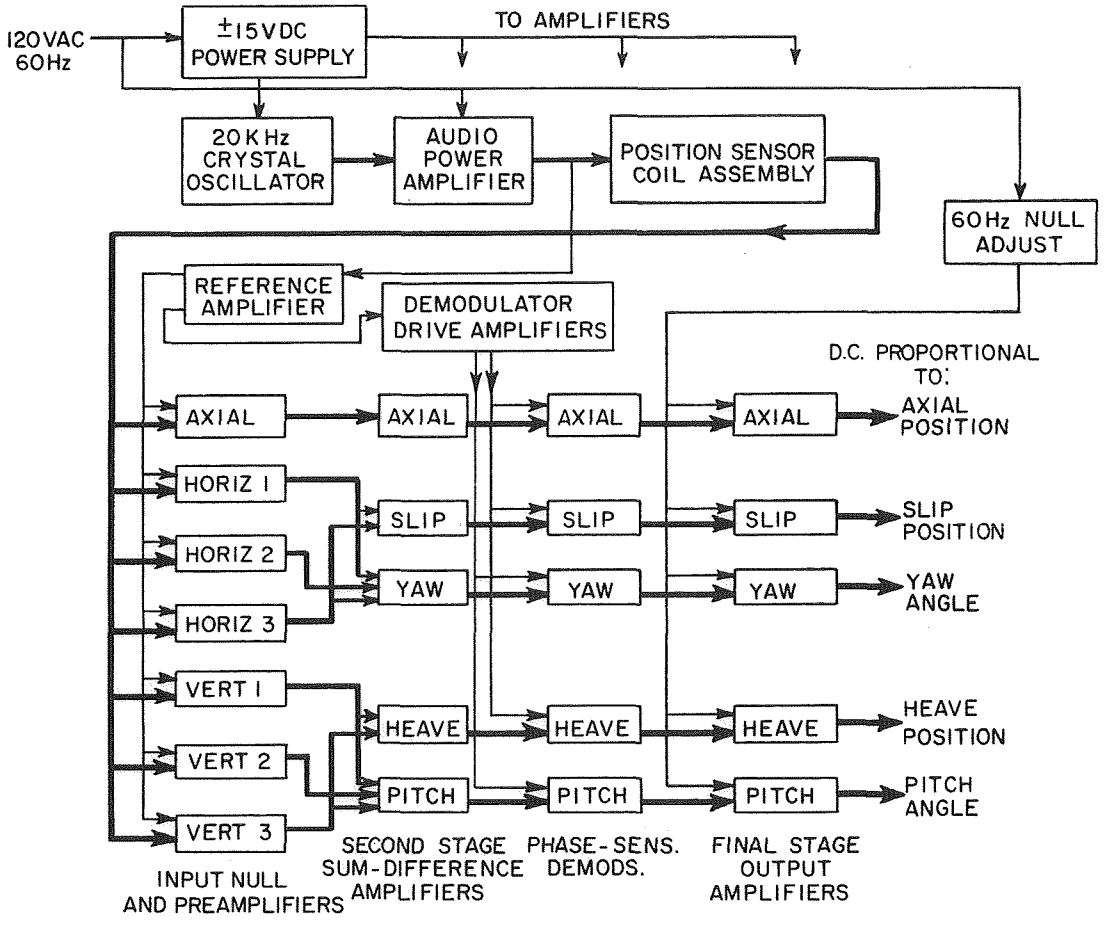

Figure 4.9. E.P.S. electronics system block diagram

4:3:4 E.P.S. ELECTRONICS SYSTEM

The electronics associated with the E.P.S. system are shown in block diagram form in Figure 4.9; the operation of the system is briefly as follows:

a) Excitation: The power required to drive the excitation windings of the E.P.S. transducer coil is provided by an audio-frequency power amplifier driven by a crystal-controlled master oscillator.

b) Preamplification: The output a.c. signals from the transducer coil (seven channels) are filtered to remove noise outside the desired bandwidth, and residual excitation-frequency voltages are nulled at this stage.

c) Signal Combination: In order to provide separate a.c. voltages proportional to lateral displacements and yaw angles, and vertical displacement at pitch angles, the preamplified signal voltages from the saddle-coil pairs must be combined, as described in 4:3:3(c,d). A further stage of amplification is provided for these functions.

The axial channel signal, which is not combined with any other signal, is also amplified further in a stage following the preamplifier.

d) Phase-sensitive Demodulation: The a.c. voltages from the second amplifier stages are rectified in full-wave phase-sensitive demodulators to produce d.c. voltages proportional to the a.c., and with polarity corresponding to the phase of the a.c. signal before demodulation.

e) Final Amplification: The demodulation output signals are filtered to remove demodulation ripple and other noise, and are amplified to a suitable level (several volts full scale). Line-frequency nulling ("hum-bucking") is also provided in this stage.

f) Position Indicators: Model positions and orientations are indicated on voltmeters driven by the output signals.

g) Reference Amplifiers: Carrier frequency signals are required for input nulling and for driving the demodulators. The basic reference signal is derived from the excitation voltage supplied to the transducer coil. This signal is attenuated and split into two balanced voltages in quadrature. These signals are used for input nulling, and for driving a pair of variable-phase square-wave generators which drive the demodulators.

The design and operation of the E.P.S. system electronics is described in greater detail in Appendix B.

4:4:1 ROLL ATTITUDE SENSING*

Active, closed-loop control of the roll attitude requires a roll angle sensor system. Optical systems have been used in the past, and there are many possible design alternatives. Such systems may be relatively simple, but a single approach is not usually adaptable to a wide variety of model geometries. A few alternatives are outlined below in 4:4:2.

As an alternative to optical systems it appears feasible to extend the operation of the E.P.S. system to include roll-angle sensing. A possible approach is outlined in 4:4:3.

---

*cf Ref. 11.

4:4:2 OPTICAL ROLL-ANGLE SENSORS

Optical systems generally are composed of a light source or sources, an electric photodetector or array of detectors, and some means of modulating the transmission from the light source to the detector, as a function of the roll attitude of the model. The various alternatives may be classified broadly as follows: (see Table)

TABLE 4.1

DESIGN CHOICES FOR AN OPTICAL ROLL ANGLE SENSOR

LIGHT SOURCE	LIGHTING	ROLL MODULATION	DETECTION
-INSIDE MODEL -OUTSIDE MODEL	-DIFFUSED -CONCENTRATED a) Collimated b) "Point Source"	-MODEL GEOMETRY -SLOTS IN MODEL -SURFACE PATTERNS ON MODEL: a) Trans-mission thru (i) gray tones (ii) black-white b) Reflec-tion by (iii) color (iv) polarizer	-SILHOUETTE IMAGE -SURFACE PATTERN IMAGE -ARRAY

The light source may be placed inside the model, and powered by battery, or may be remote from the model. In the latter case, the light may be collimated by mirror, lens, or other device within the model, or may emerge as from a point source. Modulation of the internal lights relative to a fixed axis perpendicular to the roll axis can be affected by the collimation, or by a variable density, color, or polarizing transmission filter surrounding the light source. Detection of roll angle may be accomplished by a suitable arrangement of photodetectors, imaging lenses, and color or polarizing filters if required. External light sources can be used in a variety of ways. The model may be back-lighted with a uniform diffuse or collimated source, and the roll-dependence of the silhouette of the outside shape or internal passages through the model can be sensed

with photodetectors. Alternatively, surface patterns may be applied to the model which produce image intensities which vary with roll angle to provide the roll angle signal. Some examples are shown in the following figures.

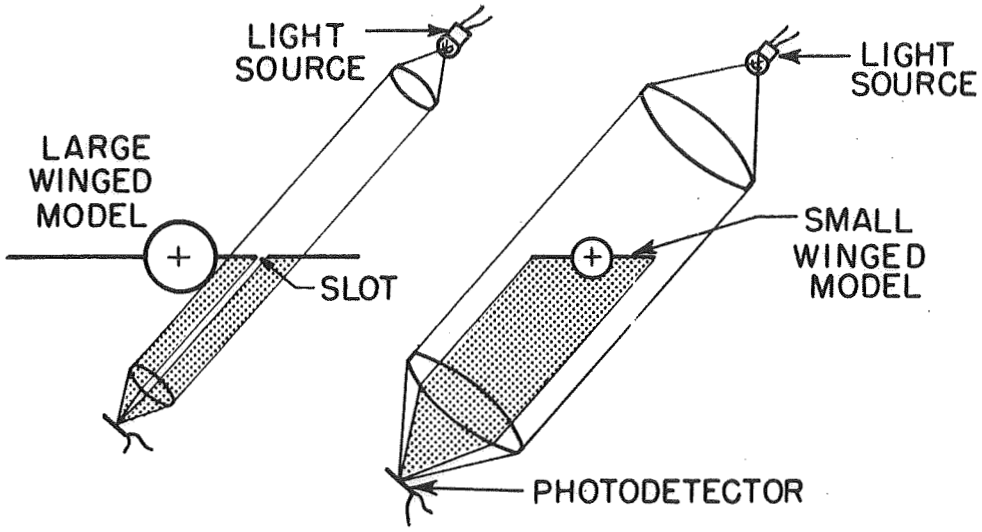

Figure 4.10. External source collimated light roll detectors for large and small-winged models

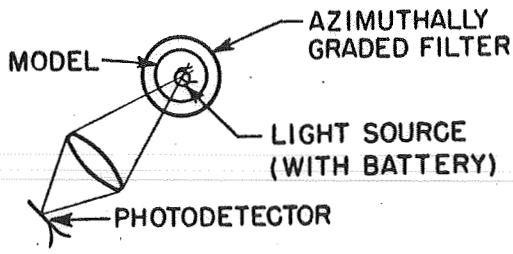

Figure 4.11. Internal point source with azimuthally graded filter

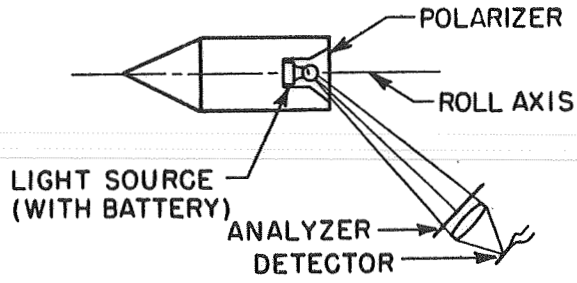

Figure 4.12. Internal point source with polarizer and analyzer

4:4:3 E.P.S. ROLL SENSOR

The E.P.S. system can be used to sense roll orientation of the model, by using the transverse pickup coils of the E.P.S. in the same manner as a synchro resolver. This requires some on-board means of generating an oscillating magnetic moment perpendicular to the model roll axis, at a frequency different from the main E.P.S. excitation. This can be done with an internal battery-powered transistor oscillator connected to a small tuned coil inside the model and perpendicular to the roll axis. This is shown schematically in Fig. 4.13 below. This scheme is obviously better adapted to larger-scale models, and may be unworkable for some model geometries.

4:4:4 ROLL ANGLE SENSING: CONCLUSIONS

There is a need for a "universal" roll angle sensor adaptable to a wide range of model configurations. However, several specialized methods are presently available using either optical systems, or an extension of the Electromagnetic Position Sensor (E.P.S.) system, depending upon the model geometry.

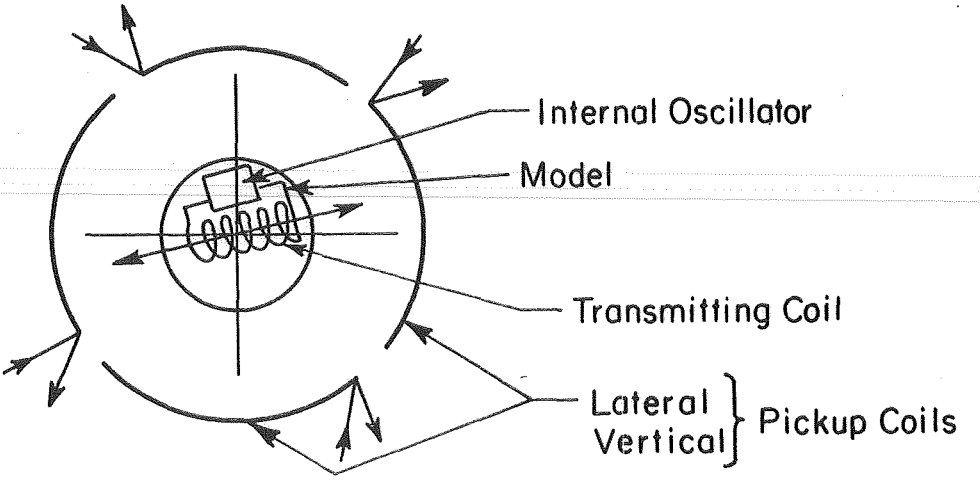

Figure 4.13. Schematic of E.P.S. roll sensor

4:5:1 ENVIRONMENTAL PROBLEMS WITH THE E.P.S. SYSTEM

The E.P.S. system is immersed in a rather hostile environment, from an electromagnetic point of view. It is surrounded by magnet coils and ferromagnetic material, and there are many modes of inductive and capacitive coupling which may cause interference with the proper functioning of the system. The interference can arise from three basic sources: (a) transformer-coupling with power amplifier generated high-frequency noise which lies within the bandwidth of the E.P.S. system, (b) variation of mutual coupling within the E.P.S. due to stray inductive and capacitive effects, changes in permeability, etc., and (c) coupling asymmetry due to nested saddle coils.

(a) Noise Coupling from Power Amplifiers

Certain power amplifier designs suitable for use with the magnetic suspension system inherently are generators of considerable electromagnetic noise power extending well into the radio frequency spectrum. The main offenders are phase-controlled SCR or thyratron converters or other types of on-off or switching amplifiers. Two-axis rotating machine-type amplifiers also produce high-frequency noise due to commutator ripple, although at typically somewhat lower relative power. Since some of the noise power lies within the bandwidth of the E.P.S. system (19 khz to 21 khz), it is necessary to attenuate it before it reaches the magnet coils, by insertion of suitable filters in the magnet coil power leads. The design of these filters depends upon the characteristics of the power amplifiers and the layout and routing of the power leads. This problem is discussed in Chapter VI.

(b) Variable Coupling Effects

The E.P.S. transducer coil is magnetically coupled with the suspension magnet system. Any variation in this

coupling will manifest itself as spurious output position signals. The major sources of this type of interference are:

(i) Changes in incremental permeability of the iron magnet cores due to variations in magnetizing level.

(ii) Variations in turn-to-turn capacitance of the magnet coils with temperature.

(iii) Variations of impedance, looking back into the power amplifiers.

(iv) Variations in suspension coil inductance, or capacitance to ground due to proximity of movable objects (such as test section doors, operations, etc).

It was found to be possible to reduce these effects significantly as follows:

(i) Core Permeability Variation

Coupling between the E.P.S. and the side and lift force magnet cores takes place predominantly at the poles. To reduce this coupling, the pole tips were covered with 1/16" thick copper shield "boots". (The 20 khz field component penetrating the iron pole tips is consequently attenuated, and the 20 khz magnetization component which results is further attenuated before it re-emerges from the pole tips.) These shields also attenuate noise from the power amplifiers.

(ii),(iii),(iv) Impedance Variations

These effects can all be reduced by addition of a shunt capacitance of at least 0.5μF across each pair of magnet coil terminals, with the exception of the saddle coils.

(c) Coupling Asymmetry

In the prototype magnet system, the "saddle-coils" used to control pitch, yaw, and roll were arranged in the nested configuration shown in Fig. 2.4. The inner pair of saddle coils couple more strongly with the E.P.S. transducer coil than do the outer pair. If the 20 khz input impedance to the saddle coils is small, and 20 khz secondary currents are therefore allowed to flow, the saddle coils behave as an asymmetric shield to the E.P.S. As a result, the zero-pitch-signal, and zero-yaw-signal axes are skewed away from the axis of the inner saddle coils. Thus, the "apparent" pitch and yaw axes are no longer orthogonal, and are also rotated from the horizontal and vertical. This condition can be corrected by making the input impedance to the saddle coils sufficiently high, at 20 khz. This can be done with parallel trap filters in the power leads, tuned to 20 khz. The design of these filters is described in Chapter VI. (This problem can be avoided completely, by use of the simpler saddle coil configuration shown in Fig. 2.3.)

Page intentionally left blank

CHAPTER V

COMPENSATION SYSTEM

5:1:1 INTRODUCTION

This chapter describes the design of the electronic compensation system which provides control of the stability and the response characteristics of the magnetic suspension system. This system is located in the control loop between the model position sensor system and the magnet power amplifiers, as shown in Fig. 5.1. The compensation system can be quite simple and effective for a wide range of models and angles of attack; refinements may be added to extend the range of the system.

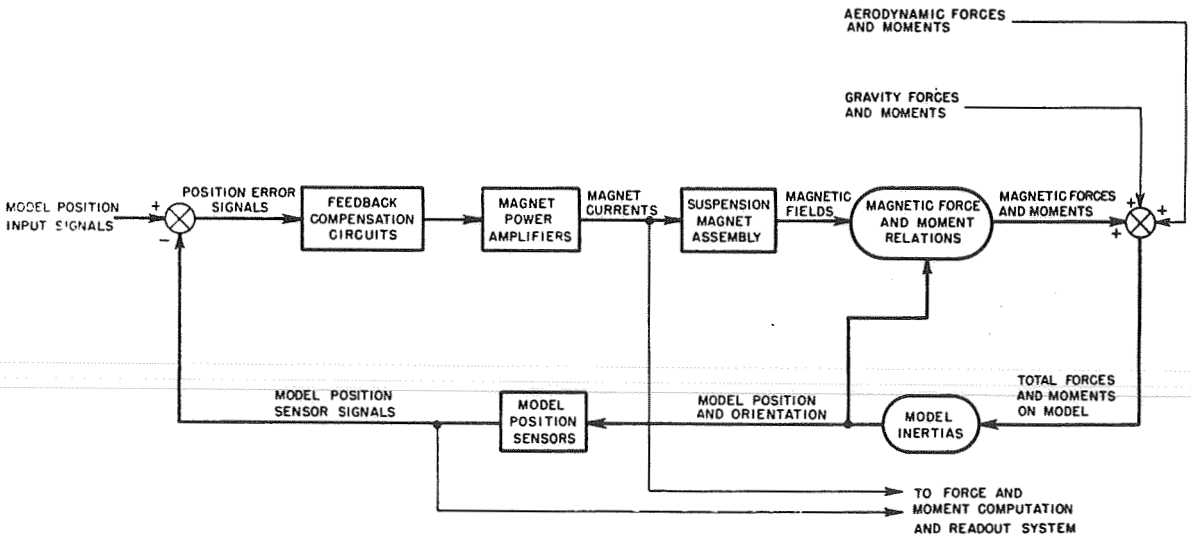

Figure 5.1. Functional block diagram of suspension system

5:2:1 UNCOUPLED COMPONENT COMPENSATION

The most simple compensation scheme is based upon the assumption that each degree of freedom is uncoupled from the others. The compensation then takes the form of electrically uncoupled channels which may be designed and analyzed independently. This assumption is approximately valid for the particular magnet system design described in this report, for small angles of attack. Consider first the translational components. One channel is shown in simplified form in Fig. 5.2.

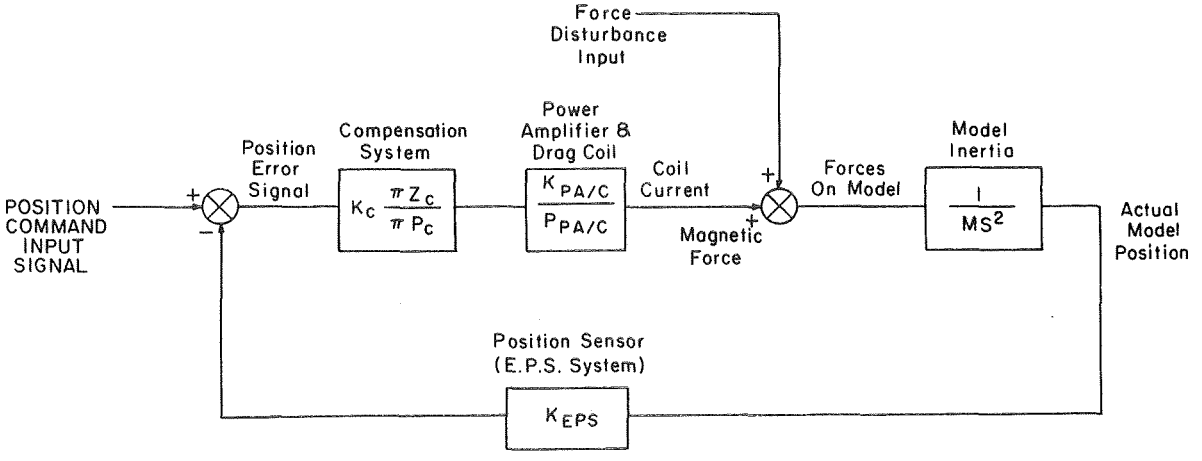

Figure 5.2. Servo-loop diagram of suspension system

The magnetic force is assumed to be proportional to and in phase with the magnet coil current. The magnet coil current/power amplifier input signal transfer function is assumed to be characterized as a first order lag. The measured model position is assumed to be proportional to and in phase with the actual model position. The effect of model inertia, defined as the

displacement/force transfer function, is characterized by a gain inversely proportional to the model mass and a double integration. The compensation system is assumed to be a ratio of two polynomial complex functions, factored into poles and zeros.

The design problem is resolved into three basic parts. These are:

a) Stabilization of the loop.

b) Minimization of position error for given force disturbance inputs.

c) Minimization of position error for given position command inputs.

The design proceeds as follows: For steady disturbance inputs, it is desirable to maintain zero position error. This requires an integration in the compensation system. The pole-zero plot of the control loop will then appear as in Fig. 5.3.

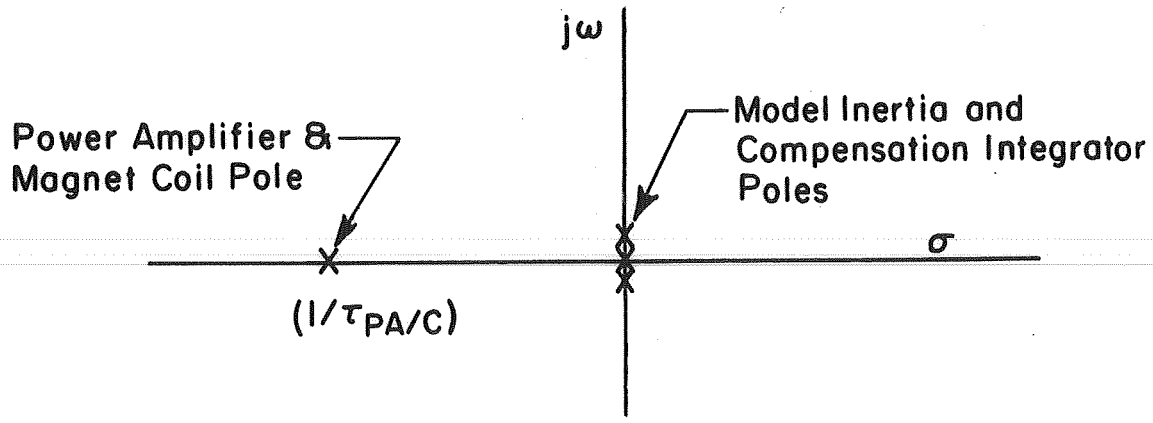

Figure 5.3. Pole-zero plot of magnetic suspension control loop with integral compensation only

The loci of the closed-loop poles of this system are sketched in Fig. 5.4.

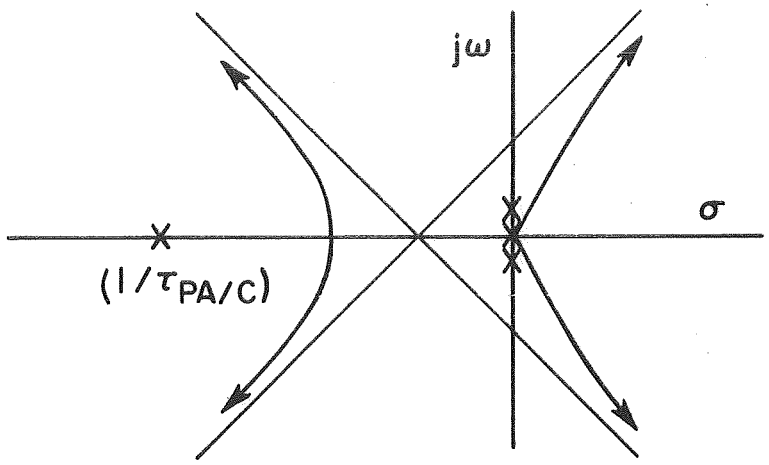

Figure 5.4. Root locus of integrally compensated suspension loop

Two closed-loop poles immediately branch into the right-half of the s-plane, and the loop is unstable for all values of loop gain.

In order to stabilize the system, lead compensation is required. That is, zeros must be introduced into the left-half of the s-plane in order to bring all of the root loci into the left-half, or stable region of the s-plane. Satisfactory stabilization of the system is not practical with a single zero. Two zeros can provide the loci shown in Fig. 5.5. The closed loop response of the system shown in Fig. 5.5 is oscillatory, with small damping ratio, and is not satisfactory. Some improvement may be made by placing the compensation zero closer to the origin, as shown in Figure 5.6.

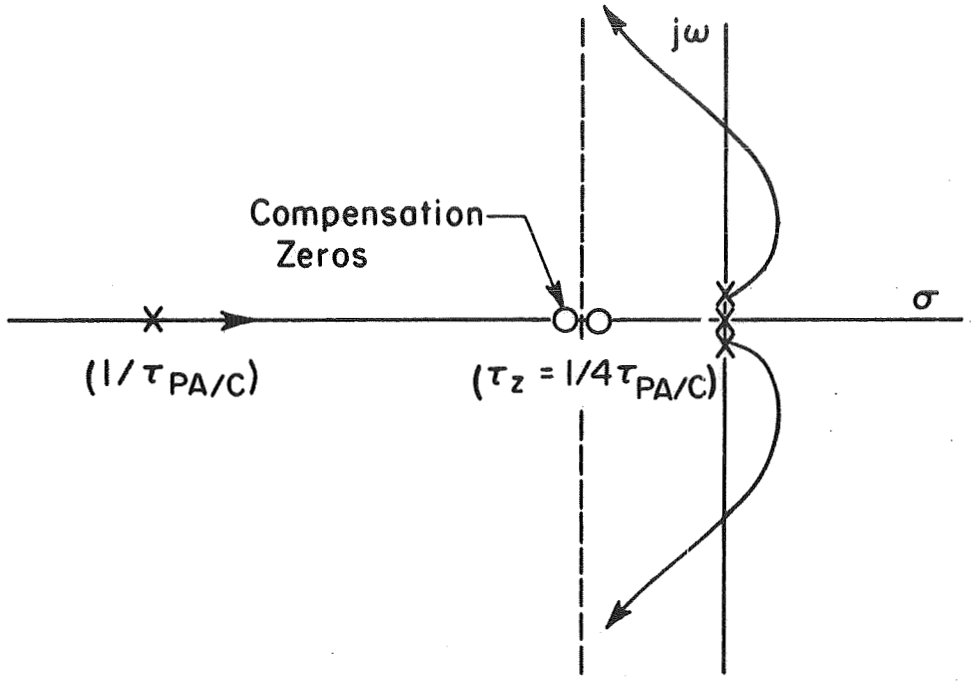

Figure 5.5. Effect of two negative real zeros on root loci ($\tau_z = 4\tau_{PA/C}$)

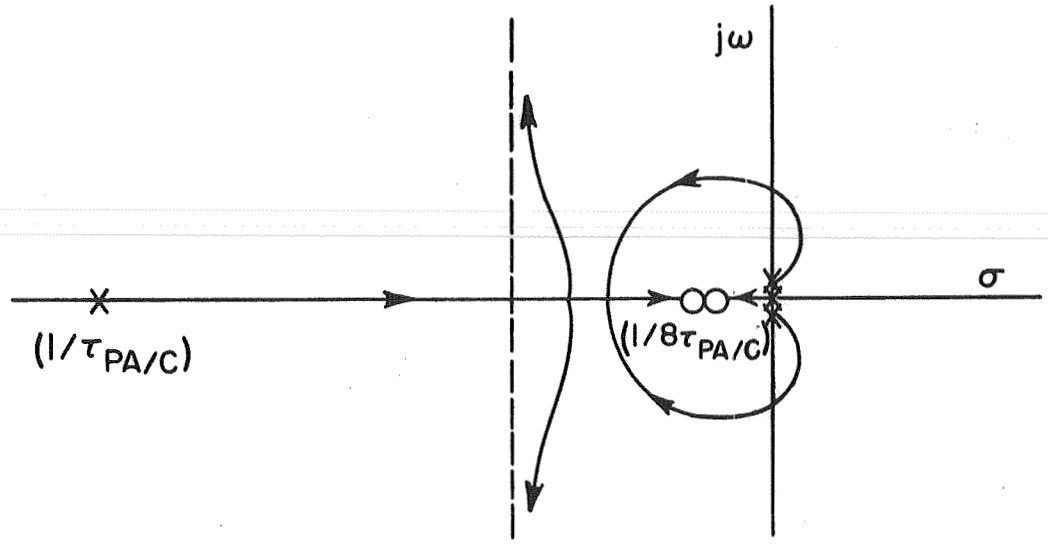

Figure 5.6. Effect of increasing compensation zero time constants ($\tau_z = 8\tau_{PA/C}$)

In this case, the closed-loop poles can be critically damped (non-oscillatory). However, the speed of response is decreased, since the closed loop poles are closer to the origin.

In practice, due to noise considerations, it is usually not practical to use a pure zero without introducing a smaller time-constant pole in association with it. Usually the associated pole is no more than twenty times as far from the origin as the zero. In the case of the system of Fig. 5.6, for example, two additional poles would be required at approximately two and one-half times the distance of the power amplifier and coil time constant from the origin. These additional poles would have only a minor effect on the dominant closed loop poles, and the response of the system.

Further improvements are possible by addition of a third compensation zero. Three zeros allow the closed loop poles to be moved farther from the origin, and hence speed up the transient response. An example of a three-zero locus plot is shown in Fig. 5.7.

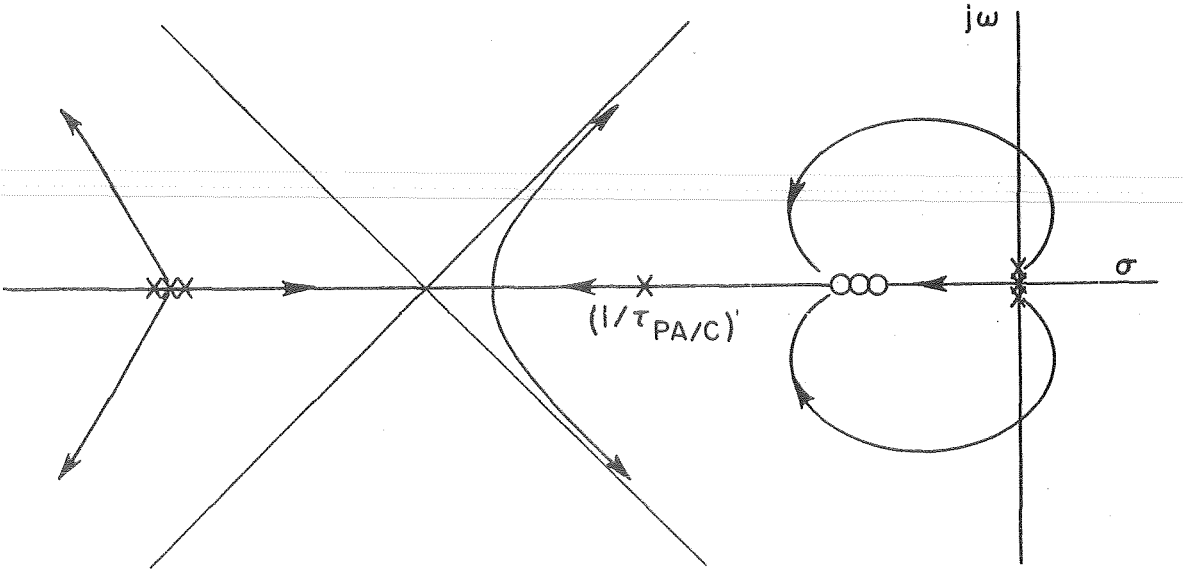

Figure 5.7. Root locus of three-zero and integral compensated translation component loop

5:2:2 PITCH AND YAW COMPONENT COMPENSATION

The pitch and yaw loop dynamics are approximately the same as the translational components. The main difference comes in the angular response of the model to coil current or moment inputs. The model behaves as if held by a torsional spring, and possesses natural frequencies in pitch and yaw corresponding to the magnetic and aerodynamic restoring moments and the moments of inertia of the model about the pitch and yaw axes. This has the effect of separating the model dynamics poles symmetrically from the origin, along the imaginary axis. A typical three-zero plus integrator root locus is shown in Fig. 5.8.

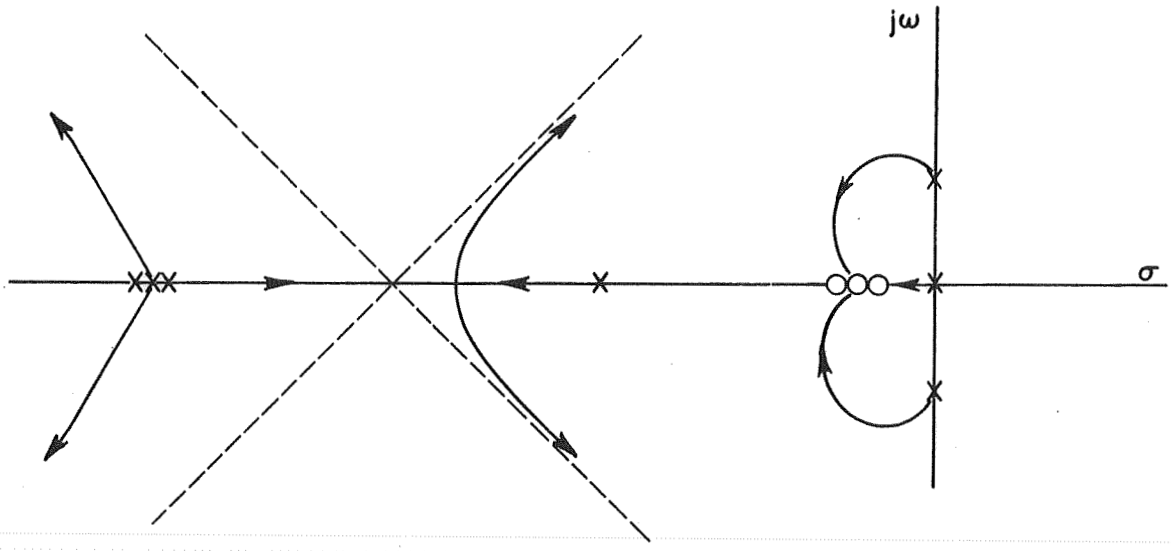

Figure 5.8. Root locus of three-zero and integral compensated angular component loop

5:3:1 IMPLEMENTATION OF COMPENSATION SYSTEM

The most effective means of implementing the compensation circuitry has been found to be by use of analog computer-type operational amplifier functional building blocks. These

building blocks may be arranged in parallel or cascade to produce the desired compensation functions. Three basic circuits have been found which satisfy most of the compensation needs. These are:

a) Input summing stage.

b) Integrator-lead-lag, with clamp.

c) Lead-lag.

Each building block is designed to enable each parameter to be varied over a suitable range either stepwise or continuously.

(a) Input Summing Stage (Fig. 5.9)

The position signal from the E.P.S. system is compared with an input signal from the position set controller (see 5.) and with a test signal which may be injected at a separate input, to form the "position error" signal.

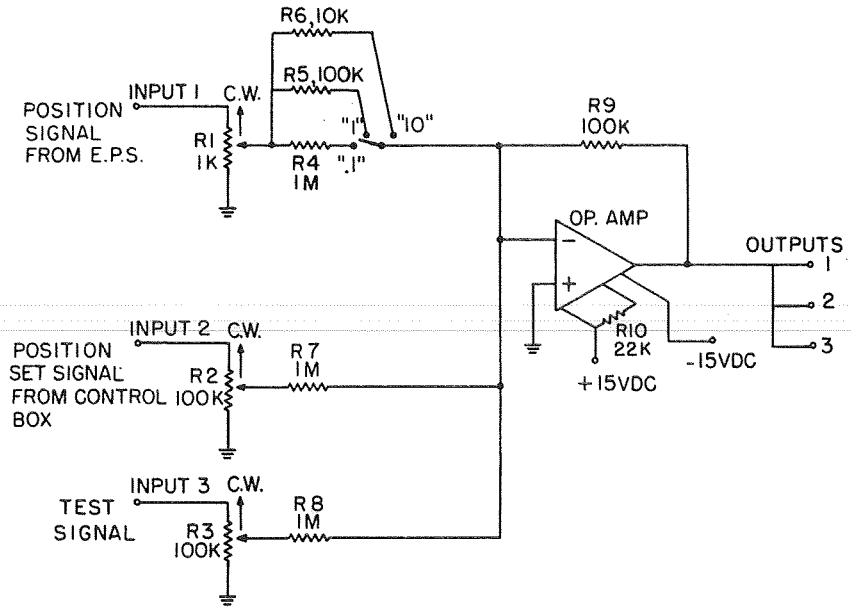

Notes: 1. R1 - 10 turn, with dial.
2. R2,R3 - single turn, log taper
3. R4→R10, 1%, ±25 ppm/°C T.C.

Figure 5.9. Compensation system input summing stage

(b) Integrator-Lead-Lag, with Clamp

A circuit combining an integrator, a lead, and a lag can be formed as shown in Fig. 5.10.

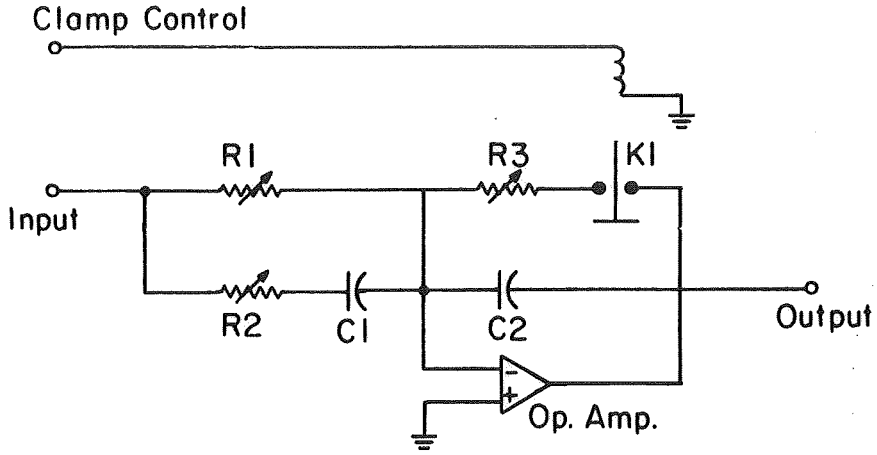

Notes:
1. C1,C2 = 1μf
2. R1,R3 = 1M - logarithmic
3. R2 = 10K, linear
4. K1 = SPST-NO reed relay, 6 v.d.c.

Figure 5.10. Integrator-lead-lag with clamp

The transfer function of this circuit is controlled by R1, R2, R3, and the clamp relay, K1, as follows:

$$\frac{V_{out}}{V_{in}} = \frac{(1+(R_1+R_2)C_1s)}{R_1C_2s(1+R_2C_1s)} \qquad (V-1)$$

$$\frac{V_{out}}{V_{in}} = \frac{R_3}{R_1}\,\frac{(1+(R_1+R_2)C_1s)}{(1+R_3C_2s)(1+R_2C_1s)} \qquad (V-2)$$

From 5.1, the transfer function contains an integrator pole (at the origin), a zero (or lead) at $\sigma = -1/(R_1 + R_2)C_1$, and a pole (or lag) at $\delta = -1/R_2C_1$. When the clamp is energized, the pole at the origin is replaced by a pole at $\sigma = -1/R_3R_2$.

(c) Lead-Lag Circuit

The circuit shown in Fig. 5.11 provides a zero and a pole (lead and lag). The locations of the zero and pole on the negative real axis can be controlled independently in steps, and the zero and pole can be moved together in fixed ratio with a separate continuous control.

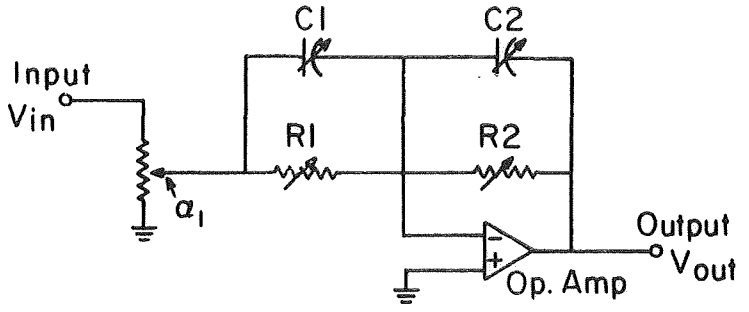

Notes: 1. C1,C2 varied independently in steps
2. $R1 = R2 = \alpha_2 R$ $(\alpha = 0 \rightarrow 1)$
3. $\alpha_1 = 0 \rightarrow 1$

Figure 5.11. Simplified schematic of lead-lag compensation circuit

The transfer function of this circuit is:

$$\frac{V_{out}}{V_{in}} = \alpha_1 \frac{R_2}{R_1} \frac{(1 + R_1C_1s)}{(1 + R_2C_2s)} = \alpha_1 \frac{(1 + \alpha_2 R\, C_1 s)}{(1 + \alpha_2 R\, C_2 s)} \qquad (V\text{-}3)$$

The circuit of Fig. 5.11 must be modified to be practical. Figure 5.12 shows additional components which are included to improve controllability and to suppress noise. The input attenuator, R1, provides variation of the d.c. gain of the stage from zero to unity. The 1.5k input resistor R2 provides improved matching with a preceding stage, and also provides a high frequency lag (pole) to aid in noise suppression. The two 100k resistors in series with the ganged 1M control potentiometers R3 and R4 provide more reliable operation at the low end of the control by limiting the turndown ratio. The capacitance is varied in steps, since continuous control is impractical for the required range of capacitance.

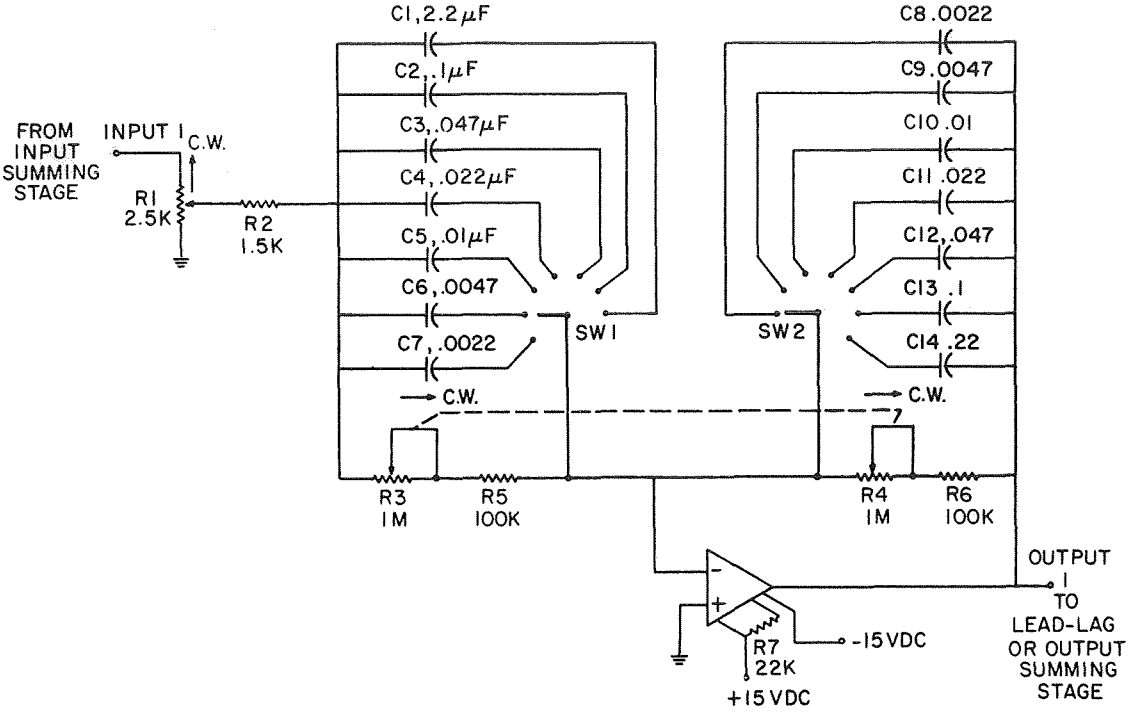

Notes: 1. R3,R4 single turn, dual ganged pots
2. Fixed resistors, ±5%, 1/4 w
3. OP amp - NEXUS SQ-10A

Figure 5.12. Prototype lead-lag compensation stage

5:4:1 CASCADED INTEGRATOR AND LEAD-LAG STAGES

The most straightforward arrangement of functional blocks might initially seem to be that shown in Fig. 5.13.

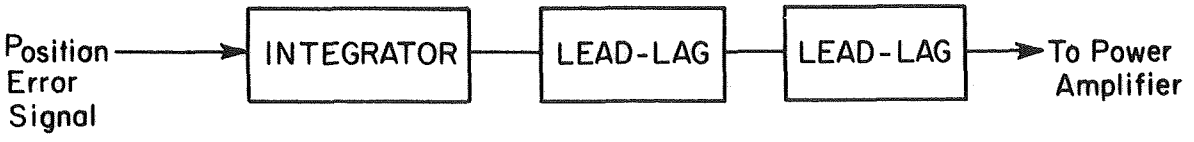

Figure 5.13. Simple compensation scheme

This arrangement provides three zeros and the integrator function plotted in Fig. 5.7 or 5.8. It is relatively free from drift effects due to the location of the integrator ahead of the lead-lag; however, a major disadvantage is apparent when saturation of the compensation stages is considered. The problem arises from the reduction in dynamic range of the lead-lag networks due to the d.c. signal, corresponding to the steady load on the model, which must be carried through the lead-lag stage from the integrator. It is essential that the compensation signals remain within the linear range of output voltage provided by the operational amplifiers. The carry-through d.c. reduces the range of excursion for the higher-frequency stabilization signals.

The d.c. carry-through problem can be avoided by placing the integrator stage after the lead-lag stages. This introduces a further problem: slowly drifting offset voltages may be introduced in the lead-lag stages, corresponding to spurious position-error signals. This effect can be obviated by means of a second integrator stage, having a relatively slow integration rate and small range, and placed in parallel with the lead-lag stages, as shown in Fig. 5.14.

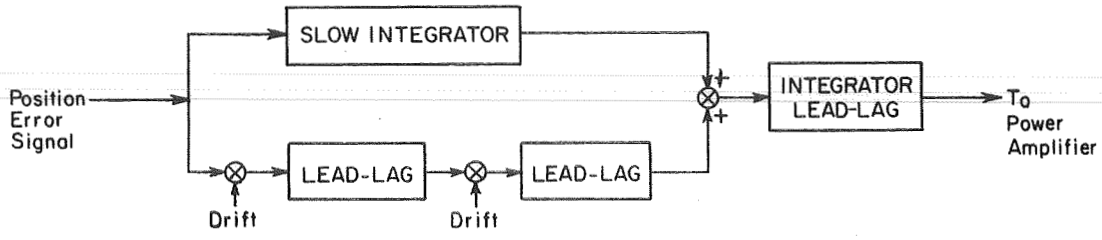

Figure 5.14. Integrator-output compensation with "slow" integrator for drift suppression

The drift rate is typically quite small, and hence the "slow" integrator can be adjusted so that is does not affect the overall dynamics, and can be ignored. A suitable integrator circuit is shown below in Fig. 5.15.

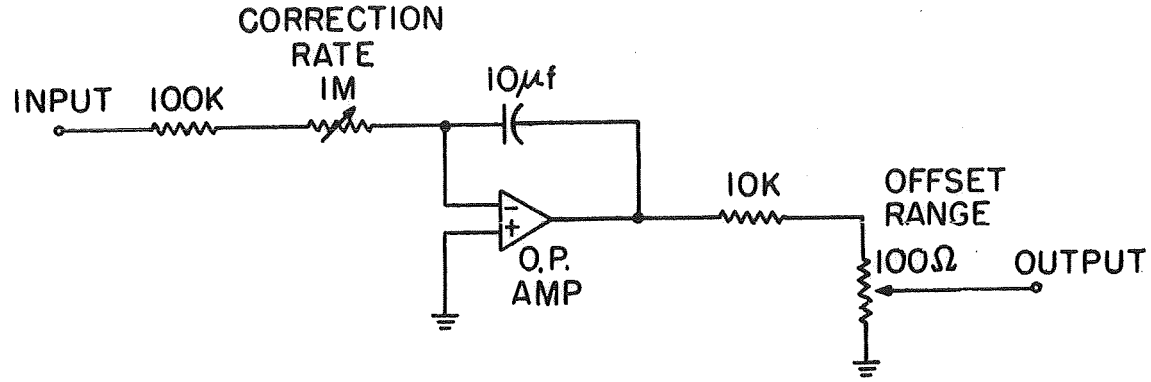

Figure 5.15. "Slow" integrator for drift suppression

5:4:2 PARALLEL INTEGRATOR AND LEAD-LAG STAGES

The d.c. carry-through problem can be avoided by placing the integrator in parallel with the lead-lag stages as shown in Fig. 5.16.

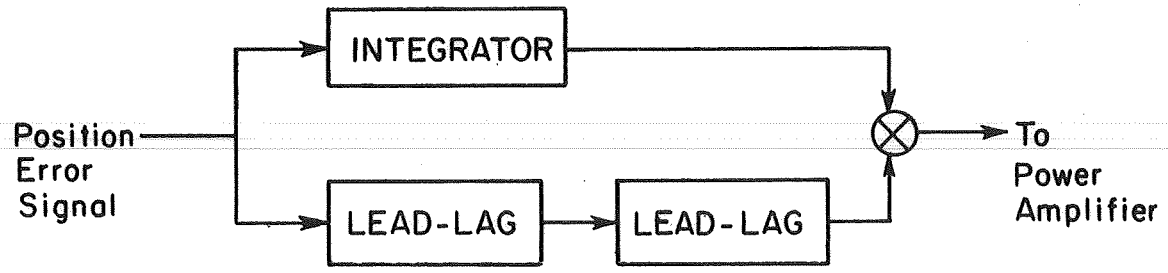

Figure 5.16. Parallel compensation

This configuration introduces considerable complexity into the setting of compensation parameters, however. The zeros of the overall compensation system transfer function are complicated functions of the poles and zeros of the individual building blocks. There is therefore no longer a straightforward correspondence between the adjustments and the open-loop pole-zero locations, and performance optimization is made difficult.

5:5:1 COMPENSATION SYSTEM HARDWARE

The compensation system may be built in any of a number of ways. Each channel can be completely hard-wired as a complete unit, or can be assembled from a group of standard modules which are hard or soft wired together. The former approach offers advantages of robustness, simplicity, and greater reliability. The latter approach offers the advantage of greater flexibility; the arrangement of functions can be changed more rapidly.

In the development of the compensation for the magnetic suspension system discussed here the modular approach was taken, to allow greater freedom of experimentation with the arrangement of functions. Each functional block was built on a small circuit board, and three boards were mounted on a "mother board" containing three operational amplifiers. The "mother boards" were mounted in chassis racks containing slides which provide side-by-side stacking. The "mother boards" were connected to a rear patch panel by roll-up cable harnesses, and could be withdrawn from the chassis rack to allow adjustment of compensation parameters, while the system was operating. Interconnection of functional blocks is made on the rear patch panel by means of coaxial patch cords. The development system is shown in Fig. 5.17.

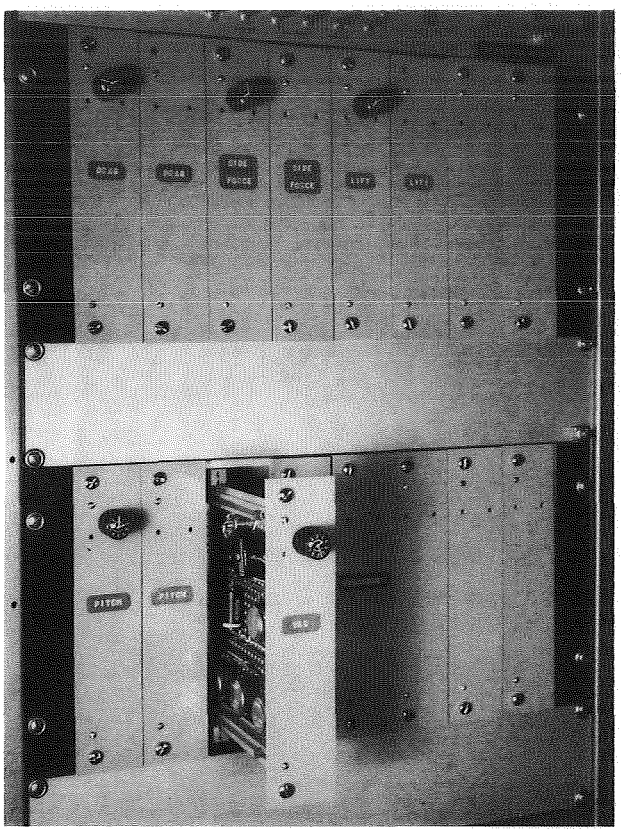

Figure 5.17. Compensation system hardware

The reliability of the system is considerably improved if all interconnectors are hard-wired. This requires that the layout of the building blocks be changed, to eliminate the drawout feature. The parameter adjustments would then all be available on the front of the control panel. It is possible to arrange all the necessary functions for each compensation channel in the space of a single standard 19" x 3 1/2" rack panel, without crowding the parameter controls.

5:6:1 POWER AMPLIFIER AND COIL WITH CURRENT FEEDBACK

The main coil power amplifiers are assumed to be approximately linear, saturating voltage amplifiers, with d.c. voltage transfer characteristics similar to those shown in Fig. 5.18.

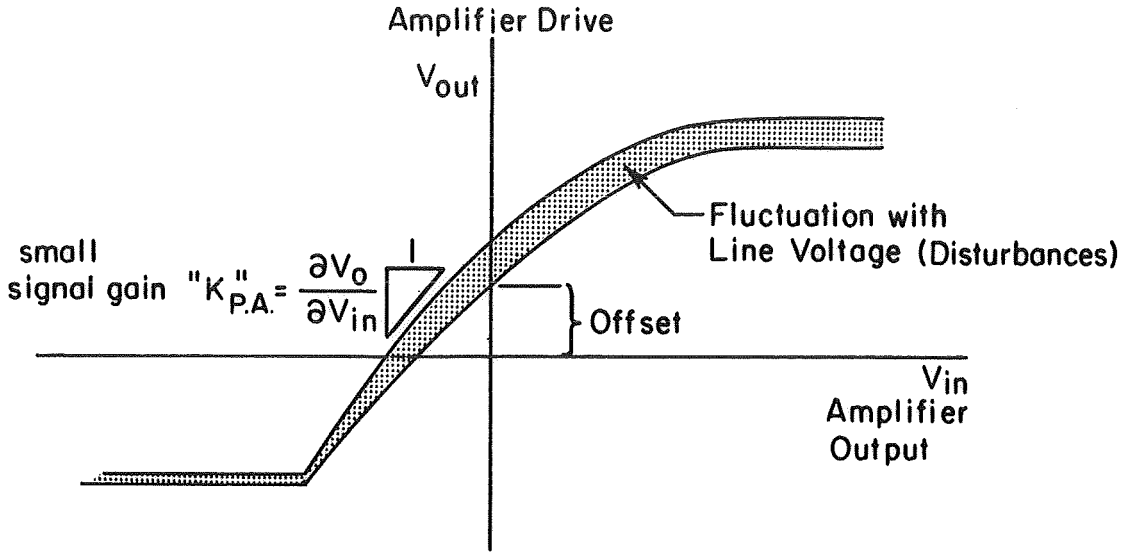

Figure 5.18. Assumed d.c. voltage transfer characteristics of coil power amplifier

The load consists of the coil resistance R_c and inductance L_c in series. The current/voltage time-constant of the coil is the ratio L_c/R_c, and for the translational components this ratio is approximately one-half second. Since linear control of the coil current is what is actually desired, (change in current proportional to control signal), the necessity of a current feedback scheme is indicated. Current feedback serves several purposes:

a) Linearizes response

b) Reduces output sensitivity to line-voltage fluctuations

c) "Speed-up" current response

The current feedback function is shown in Fig. 5.19.

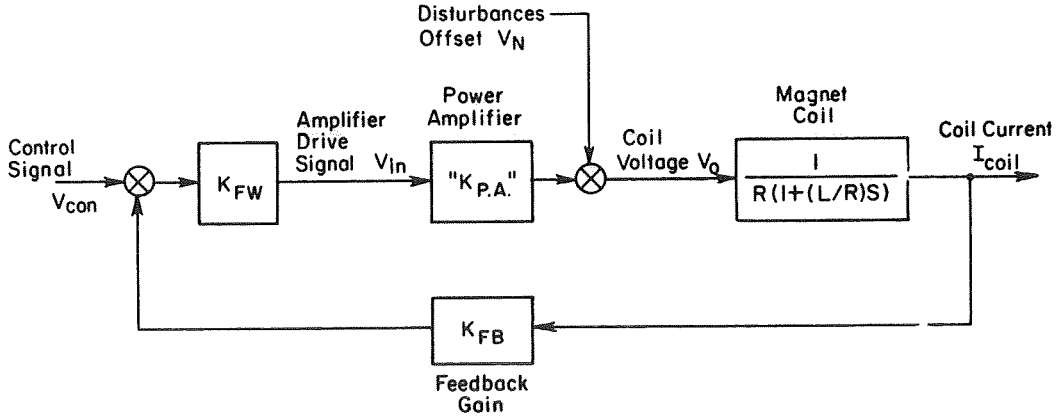

Figure 5.19. Power amplifier and coil with current feedback

The small-signal current/voltage function for the system of Fig. 5.19 is:

$$\frac{I_{coil}}{V_{con}} = \left[\frac{1}{K_{fb} + \frac{R}{K_f K_{pa}}}\right]\left[\frac{1}{1 + \frac{1}{\left(1 + \frac{K_{fw} K_{fb} K_{pa}}{R}\right)} \frac{L}{R} s}\right] \qquad \text{(V-4)}$$

If $K_{FW}K_{FB}K_{PA}/R >> 1$, the lag time constant is considerably reduced, the overall gain is relatively independent of K_{PA}, and the output current is relatively insensitive to disturbance or offset voltages, V_N.

5:7:1 RESOLVER NETWORK FOR DRIVING NESTED SADDLE COIL POWER AMPLIFIERS

In the prototype magnetic suspension system, pitch and yaw control is provided by two nested pairs of saddle coils transverse to the tunnel axis, (see Fig. 2.4) and at 45° to the horizontal and vertical (pitch and yaw axes). The compensated pitch signal must therefore be split into two parts; one part driving the inner saddle coil power amplifier, and the other part driving the outer saddle coil power amplifier. The yaw signal must likewise be split into two parts. An appropriate resolver or crossover system is shown in Fig. 5.20.

5:8:1 POSITION SET CONTROLLER

The position of the model is controlled by the operator by means of a control box which regulates the command input signals to the compensation input summing stage. The control box circuit is shown in Fig. 5.21.

Precision, multi-turn potentiometers are powered by two mercury batteries. The bipolar variable wiper voltages provide

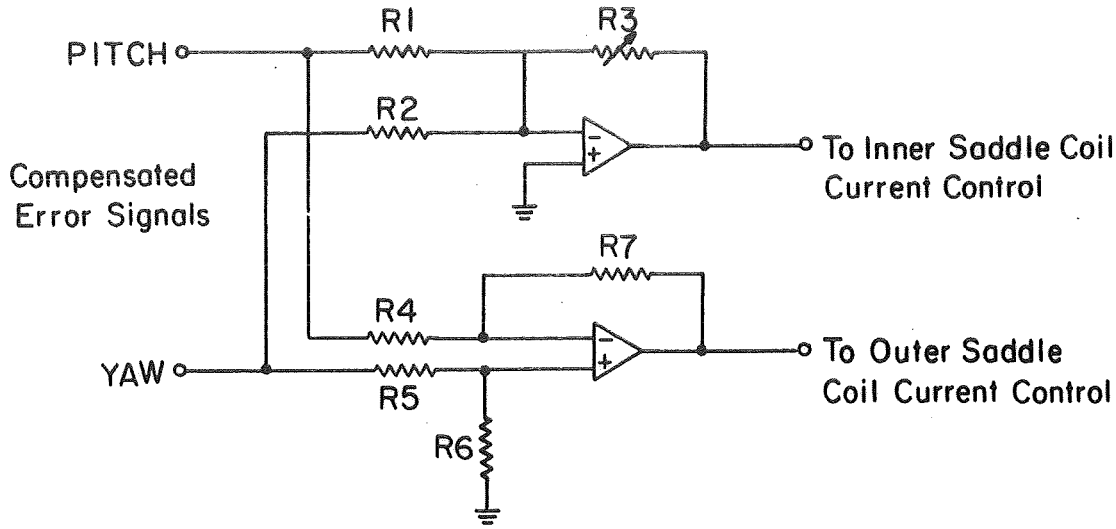

Notes: 1. R1,R2,R4,R5,R6,R7 = 27K
2. R3 = 50K (max)

Figure 5.20. Resolver network for driving nested saddle coil power amplifiers

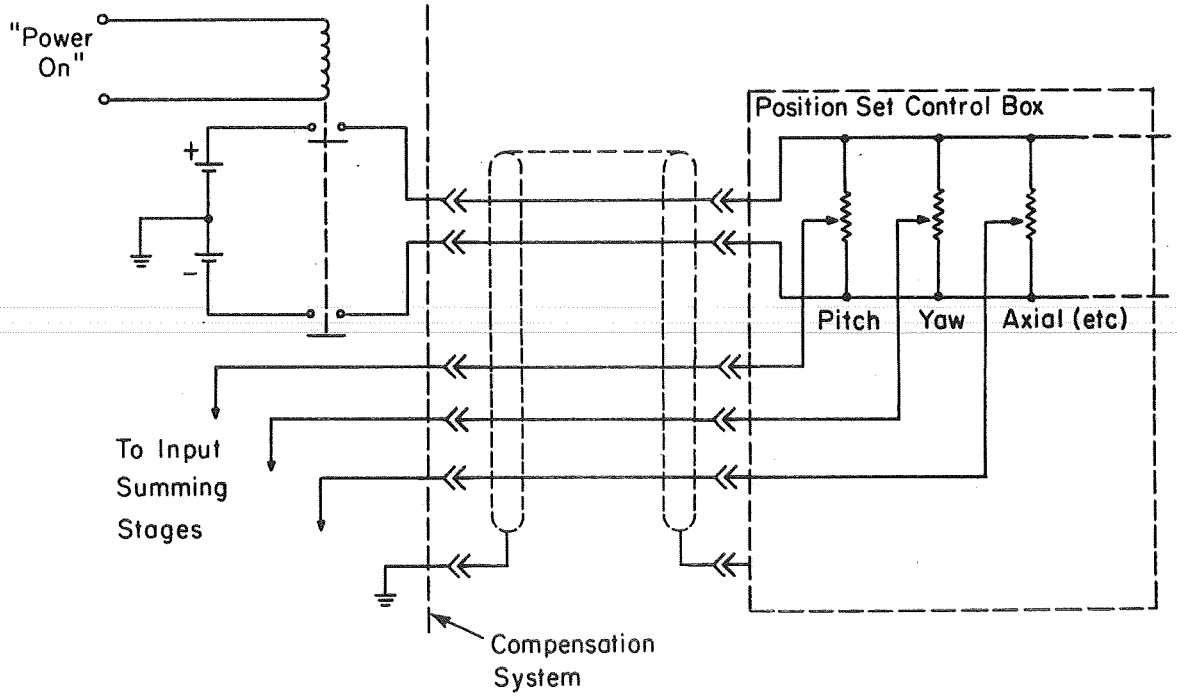

Notes: 1. Batteries - 5.4 volt, mercury
2. Control pots - 10K, 10-turn with dials

Figure 5.21. Schematic of position set control box

the position set signals to the compensation system input summing stages.

The control box can be operated at a distance from the main control panel and is connected to the panel by a cable as shown. The control box is ruggedly built, and the control potentiometers are recessed as shown in Fig. 5.22.

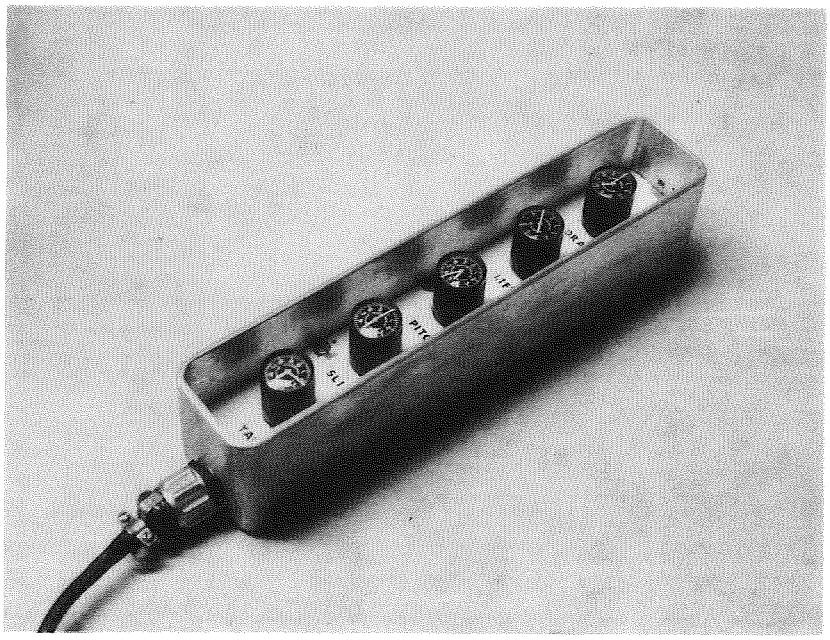

Figure 5.22. Position set control box

Page intentionally left blank

CHAPTER VI

MAIN POWER AMPLIFIERS

6:1 INTRODUCTION

A significant part of the cost of any magnetic suspension system is invested in the electrical power supply and amplifier subsystems required for control of the magnet coil currents. The complexity and size of these subsystems is governed by the performance that is required of the suspension system, in terms of magnetic loads, frequency response, and electrical noise levels. This chapter outlines the basic requirements and the various design approaches which are available. The particular approach that was used in the prototype system is described also.

6:2 BASIC REQUIREMENTS

Several electrical conversion subsystems provide the d.c. and a.c. electrical power required for control of the magnetic field variables. These are as follows:

a) Axial Magnetizing Bias d.c. Power Supply
   - Single polarity, regulated, adjustable direct current, low output ripple.

b) Drag, Side, Lift Force, Pitch, Yaw Power Amplifiers
   - Reversing voltage and current d.c.-coupled amplifiers, capable of four-quadrant volt-ampere operation.
   - Output noise filter networks.

c) Roll-Control Power Amplifiers
   - A.C.-coupled power amplifiers, 60 Hz to 400 Hz output.
   - Coupling networks to match, yaw and roll power amplifiers to saddle coils.

6:3 SPECIFIC REQUIREMENTS

Specification of the performance of the power supplies and amplifier will generally be based upon the desired performance of the suspension system and limits imposed by saturation of the magnet cores. In addition, the variation of the specifications with size can be related to the performance. In the following sections specifications are outlined for a family of four suspension systems similar to the prototype, and ranging in size from 7.5 inches to 5 feet in inside diameter.

6:3:1 AXIAL MAGNETIZING BIAS D.C. POWER SUPPLY

The "magnetizing" coils, which provide the uniform axial field component, are supplied with filtered and regulated direct current. The range of control must be quite large; the maximum current is dictated by the saturation limit of the magnet cores, and the minimum current corresponds to the incipient saturation of the most slender model (minimum axial demagnetizing factor). For the prototype suspension system, this upper saturation limit (See section 3:3:1) corresponds to an axial field strength of B_x = 4.6 kilogauss, at a current of 230 amps, into the 2-ohm resistance of these windings. This level is appropriate for magnetization of a body such as a sphere (demagnetizing factor = 1/3). For extremely slender models, the magnetizing current must be reduced by a large factor. For example, with a model slenderness ratio (ℓ/d) of 20, the axial demagnetizing factor, D_a, is approximately 0.006, and the allowable axial field and coil current is reduced to 90 gauss and 4.5 amps respectively.

Figure 6.1 illustrates the range of magnetizing power required as a function of the model geometry.

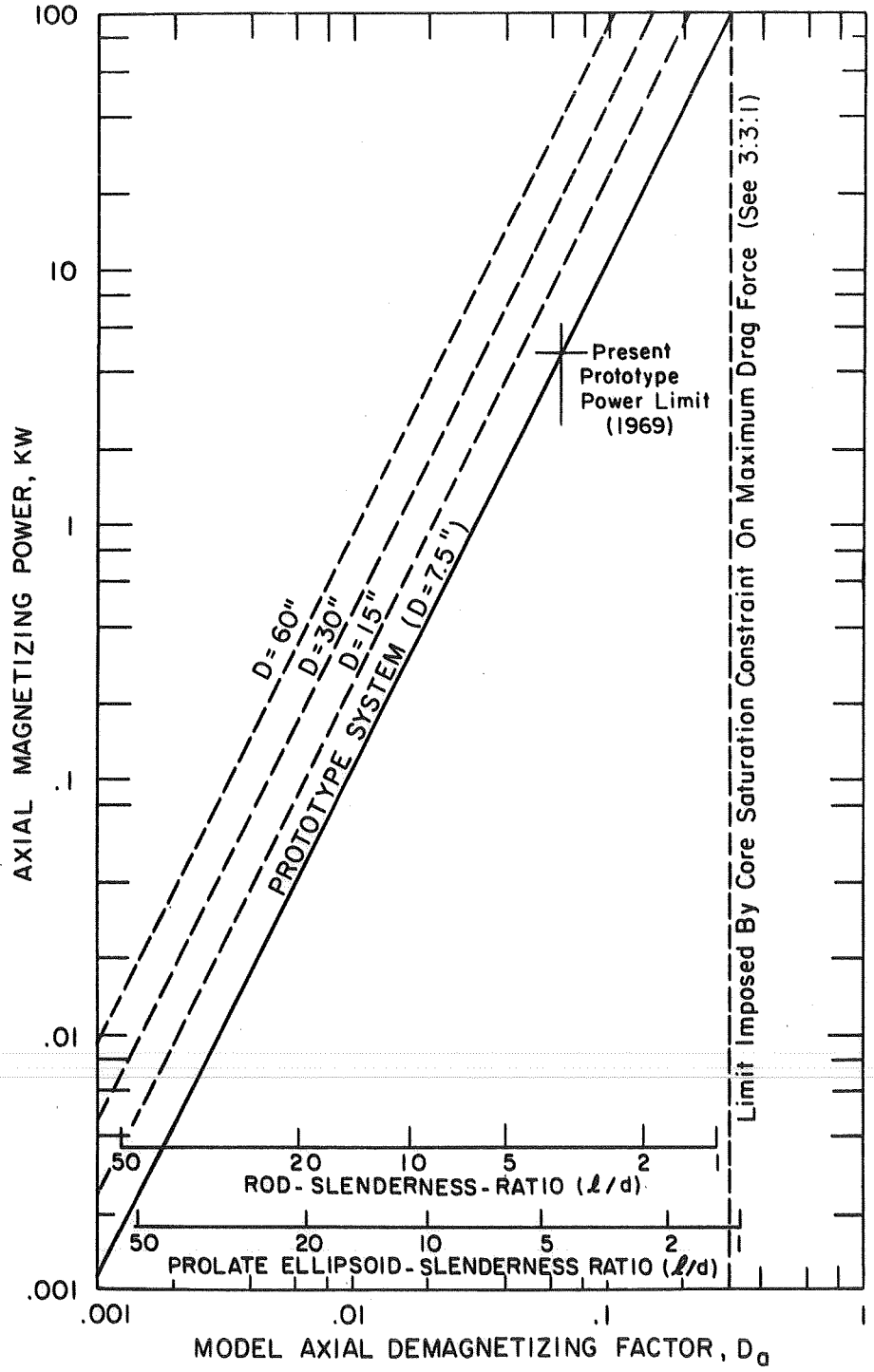

Figure 6.1. Magnetizing power requirements as a function of model geometry and system size

The power required to produce a given magnetizing field level is proportional to the size of the magnet system, all other factors being equal. Figure 6.1 indicates the power requirements of larger-scale magnet systems, similar to the prototype. The nominal size "D" (Eq. D = 7.5", for the prototype) refers to the clear inside diameter of the position sensor transducer coil (which is the limiting size). For a D = 5 ft system, the maximum magnetizing power is 800 kw.

The present power limit of 5 kw for the prototype is shown in Fig. 6.1. This range was found to be satisfactory except for the least slender models ($\ell/d \simeq 3$). This corresponds to a quite modest power level, even for the largest scale shown (i.e. 40 kw @ D = 60").

Continuous control of the magnetizing current from zero to the maximum level is clearly desirable. Automatic regulation of the current is also desirable in order to simplify the data reduction process. (The axial magnetization field (or current is an important parameter in all data reduction equations). In addition, ripple and high-frequency noise must be attenuated to minimize interference with the position sensing system.

6:3:2 DRAG, LIFT, AND SIDE FORCE POWER AMPLIFIERS

a) Static Power Requirements (Resistive Power)

The saturation-limited ratios of forces to model weight were related to the static power required for the coil windings in Section 3:3:1 (b,c). In each case, the static power is proportional to the square of the force/core weight, and to the cube of the size of the suspension system. The static power curves for the prototype (D = 7.5") and three larger sizes (D = 15", 30", 60") are shown in Figures 6.2 and 6.3.

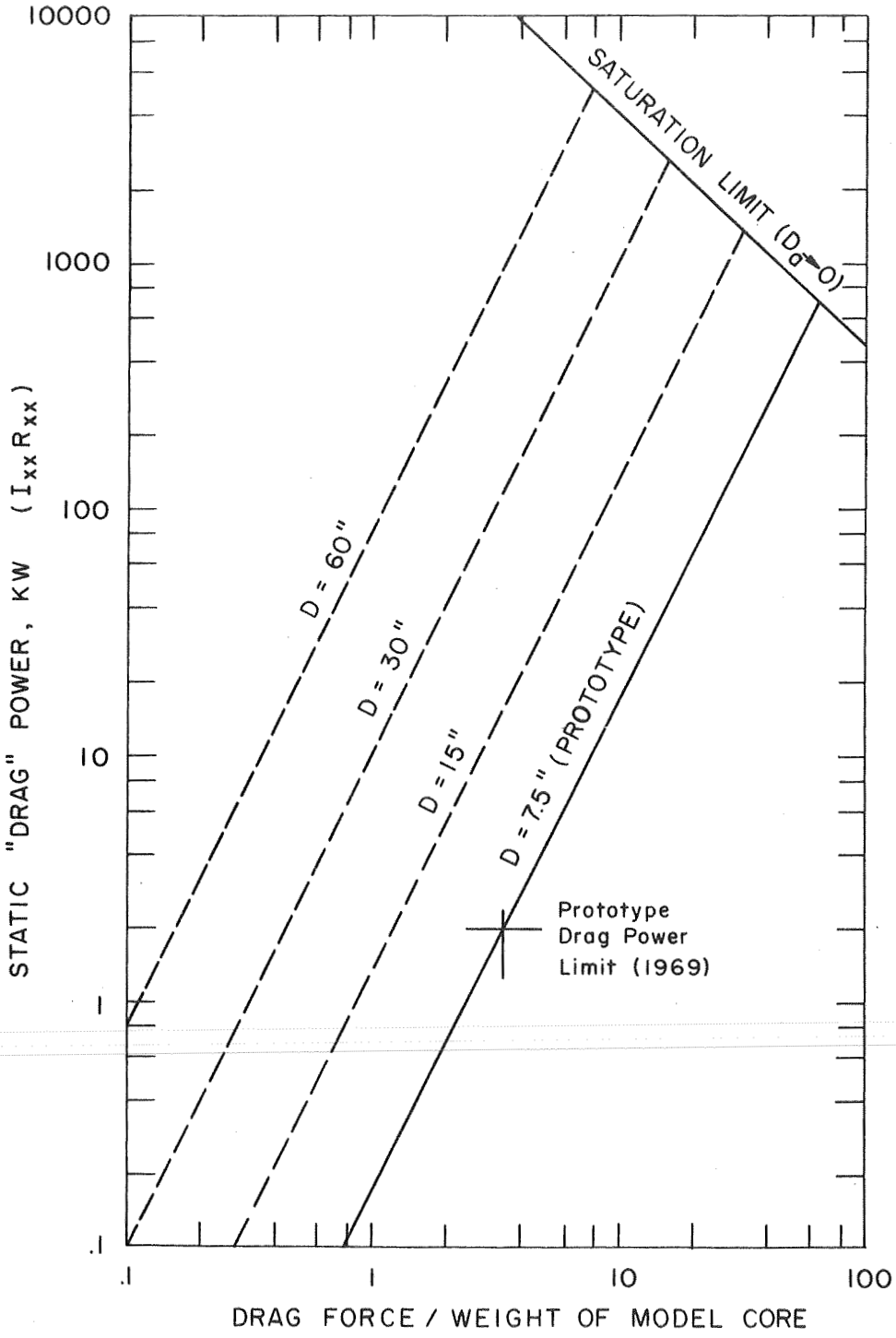

Figure 6.2. Static power requirements of drag force power amplifier

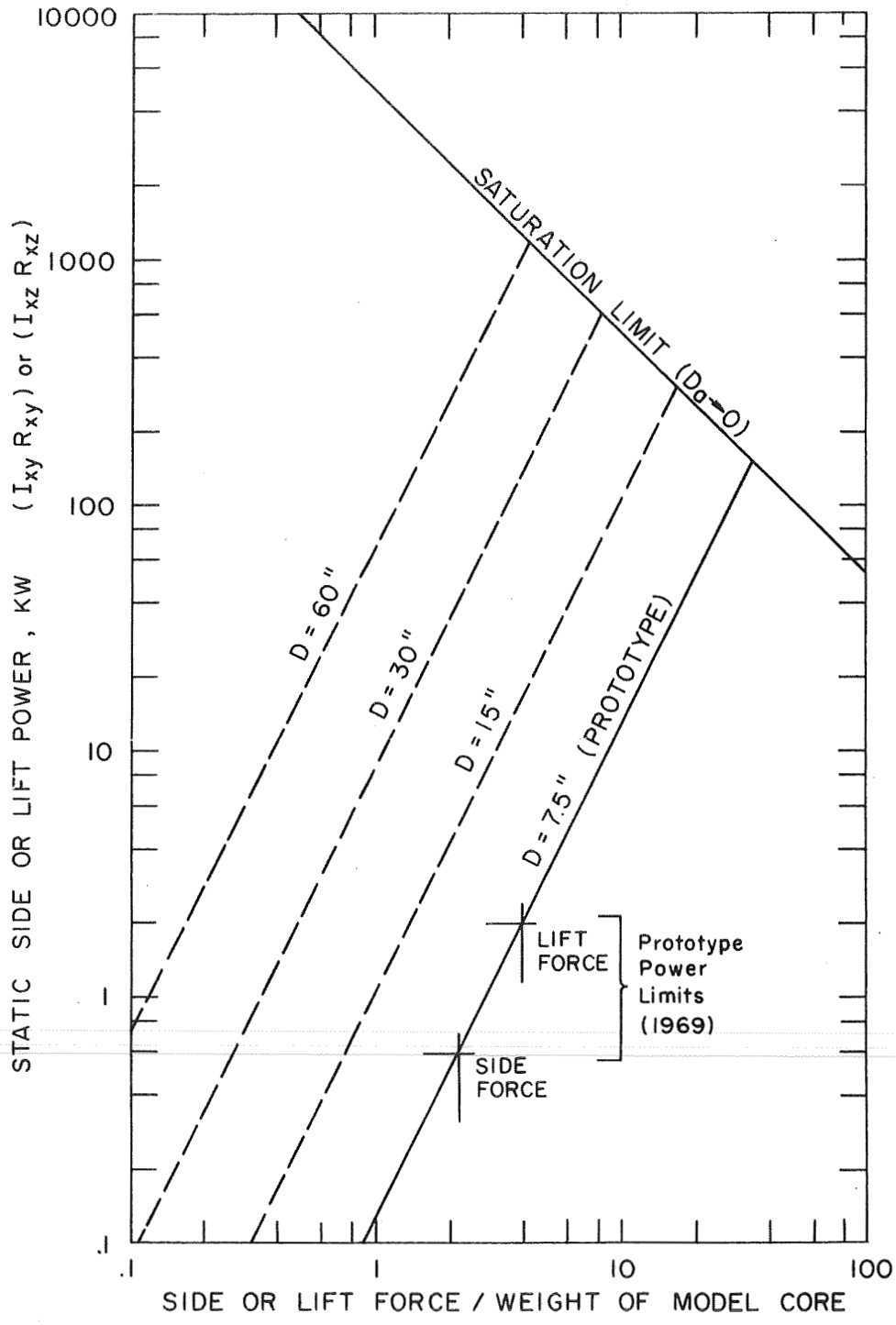

Figure 6.3. Static power requirements of lift or side force power amplifiers

b) Reactive Power Requirements

The magnet coil windings are inductive and hence require additional voltages proportional to the rate of change of the coil current. That is, voltage in excess of that required to overcome the ohmic losses is required to provide ability to vary the current at a sufficiently high rate to stabilize the model when subjected to disturbances (aerodynamic loads) or dynamic testing conditions (forced oscillations). Specification of this overvoltage capability is dependent upon the anticipated aerodynamic disturbances and spectrum of dynamic test conditions. as a general rule it is desirable, for a given maximum continuous rated coil current, to specify a maximum voltage <u>at least</u> twice the maximum resistive voltage drop. This ensures that the current slewing rate at maximum current is no less than one half the zero-current rate. Another way to approach the problem of specification of the overvoltage capability is to consider the characteristic time-constants of the system. The current-voltage time constant of each magnet system increases as the square of the size. It appears reasonable to assume that characteristic frequencies should decrease with size (pitch and yaw magnetic natural frequencies, for example, behave this way). As a result the maximum frequency at which the current limits can be reached should be inversely proportional to the size. This in turn implies that the ratio of the overvoltage to the voltage corresponding to maximum steady current should be proportional to the size of the system. Note that the saturation-limited ($D_a \rightarrow 0$) peak static power varies only as the first power of the size. (See Figs. 6.2, 6.7). Therefore, the peak reactive plus resistive power corresponding to these saturation limits would vary as the square of the size.

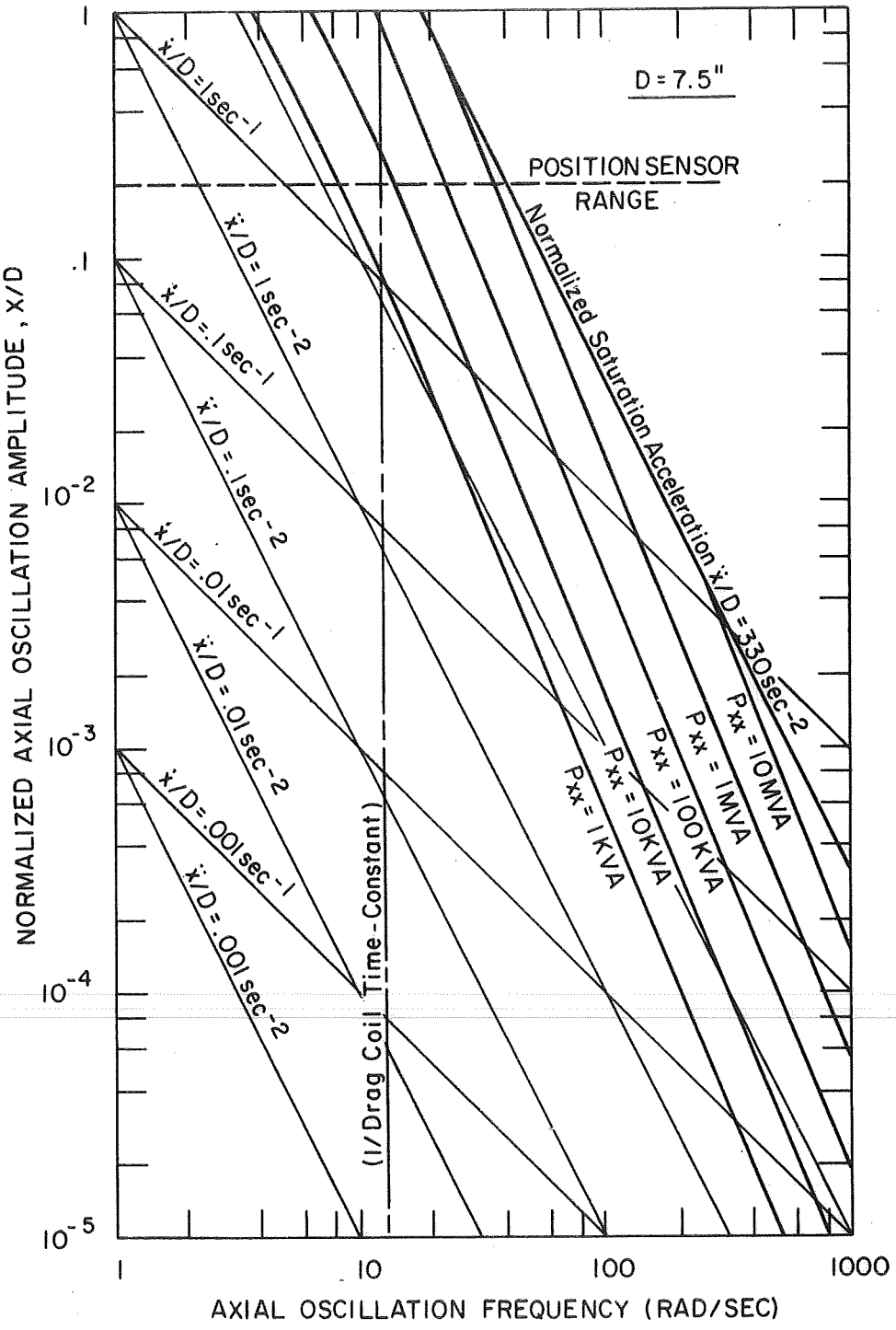

Figure 6.4. Reactive power requirements for drag power amplifier, D = 7.5"

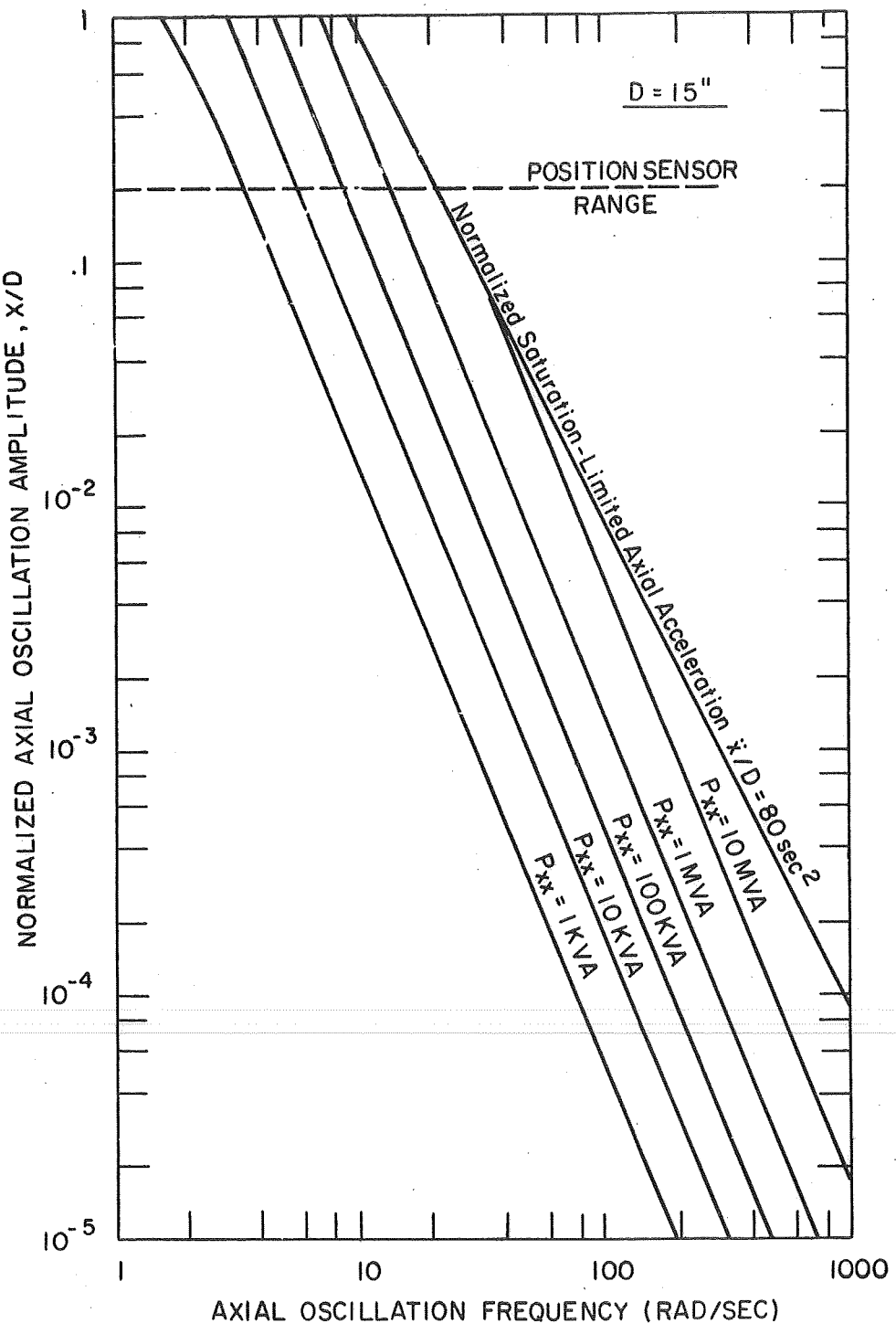

Figure 6.5. Reactive power requirements for drag power amplifier, D = 15"

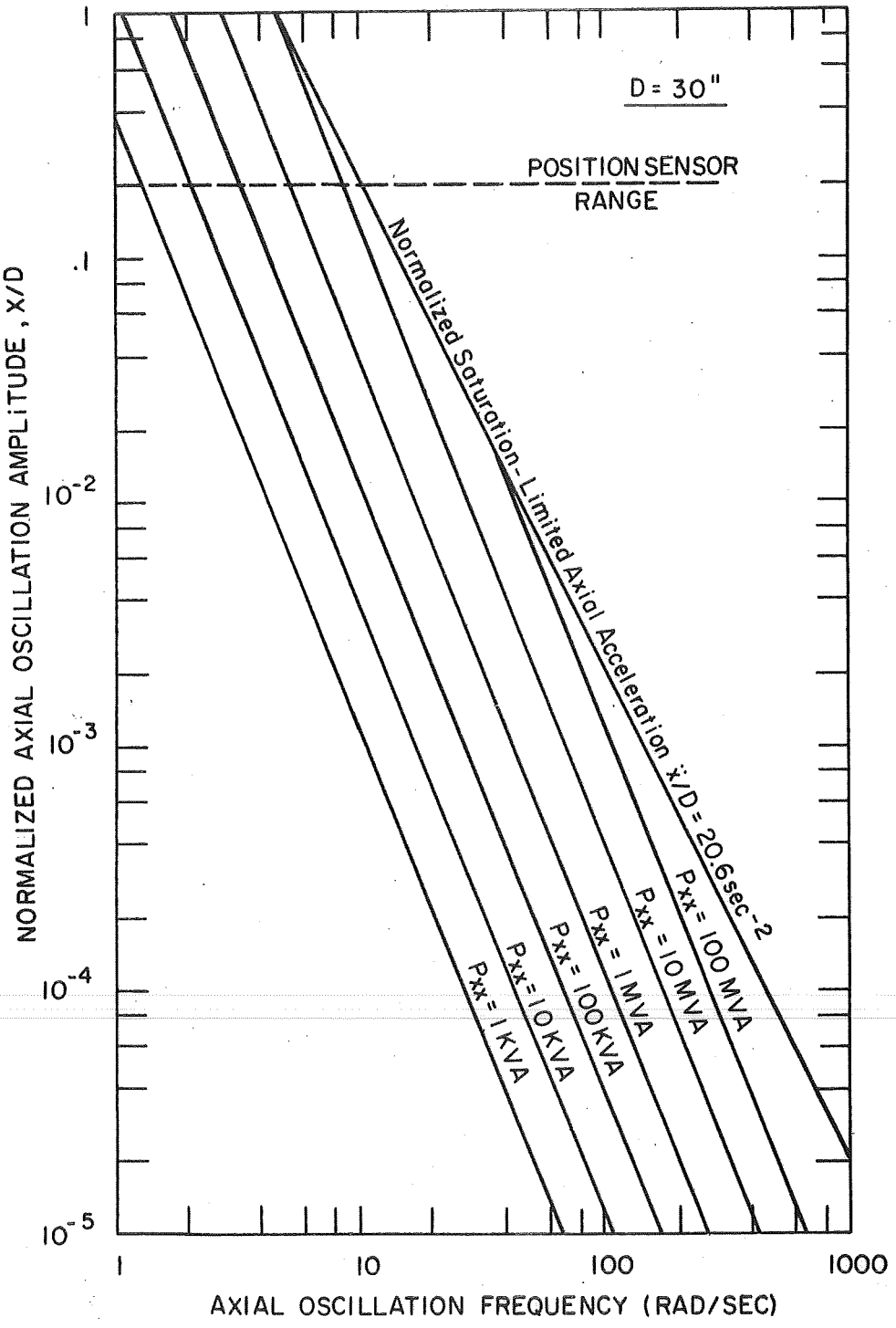

Figure 6.6. Reactive power requirements for drag power amplifier, D = 30"

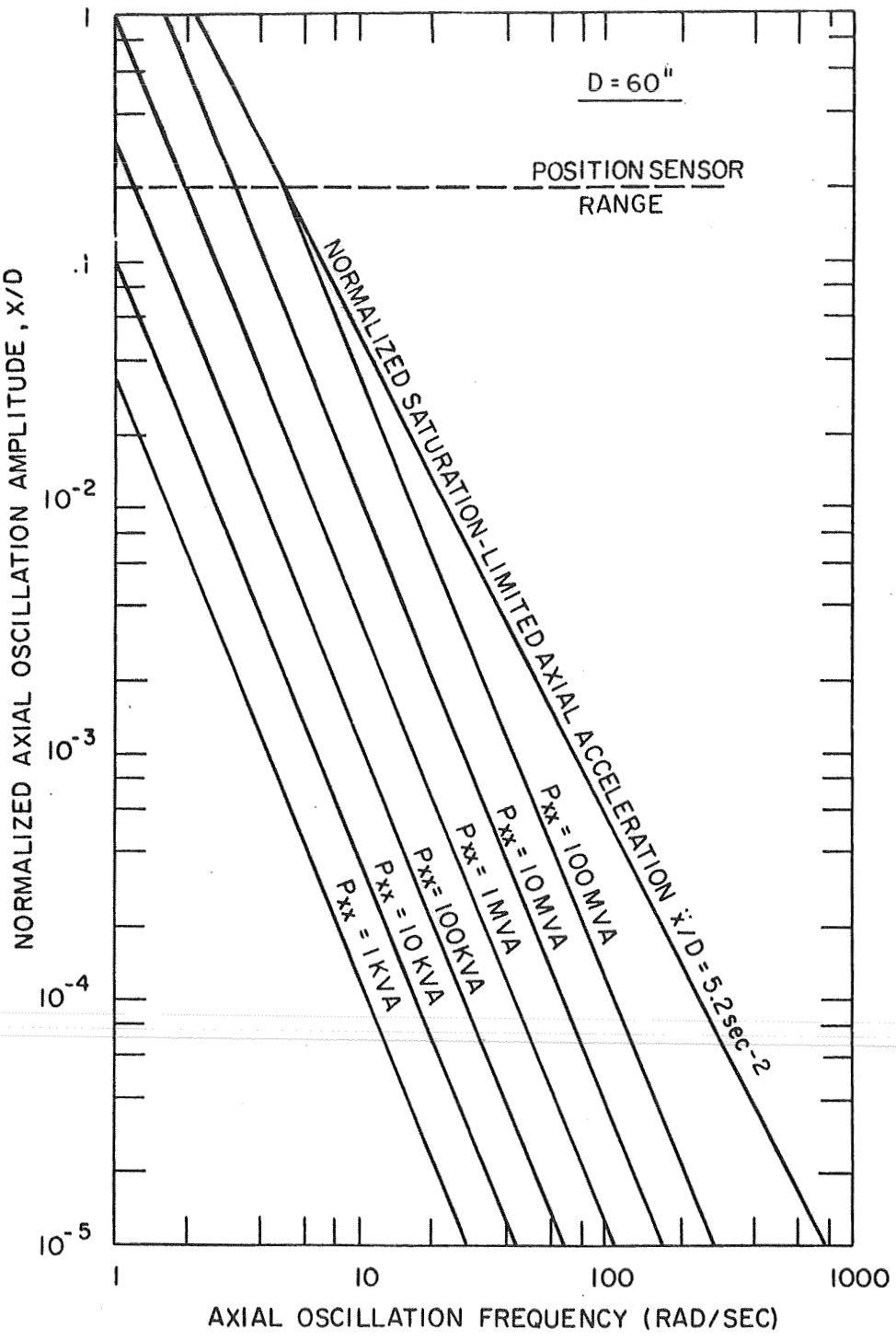

Figure 6.7. Reactive power requirements for drag power amplifier, D = 60"

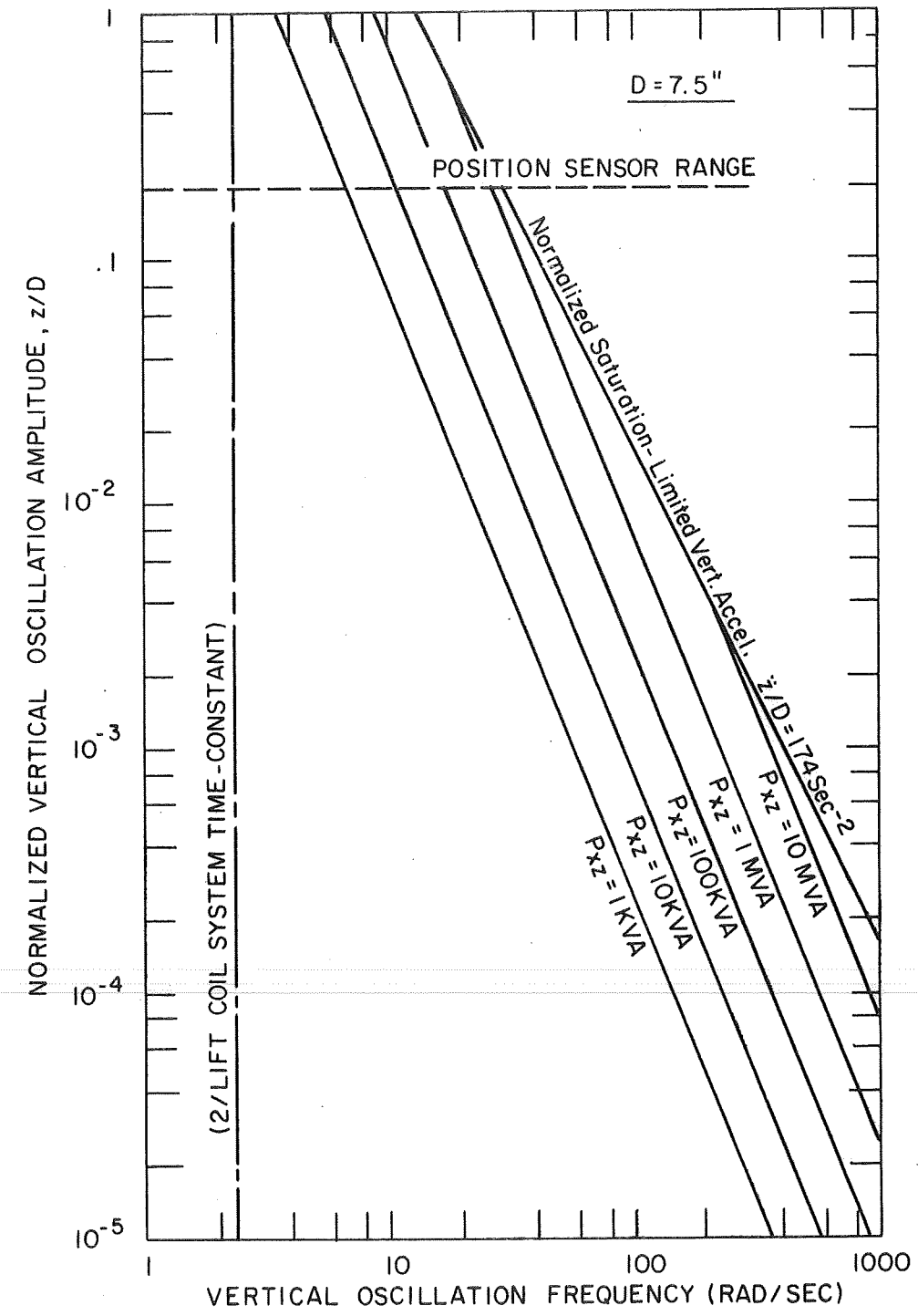

Figure 6.8. Reactive power requirements for lift or side force power amplifier, D = 7.5"

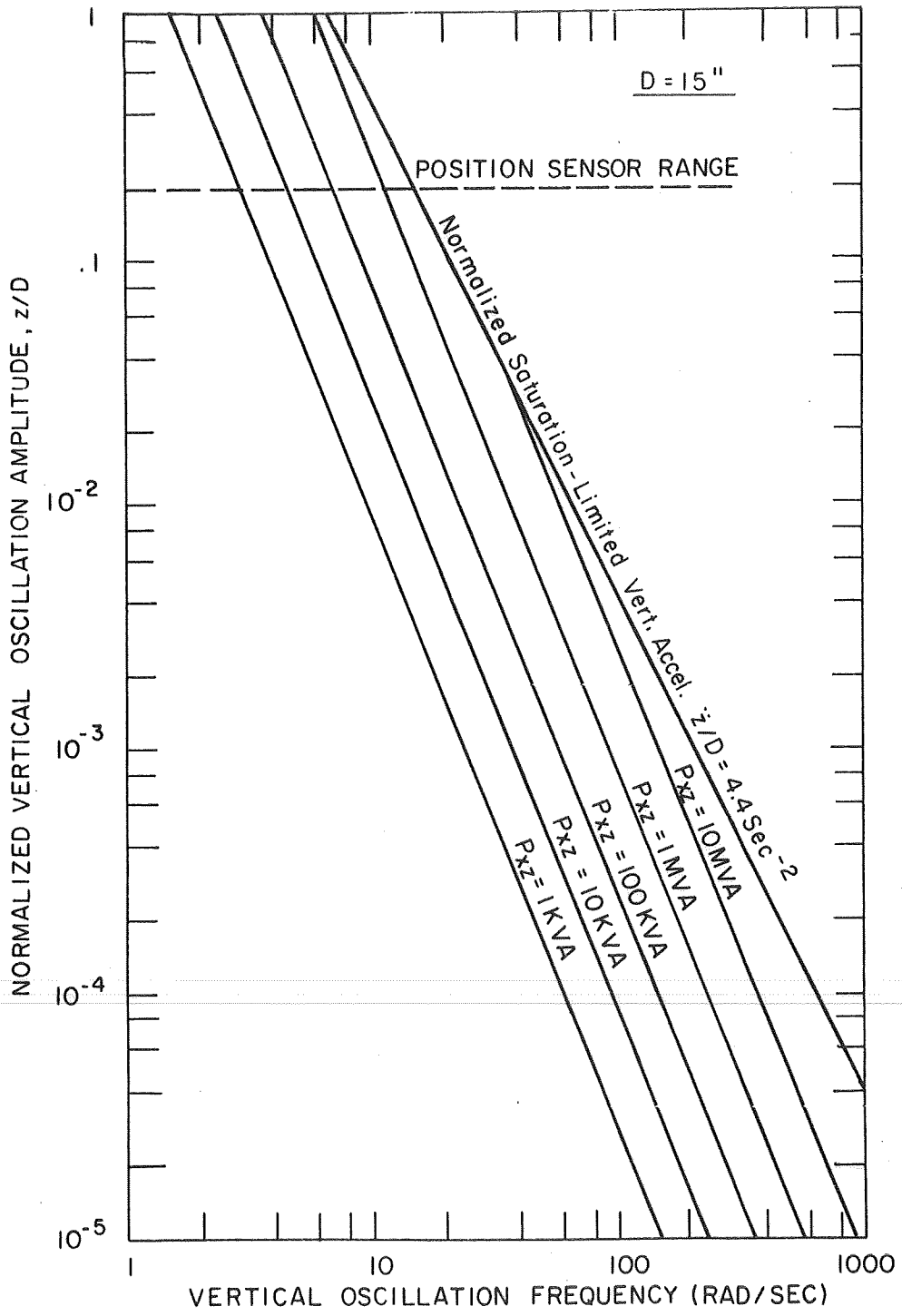

Figure 6.9. Reactive power requirements for lift or side force power amplifier, D = 15"

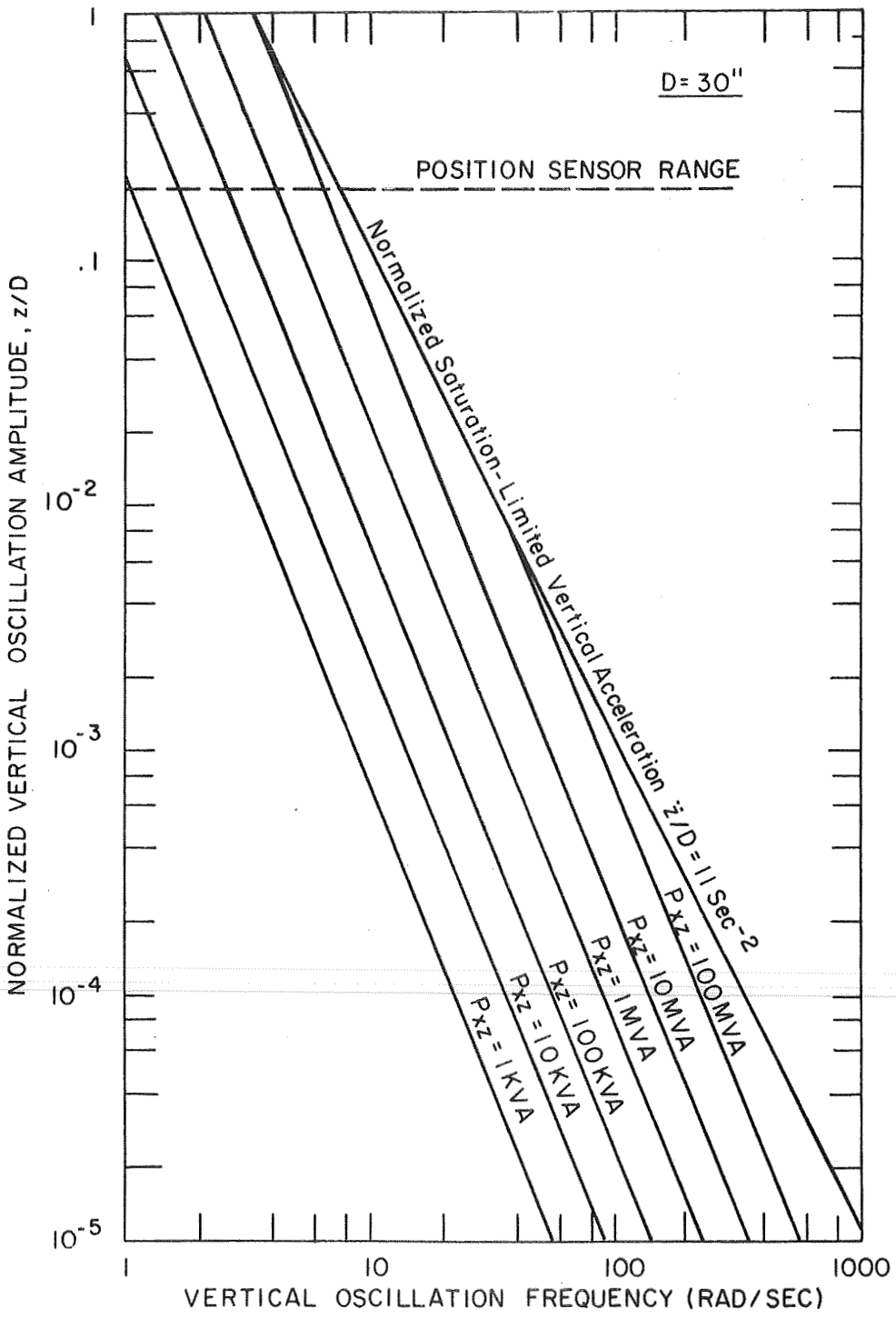

Figure 6.10. Reactive power requirements for lift or side force power amplifier, D = 30"

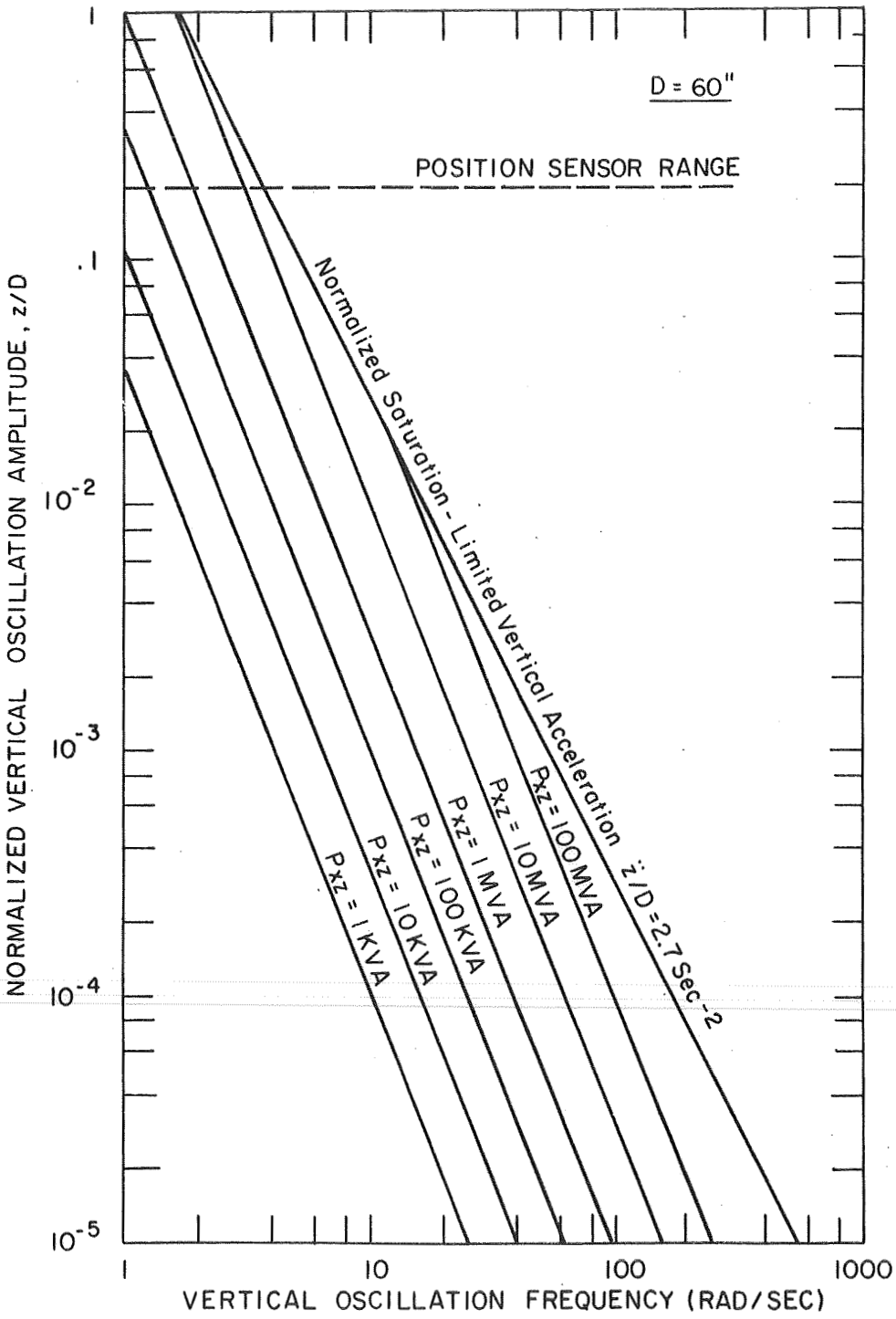

Figure 6.11. Reactive power requirements for lift or side force power amplifier, D = 60"

The power required to obtain given oscillation amplitudes is shown in Figs. 6.3 - 6.6 and 6.8 - 6.11 as a function of frequency and system size.

6:3:3 PITCH AND YAW POWER AMPLIFIERS

a) Nested-Saddle Coils (Prototype Design)

Using arguments similar to those outlined in 3:3:1, it can be shown that for the prototype system, core-saturated-limited optimum levels of transverse field B_y and B_z exist. These limits are approximately the same for the inner and outer saddle coils, and are approximately 2.3 kilogauss. For the inner saddle coils, this corresponds to a static power of 90 kw, and for the outer saddle coils, 190 kw.

The static power required for given levels, $B_{y'}$ and $B_{z'}$ (and hence the saturation-limited power) varies directly with the system size.

If it is assumed that the bandwidth of the pitch and yaw system is inversely proportional to the system size, then the peak power (ohmic plus reactive) will vary as the square of the system size. The characteristic pitch and yaw frequencies due to magnetic restoring moments in the prototype system are in the range of 30 sec^{-1} to 150 sec^{-1}. The time-constants of the inner and outer saddle coils are both approximately 0.04 sec^{-1}. The voltage requirements are shown in Fig. 6.12 as a function of frequency, system size, and angular displacement amplitude. Above the resonant frequency, the voltage required for a given displacement amplitude increases as the cube of the frequency; below resonance, as the first power of frequency. The voltage/displacement is normalized with respect to the low frequency response. Fig. 6.13 shows the relative power requirements as a function of system size.

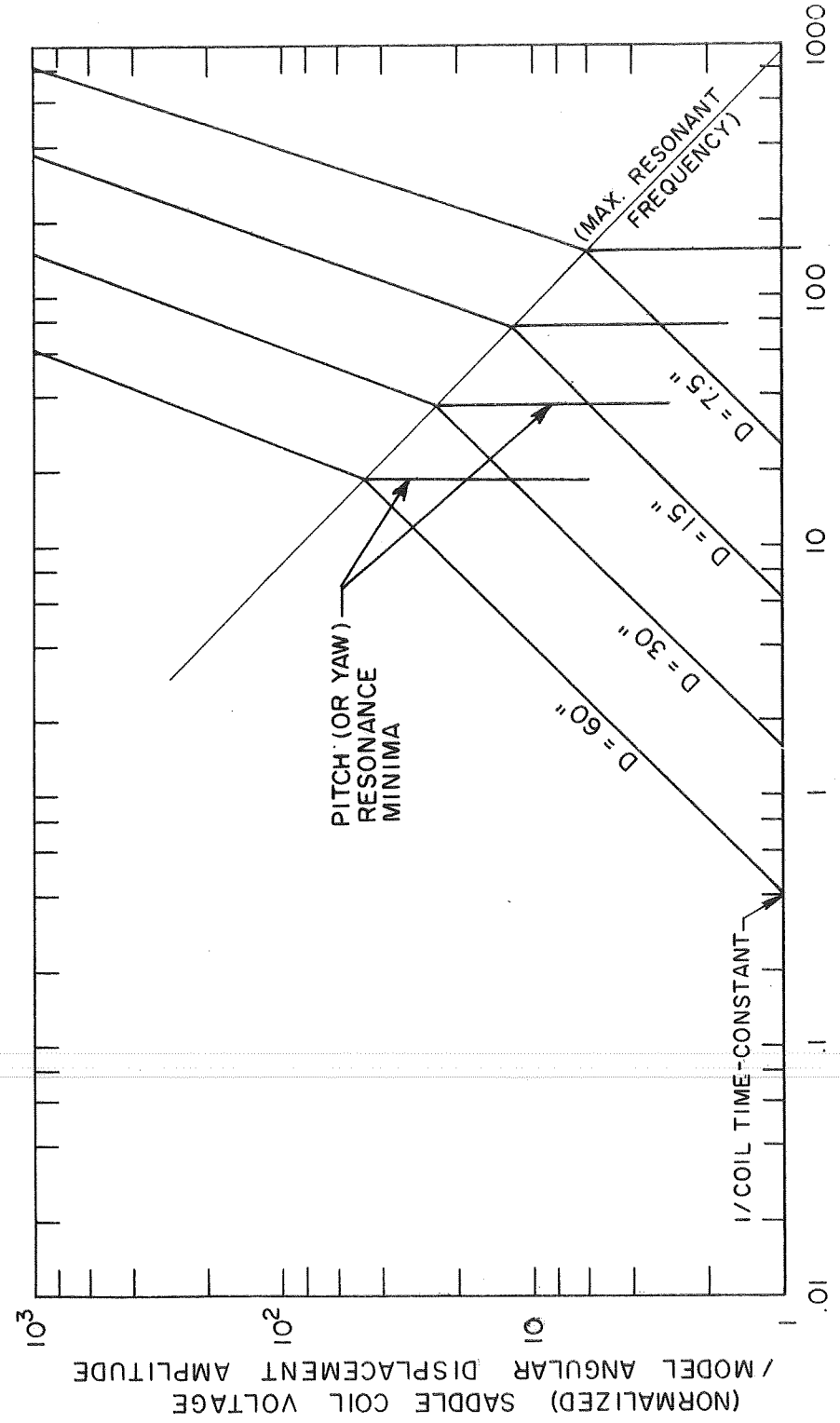

Figure 6.12. Over voltage requirements of pitch and yaw power amplifiers

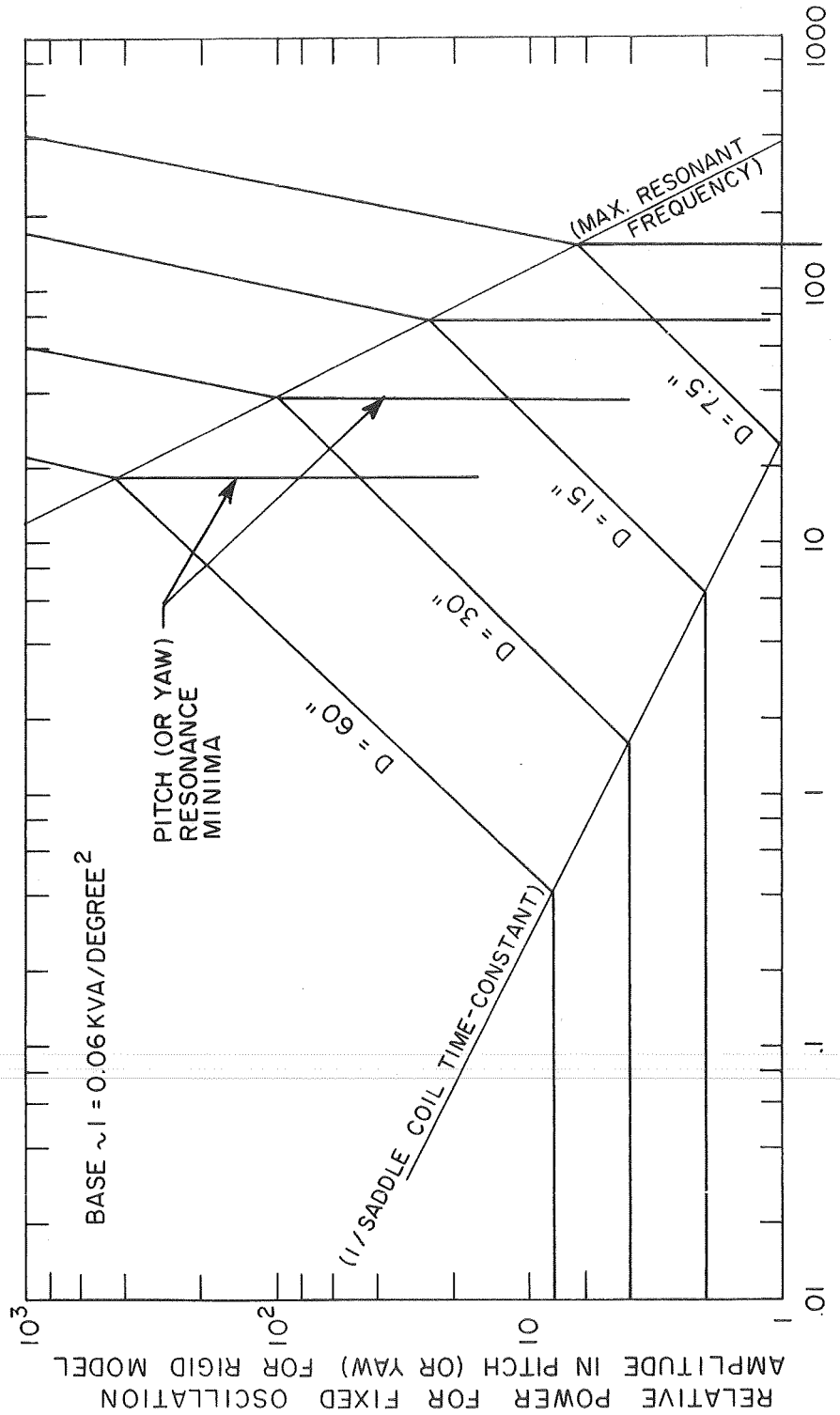

Figure 6.13. Relative power for fixed oscillation amplitude in pitch (or yaw)

6:3:4 PROTOTYPE POWER AMPLIFIERS (DRAG, LIFT, SIDE FORCE, PITCH, YAW)

The prototype power amplifiers consist of 60 Hz, 3-phase full-wave thyratron controlled unipolar output amplifiers d.c. biased through resistor networks with opposite polarity. The general arrangement is shown in Fig. 6.14.

With this arrangement, reasonable response can be expected up to 30 Hz; above this, the response breaks up into side loads of 60 Hz, and overall system response is relatively poor. This presents problems at the highest pitch and yaw natural frequencies in the prototype, and in fact imposes the most important limit on the response and stability of the system.

Since the pitch and yaw natural frequencies decrease with increasing system size, and since it appears appropriate to accordingly reduce system bandwidth, the 30 Hz limit inherent in this basic power amplifier design is satisfactory for systems larger than the prototype. This presents important advantages, since reversing, 3-phase, full-wave SCR controlled amplifiers are readily available as off-the=shelf systems and have all the corresponding cost and reliability advantages. Furthermore, the market for such systems (primarily variable speed mill motor drives) is quite large and competitive.

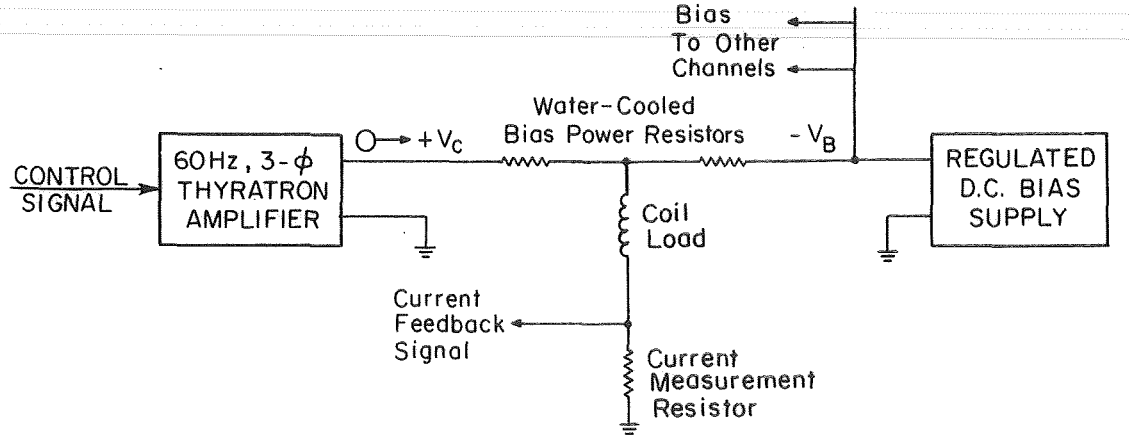

Figure 6.14. Schematic of prototype power amplifiers

6:3:5 OUTPUT NOISE ATTENUATION

It is necessary to minimize high frequency noise at the output of the power amplifiers in order to prevent interference with the position sensing system. If the power amplifier is of the phase-controlled SCR or thyratron type, then relatively high noise levels are encountered. The most straightforward method of attenuating this noise is by passive filtering of the output. Two filter configurations are shown in Fig. 6.15.

In configuration 6.15(a), the shunt capacitance C1 is made to tune the load inductance at approximately 150 Hz, and the series inductance L1 is made no larger than 0.1 times the load inductance. At the position sensor carrier frequency (20 kHz, for prototype), the attenuation contributed by the filter is therefore approximately 60 db, and insertion loss is approximately 1 db, at low frequency. The series filter inductor L1 must be designed to carry the maximum rated current and must have negligible parallel capacitive reactance at the position sensor carrier frequency.

The band-reject filter scheme of 6.15(b) offers better performance; the attenuation is proportional to the product of the quality-factor "Q" (= $\omega L/R$) of each of the two filter inductors, and the ratio of the series inductance to the shunt inductance. The series filter inductance must carry the full load current, and since it is tuned, it must be air-cored (inductance independent of current). The shunt inductor carries no d.c. and very little a.c., and can thus be relatively easily designed with a high Q. If $L_2/L_3 \cong 10$, $Q_2 \cong 30$, $Q_3 \cong 300$ (at 20 kHz) and stray coupling effects are negligible, the attenuation is thus approximately 96 db, or almost a factor of 100 better than the low-pass filter design described above.

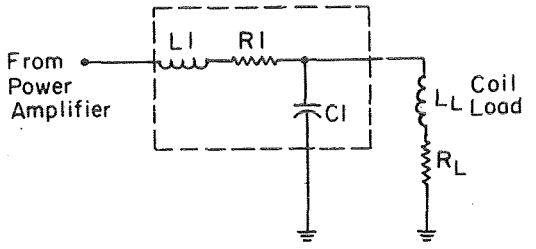

Figure 6.15(a). Low-pass single-stage output filter

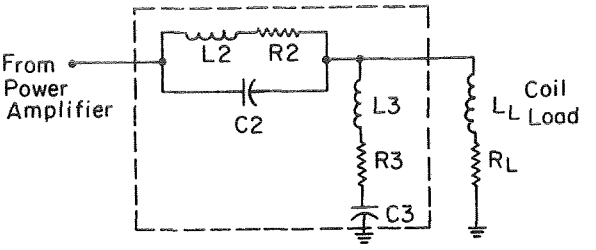

Figure 6.15(b). Band-reject single-stage output filter

6:3:6 ROLL-CONTROL POWER AMPLIFIERS AND COUPLING NETWORKS

The power amplifiers required for roll control consist essentially of a pair of amplitude-modulated fixed center-frequency power supplies. For a given model configuration and size relative to the suspension system, the minimum required center frequency varies inversely with the square of the size. For the prototype system (D = 7.5"), a roll-control center frequency of 400 Hz appears to be acceptable. For systems twice the size of the prototype or larger, the line frequency (60 Hz) would be acceptable and has the advantage that it is readily available and easily controlled.

The roll-control amplifiers must be coupled to the saddle coils in such a way as to ensure the maximum power transfer to the coils and a minimum loss through the pitch and yaw power amplifiers. The prototype arrangement is shown in Figure 6.16.

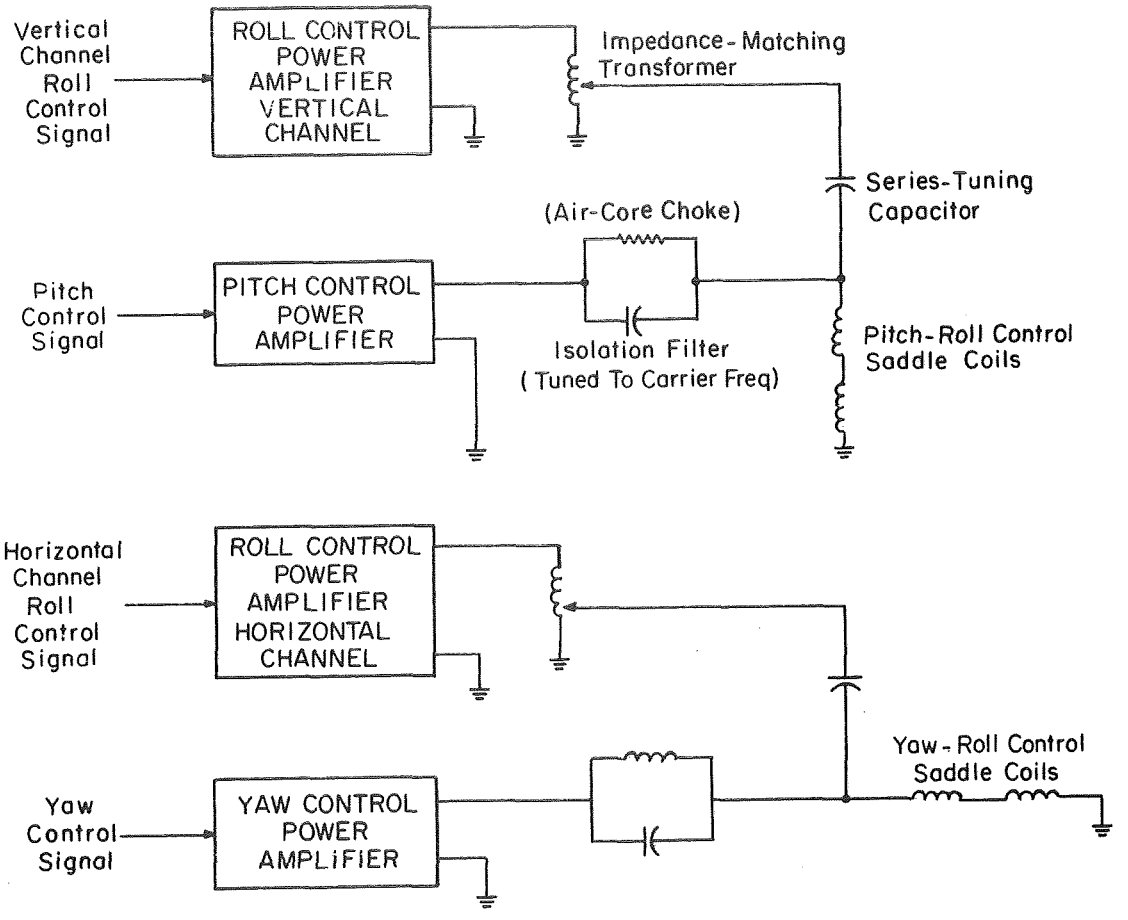

Figure 6.16. Pitch-yaw-roll power amplifier coupling scheme using separate roll power amplifiers

Parallel-tuned trap filters present high impedance to the roll control power and prevent significant losses through the pitch and yaw control amplifiers. The saddle coils are series-tuned with the roll-control amplifiers, and optimum coupling is obtained by adjustment of the impedance-matching output auto-transformers.

6:3:7 ROLL-CONTROL POWER REQUIREMENTS

Performance of the a.c. roll system is not well defined at this point, and is dependent to a large degree upon the

model geometry. Therefore, only general limit specifications can be given. The maximum steady rolling moment for a particular model, system size and carrier frequency is proportional to the roll power supplied to the saddle coils. The maximum power is related to the saturation limits. This power limit corresponds to roll control fields of the order of 2500 gauss and roll power levels at the saddle coils of 120 kva for the prototype. From the limited experience with the prototype, usable rolling moments have been obtained with 1 kva; however, a more suitable level would appear to be at least 10 kva.

The saturation-limited power increases in proportion to the system size, and the maximum rolling moment for a given model configuration varies as the cube of the size.

Page intentionally left blank

CHAPTER VII

COOLING SYSTEM

7:1 HOLLOW-CONDUCTOR COOLING

Heat dissipated in the magnet coils due to ohmic losses must be removed. In the prototype system, square o.d., circular i.d. copper hollow conductor was used and cooled by forced convection of water through the conductor. The magnet coils are designed to provide multiple parallel hydraulic paths, in order to reduce the impedance to coolant flow.

The eight side and lift force coils and the two Helmholtz coils were wound in layers, with all coolant inlets at one end of each coil and all outlets at the other end. The general method is shown schematically in Fig. 7.1.

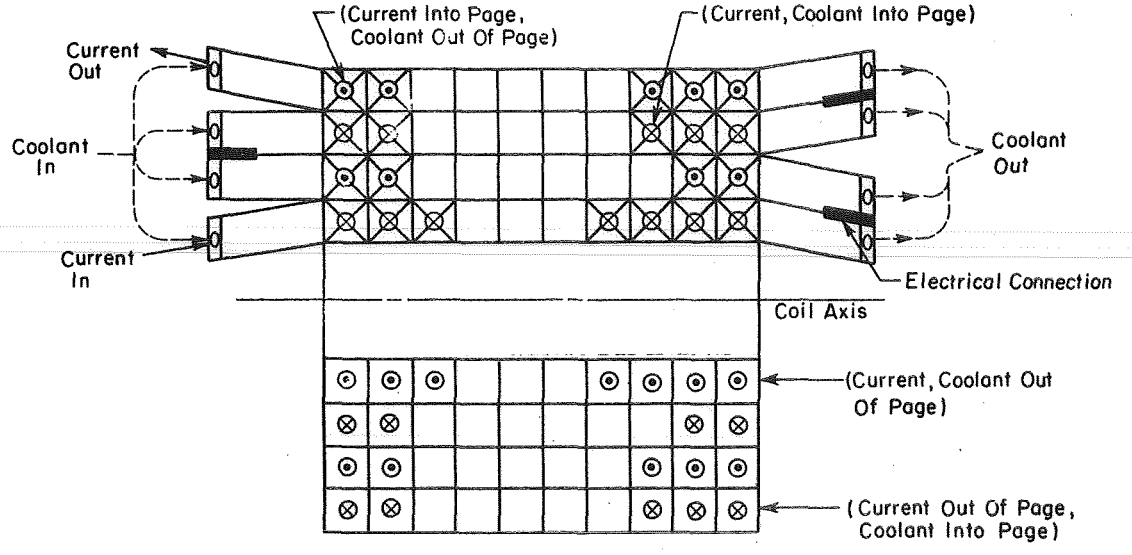

Figure 7.1. Layer-wound hollow conductor coil cooling and electrical paths

The coolant connections are made to the coil by means of tube fittings which are adapted to fit either single or double (siamesed) hollow conductor ends. The fittings which were used in the prototype were commercial brass "Tube-end reducers", which were annealed, swaged to fit, and soft-soldered to the hollow conductor ends. The adapters fit 1/4" o.d. nylon tubing which is used to connect the coils to the inlet and outlet coolant manifolds.

The saddle coils were wound in a different manner. These were formed from a stack of double-layer pancake coils which were bent together to form the curved shape. The inlets and outlets were brought out at opposite ends, and connected using the same tube fittings described above. The double-layer pancakes were provided with additional thermal insulation between layers to reduce regenerative heat exchange which tends to increase local coolant temperature.

7:2 COOLING MANIFOLDS

Cooling water is supplied to and collected from the magnet coils by means of a set of manifolds. Due to space limitations in the wind tunnel, the manifolds are of compact design. Six manifolds are used. Four inlet manifolds consisting of short lengths of heavy-wall brass pipe with silver-soldered end caps are located between the tie rods and the iron cores, on opposite sides of the system, and are piped together with copper tubing, using solder fittings. These manifolds supply coolant to the side and lift force coils and the saddle coils. Two tubular manifolds running the length of the balance and located close to the other two opposing tie rods are used both for inlets and outlets. Each manifold is made with an annular section in the middle which serves as an inlet manifold, and the two internally connected ends serve as outlet manifolds. The overall plumbing is shown schematically in Fig. 7.2.

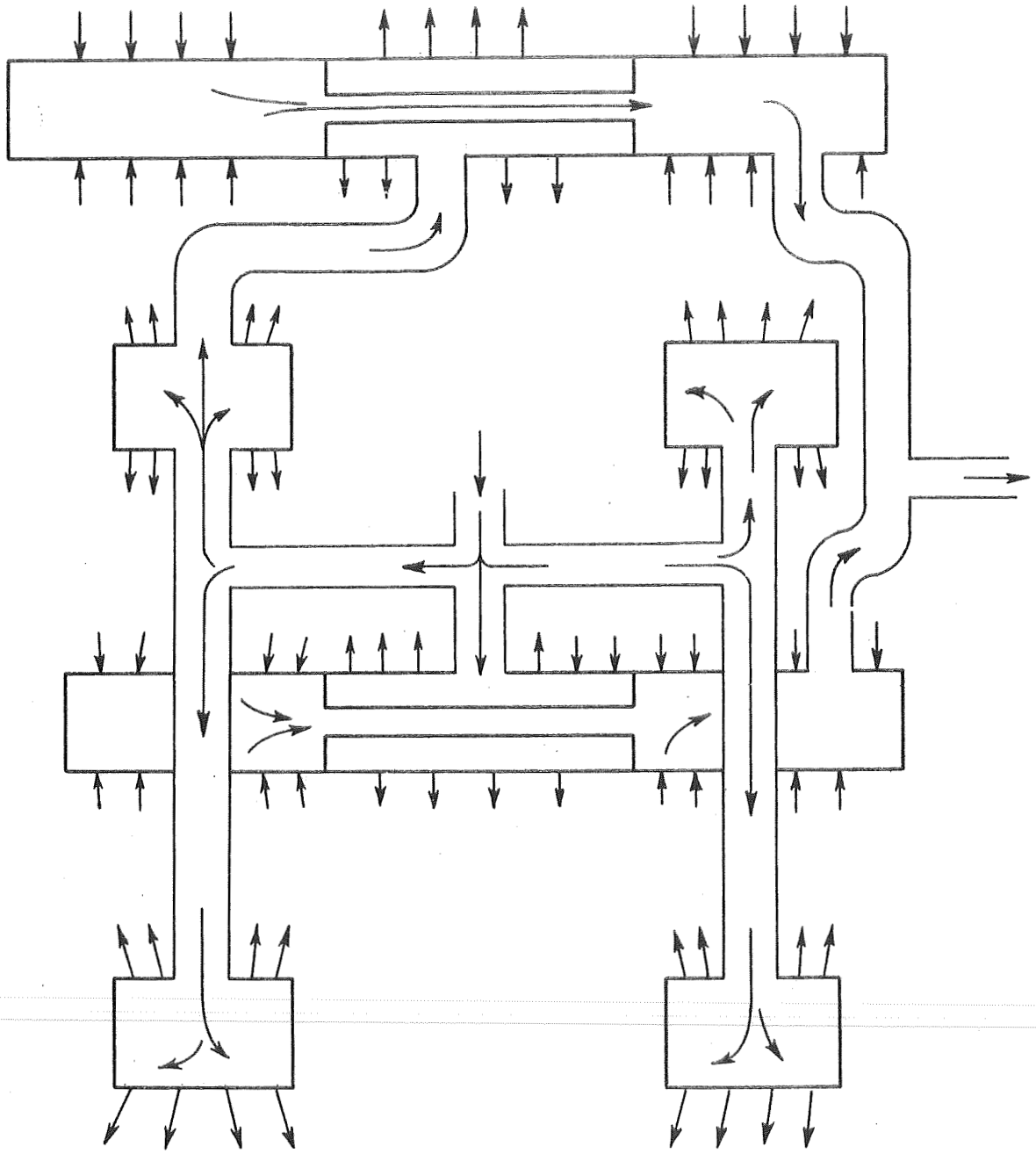

Figure 7.2. Prototype coolant manifold: developed schematic

The external arrows indicate inlet or outlet fittings leading to the magnet coils These fittings are screwed into pipe-threaded holes in the heavy walls of the manifolds, and accept the 1/4" o.d. nylon coolant tubes from the coils.

7:3 PROTOTYPE COOLANT SUPPLY

The coolant used in the prototype system is service water with no chemical treatment. The water is controlled with an inlet globe valve, filtered with a 100 mesh/in. screen, and the flow rate monitored with a rotameter-type gauge. The system is normally run at the full supply pressure of 45 to 60 psig, with a total flow rate of approximately 30 gpm. Water temperature ranges between 40° F and 60° F depending upon the season. No attempt is made to economize on cooling water; it passes directly to the drain.

7:4 MORE ELABORATE SYSTEMS

Since it is desirable to operate the magnet system at approximately constant temperature and also to economize on cooling water, then more elaborate cooling systems are called for.

A simple scheme suitable for intermediate power levels is shown in Fig. 7.3, which provides regulation of the temperature of water leaving the magnet system. It also provides a means of raising the mean operating temperature of the system substantially higher than the cold service water. This eliminates the problem of condensation on the magnet system during periods of high humidity and low service water temperature (typical of early summer).

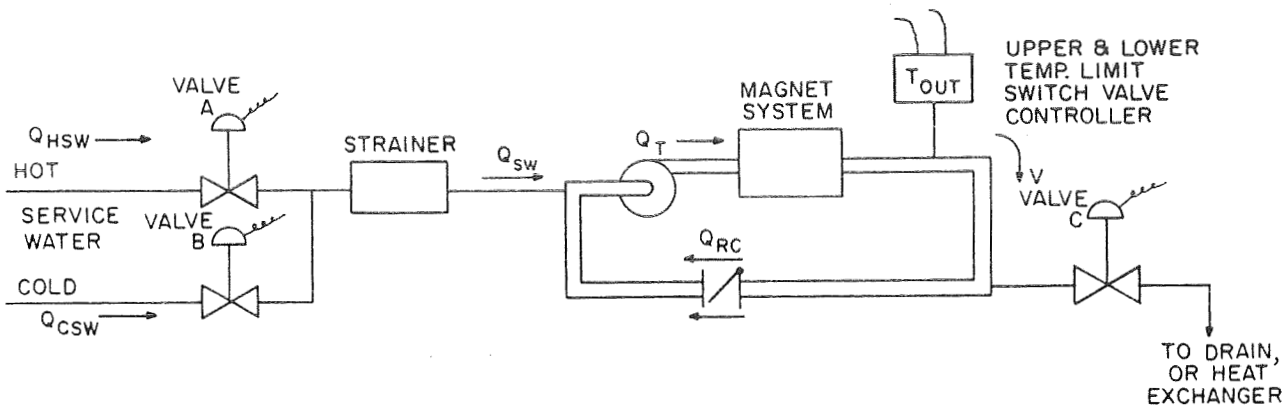

Coolant Temperature	Valve Position A	B	C
Below low limit	Open	Closed	Open
Between limits	Closed	Open	Closing
Above high limit	Closed	Open	Opening

Figure 7.3. Partly-closed circulating loop cooling system with temperature regulation

The average flow rate of cold service water, "Q_{csw}", is related to the outlet temperature "T_{out}", the cold service water temperature "T_{csw}", and the total power (magnet dissipation "P_{mag}" and pump power "P_{pump}."

$$\text{i.e.} \quad Q_{csw} = 7.5 \frac{(P_{mag} + P_{pump})}{(T_{out} - T_{csw})} \quad \text{gal/min}$$

where: P_{mag}, P_{pump} = kw

T_{out}, T_{csw} = °F

The warm water leaving the system can be exhausted to the drain or can be passed through a heat exchanger and returned to the inlet.

The total flow rate "Q_T" through the pump and magnet system should exceed the maximum required Q_{csw}.

If a controllable-speed reversing motorized actuator is used on Valve "C", then full proportional temperature regulation will be obtained.

7:5 COOLING SYSTEM SAFEGUARDS

Since a considerable amount of power can be dissipated in the magnet windings, failure of the cooling system can result in rapid overheating and destruction of the magnet system. For example, at maximum rated power density in the prototype (approximately 1 kw/lb of copper, in the "drag" windings), the corresponding rate of conductor temperature rise is approximately 10° F/sec if coolant flow is stopped. (The rate of temperature rise is reduced as soon as boiling begins. However, the remaining coolant may be promptly expelled by the generated steam.) Some means of sensing incipient overheating must therefore be provided. Monitoring of several variables and coupling with an interlock system should give adequate protection through redundancy. The following are simple installations:

a) Total outlet flow rate of magnet system (flow switch)
b) Flow rate from individual outlet manifolds (flow switches)
c) Coil conductor temperatures (thermal switches)

Failure of the circulating pump, or extreme supply pressure drops will result in an immediate input from sensors (a) and (b), and a delayed input from (c). Rupture or blockage of an individual coolant passage may be indicated by the coil conductor thermal switches (c), at the higher power levels.

(Rupture will usually be obvious to the operator.) For the thermal switches to be effective, several must be attached to each coil in the system. For example, a minimum of four for each of the eight side and lift coils, power for each of the four saddle coils, and sixteen for each of the Helmholtz coils. The thermal switches are placed in intimate thermal contact with the coils, on the outlet ends.

The interlock system should perform the following functions: It must prevent startup of the main magnet power systems if adverse inputs come from (a), (b) or (c); it must indicate and remember location of faults; and it must provide warning of faults, and delayed automatic shutdown of the power systems.

The saturation-limited power density (kw/lb) varies inversely with the square of the system size. Thus the maximum rate of conductor temperature rise will be less for the larger sizes. For example, in a 5-foot i.d. system the maximum rate of rise will be no more than 0.2° F/sec, which allows several minutes for shutdown in case of coolant failure.

Page intentionally left blank

CHAPTER VIII

DATA ACQUISITION SYSTEM

8:1 GENERAL REQUIREMENTS

In order to use the magnetic suspension system as a wind tunnel balance, the variables which are related to magnetic forces and moments on the model must be measured. The most useful and readily available variables are the currents in each coil system, and the position sensor outputs. Differential voltage signals proportional to the coil currents are obtained from small resistors ("shunts") in series with the coils, and the position sensor signals are obtained directly from a multiple output jack for this purpose. The current and position sensor signals are brought to a central distribution panel, which provides individual outputs, and a scanning switch with single output to provide sequential measurement of the data variables.

In the prototype system, for steady measurements, each variable is measured in sequence with an integrating digital voltmeter having floated and guarded differential input, and capable of giving six-figure measurement accuracy. Signal-averaging periods up to one second are available internally, and with external reference frequency, can be increased by orders of magnitude. The output of the digital voltmeter is printed on paper tape. With slight further modification, the complete scanning, digitizing, and recording can be automatically sequenced.

In the prototype, unsteady measurements have so far been limited to pitch damping. Forced oscillation techniques were used, and commercial signal conditioning equipment was used

to filter the signals and derive amplitude ratio signals, which were measured with the digital voltmeter.

The recorded data is transferred from the recorder output printed paper tape to punch cards, and converted to aerodynamic coefficient form using a digital computer.

Calibration equipment and procedures are being developed and evaluated at present.

REFERENCES

1. Tournier, M. and Laurenceau, P., "Suspension Magnetique d'Une Maquette en Soufflerie," La Recherche Aeronautique, No. 59, pp 21-27, July-August 1957.

2. Tilton, E. L., Parkin, W. J., Covert, E.E., Coffin, J.B., and Chrisinger, J. E., "The Design and Initial Operation of a Magnetic Model Suspension and Force Measurement System," Massachusetts Institute of Technology Aerophysics Laboratory, USAF-OAR-Aerospace Research Laboratories Report ARL 63-16, January 1963.

3. Copeland, A.B., Covert, E. E., Stephens, T., "Recent Advances in the Development of a Magnetic Suspension and Balance System for Wind Tunnels (Part III), M.I.T. Aerophysics Laboratory, USAF-OAR Aerospace Research Laboratories Report ARL 65-113, June 1965.

4. Copeland, A. B., Covert, E. E., Tilton, E. L., "Measured Aerodynamic Characteristics of a Cone-Cylinder-Cone Model with Base Separation, at M = 4.8," Journal of Spacecraft and Rockets, November-December 1965.

5. McLaughlin, D. K., Carter, J. E., Finston, M., "Experimental Investigation of the Near Wake of a Magnetically Suspended Cone at M = 4.3," AIAA 7th Aerospace Sciences Meeting, New York, AIAA Paper No. 69-186, January 20-22, 1969.

6. Copeland, A.B., "Measurement of Damping in Roll of a Finned Body Using a Magnetic Wind Tunnel Model Suspension System," Massachusetts Institute of Technology, Department of Aeronautics and Astronautics, M.S. Thesis, June 1965.

7. Rostron, A. J., "Levitation Melting," Science Journal, Volume 3, No. 7, July 1967.

8. Basmajian, V.V., Copeland, A.B., Stephens, T., "Studies Related to the Design of a Magnetic Suspension and Balance System," M.I.T. Aerophysics Laboratory, NASA Langley Contractor Report CR-66233.

9. Stephens, T., "Methods of Controlling the Roll Degree of Freedom in a Wind Tunnel Magnetic Balance," M.I.T. Aerophysics Laboratory, USAF-OAR-ARL Report ARL 65-242.

10. Montgomery, D. B., Solenoid Magnet Design, Wiley-Interscience, 1969.

11. Goodyer, M. J., "The Roll Control of Magnetically Suspended Wind Tunnel Models by Transverse Magnets," Unversity of Southampton, Dept of Aeronautics and Astronautics Report No. 291.

12. Wright, M. J., "A Transistor Phase-Sensitive Demodulator of High Performance," Electronic Engineering, October 1962

13. Chrisinger, J.E., "An Investigation of the Engineering Aspects of a Wind Tunnel Magnetic Suspension System", Massachusetts Institute of Technology, Aeronautical Engineering Thesis, TR 406, 1959.

14. Tilton, E.L. and Schwartz, S., "Static Tests of the Magnetic Suspension System", Massachusetts Institute of Technology, AR Memo 399, July, 1959.

15. Tilton, E.L., Baron, L., "Design, Construction, and Testing of an Automatic Control System for a Wind Tunnel Magnetic Suspension System", Thesis for B.S. Degree, Department of Aeronautics, Massachusetts Institute of Technology, May 1960.

16. Daum, F.L., "Summary of ARL Symposium on Magnetic Wind Tunnel Model Suspension and Balance Systems", Aerospace Research Laboratories, ARL 66-0135, July 1966.

APPENDIX A

PERFORMANCE ESTIMATION ANALYSIS OF MAGNET SYSTEM

A:1 HELMHOLTZ COILS

The Helmholtz coils are shown in partial section in Fig. A.1.

The axial field at the center of symmetry is composed of an even part due to the magnetizing windings, and an odd part due to the drag windings. The magnetization field contribution B_x is given by:

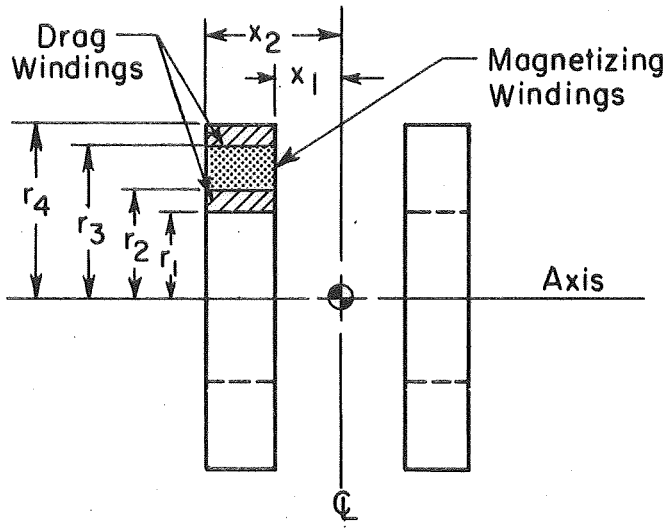

Figure A.1. Partial section of Helmholtz coils

$$B_x(0,0,0) = K \frac{\mu_o N_x I_x}{2(x_2 - x_1)(r_3 - r_2)} \left[x_2 \ln \left[\frac{r_3 + \sqrt{r_3^2 + x_2^2}}{r_2 + \sqrt{r_2^2 + x_2^2}} \right] - x_1 \ln \left[\frac{r_3 + \sqrt{r_3^2 + x_1^2}}{r_2 + \sqrt{r_2^2 + x_1^2}} \right] \right] \qquad \text{(A-1)}$$

where: x_1, x_2, r_2, r_3 = inches

K = 39.7 in/meter

μ_o = 4×10^{-3}

N = total number of turns

I_x = magnetizing current in each coil

B_x = gauss

For the prototype:

$x_1 = 4"$ $\quad r_2 = 10"$ $\quad N = 800$ turns

$x_2 = 8"$ $\quad r_3 = 14"$

$\therefore \quad B_x = 13.0\ I_x$ gauss (without iron contribution)

Compare this with the measured value (3:1:1)

$B_x = 20\ I_x$ (measured, including iron contribution)

The iron cores of the lift and side force assemblies therefore contribute approximately 54% to the central field.

The odd component of B_x due to the drag windings produces the desired gradient $\partial B_x/\partial x$ for control of drag force. Due to the windings alone:

$$B_{xx}(0,0,0) \approx K \frac{\mu N_{xx} I_{xx}}{2} \cdot \frac{3\,\bar{r}^2 \bar{x}}{(\bar{x}^2 + \bar{r}^2)^{5/2}} \qquad \text{(A-2)}$$

where

$$\bar{x} = \frac{x_1 + x_2}{2} \qquad \bar{r} = \frac{r_2^2 + r_4^2 - r_1^2 + r_3^2}{r_2 + r_4 - r_1 + r_3}$$

$N_{xx} = 800$

$\therefore \quad B_{xx}(0,0,0) = 1.21\ I_{xx}$ gauss/in (without iron contribution)

Compare this with the prototype measured gradient (3:1:1)

$B_{xx}(0,0,0) = 1.7\ I_{xx}$ (measured on prototype, includes iron)

The iron cores therefore contribute approximately 40% to B_{xx}, the axial gradient of the axial field.

A:2 SADDLE COILS

The geometry of the saddle coils can be approximated by the "mean-turn", corresponding to the centroid of the winding cross-section, as shown in Fig. A.2.

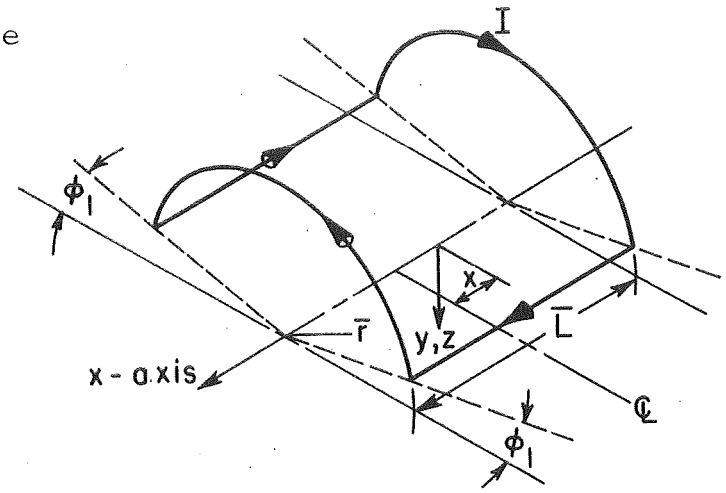

Figure A.2. Mean-turn geometry of saddle coils

The transverse field $B_{y'}$ (or $B_{z'}$) at the central point (x,y,z = 0) is:

$$B_{y'}(0,0,0) \simeq K \frac{\mu_0}{4\pi} N_y I_y \frac{4}{\bar{r}} \left[\frac{1}{\left(1+\left(\frac{\bar{r}}{\bar{L}/2}\right)^2\right)^{1/2}}\right]\left[1+\frac{1}{\left(1+\left(\frac{\bar{L}/2}{\bar{r}}\right)^2\right)}\right]\cos\phi \qquad \text{(A-3)}$$

For prototype,

(a) Inner Saddle coils - $B_{y'}$

$$\bar{L}/2 = 5.5" \quad \bar{r} = 5.2" \quad \theta_1 = 15° \quad N = 176$$

$$\therefore \quad B_{y'} = 5.4\ I_y,\ \text{gauss (without iron contribution)}$$

Compare with 3:1:1:

$$B_{y'} = 4.7\ I_y,\ \text{gauss (measured, with iron)}$$

The iron cores thus subtract from the central $B_{y'}$ field approximately 13% of the iron-free flux density due to the inner saddle coils alone.

(b) Outer Saddle Coils - $B_{z'}$

$$L/2 = 5" \qquad \bar{R} = 7" \qquad \theta_1 = 15° \qquad N = 266$$

$$B_{z'} = 7.8 I_z, \text{ gauss (calculated, without iron contribution)}$$

Compare with 3:1:1:

$$B_{z'} = 4.7\ I_z, \text{ gauss (measured, with iron contribution)}$$

The iron cores subtract from the central $B_{z'}$ field approximately 40% of the iron-free flux density due to the outer saddle coils alone.

(c) Simplified Saddle Coil Design

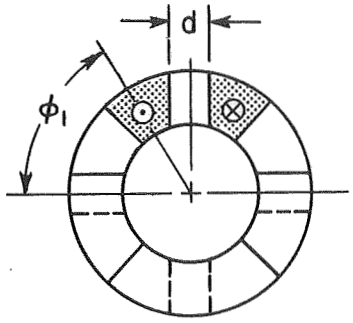

Figure A.3. Simplified saddle coil design

Consider the alternate saddle coil design shown in Fig. A.3. For the aperture "d" as used in the nested saddle coil arrangement of the prototype, the number of turns per coil of Fig. A.3 can be equal to the sum of the turns on the innter and outer saddle coils. The angle ϕ_1 however is much larger, (approximately 60°). For the same overall dimensions, the arrangement of Fig. A.3 provides:

$$B_y, B_z \tilde{\sim} 5.7\ I_y, I_z \text{ gauss}$$

The current and power levels are approximately equal for the two alternative schemes. However, the second derivative, $\partial^2 B_y / \partial y^2$, at the central point is at least an order of magnitude larger for the simpler arrangement.

Page intentionally left blank

APPENDIX B

ELECTROMAGNETIC POSITION SENSOR: DESIGN AND OPERATION DETAILS

B:1 INTRODUCTION

As a supplement to Chapter IV, further details related to the prototype E.P.S. system are given here. These include mechanical and electrical details, preliminary alignment details, and general operating procedures.

B:2 TRANSDUCER COIL ASSEMBLY

The transducer coil is wound on a tubular coil form as shown in Fig. B.1. Grooves and slots are machined into the form to control the shape of the coils and also to provide paths for the wires leading from the coils to the excitation and signal connectors. The windings are shown in the developed view, Fig. B.2. Each pair of coil leads is twisted together to minimize stray pickup.

B:3 EXCITATION POWER SUPPLY

The excitation windings of the transducer coil are powered by a master-oscillator power-amplifier. The master-oscillator consists of a commercial self-contained crystal controlled transistor oscillator providing a sinusoidal output voltage of 8 v.p.p. at 20 khz with a frequency stability of ±0.025%. The oscillator is powered by the positive 15 v.d.c. supply common to all the E.P.S. signal processing electronics. The oscillator drives a modified commercial vacuum-tube audio "hi-fidelity" power amplifier, and output level is controlled

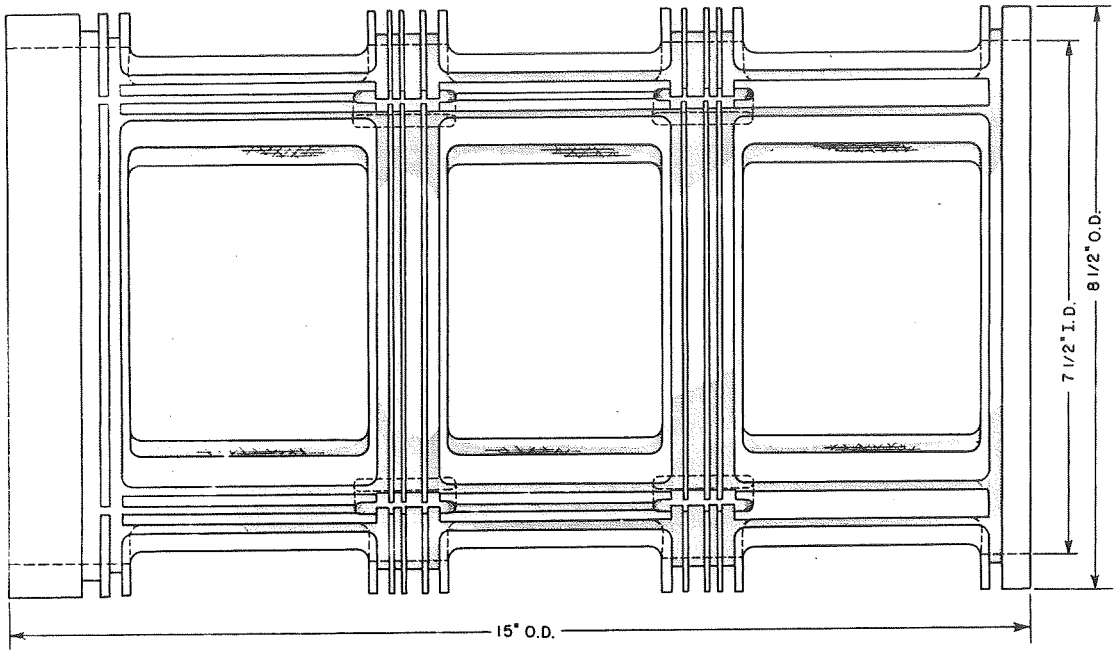

Figure B.1. E.P.S. transducer coil form

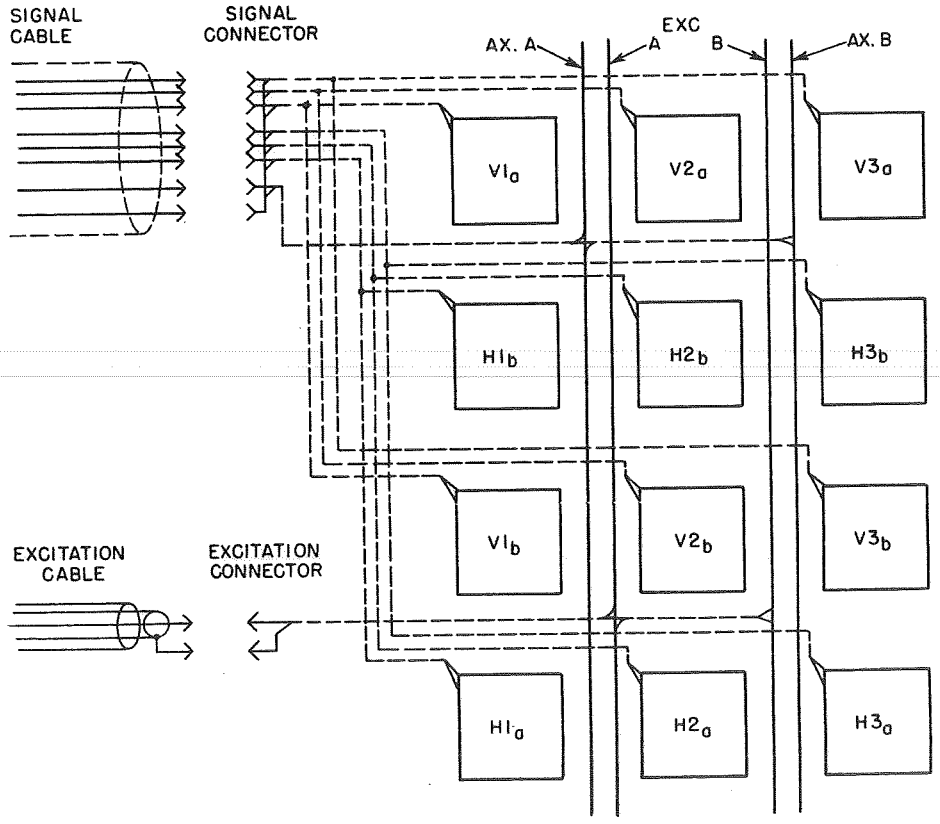

Figure B.2. E.P.S. transducer coil windings: developed view showing wire routing

by a variable attenuator between the oscillator and amplifier. Modifications to the power amplifier bias and plate supplies were required to reduce line-frequency modulation and gain drift. The bias supply was zener-regulated, and the plate supply was provided with a large L-C filter, and was also zener-regulated. A fan was installed to cool the entire amplifier.

The excitation coils are designed to match the range of output impedance of the power amplifier (4 ohms to 16 ohms) when series-tuned with a suitable capacitance. The tuning capacitance must be large enough to neutralize the inductive reactance of the excitation coils, and also the output reactance of the amplifier output transformer. The correct output tap and tuning capacitance is determined by trial and error, by observing the amplitude of the excitation coil voltage as the tap and capacitance is varied. The optimum tap and capacitance will provide the maximum coil voltage amplitude with constant drive level. Stability of the tuning capacitance is important and high-quality components must be used. Large transmitter-type mica-ceramic types are the most suitable. The tuning capacitors are mounted on the outside of the power amplifier and are hard-wired to two coaxial output receptacles, one for the excitation cable, the other for the reference signal to the E.P.S. electronics system.

The excitation cable consists of a shielded coaxial line ("triax") with a relatively large center conductor (#14). The inner and outer shields are connected to the outer part of the plug at the amplifier output end, and at the transducer-coil end, the inner shield and center conductor are connected to the two pins of the excitation connector plug and the outer shield is open.

B:4 REFERENCE AMPLIFIERS

Signals proportional to the excitation voltage are required for nulling the pickup coil signals and for driving the demodulators. The excitation voltage is amplified as shown in Fig. B.3. First, the excitation signal is attenuated, then split into two phases in quadrature, by means of a 45° phase-lead network in one channel, and a 45° phase-lag in the other channel. Each phase-shifted signal is then current-amplified in two-stage complementary-symmetry emitter-follower amplifiers, and is transformed into two equal output signals which are balanced with respect to ground.

B:5 PICKUP-COIL VOLTAGE PREAMPLIFIERS

Due to stray coupling effects, each pickup coil input to the E.P.S. electronics will have some 20 khz voltage even when a model is absent from the transducer coil assembly. In order to be able to amplify the actual useful pickup coil signals to a usable level, it is necessary to first null out the stray voltages. In addition to nulling the 20 khz components, it is also necessary to filter out any interference outside the desired bandwidth of the system. Therefore, bandpass filtering is employed in this preamplifier stage. Finally, the gain and phase shift through the preamplifier stage must be the same for all channels; thus, gain and phase trimming adjustments are provided.

The circuit is shown in Fig. B.4. The input signal is first filtered in an R-C high pass stage to attenuate the strongest interference components. The residual low-frequency interference is attenuated strongly in a multi-stage maximally flat L-C high-pass filter. The filtered signal is then amplified using a standard transistor operational amplifier, in the summing-inverting mode with positive input grounded. The

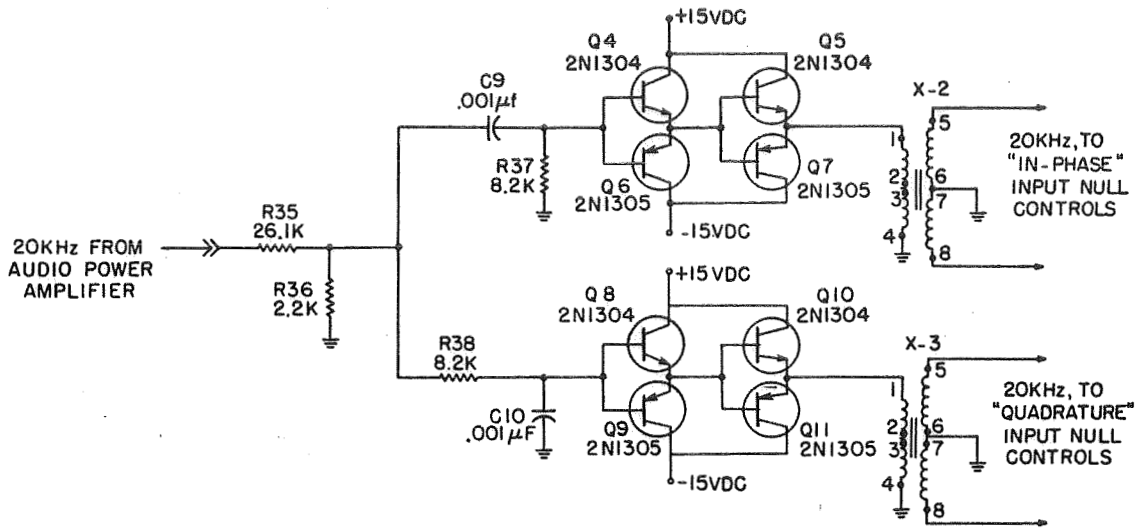

Notes: 1. X-1, X-2. U.T.C. #H-26 (or equiv)
2. Fixed resistors 1% precision, ±25 ppm/°C T.C. 1/2 w

Figure B.3. Reference amplifiers for input null control

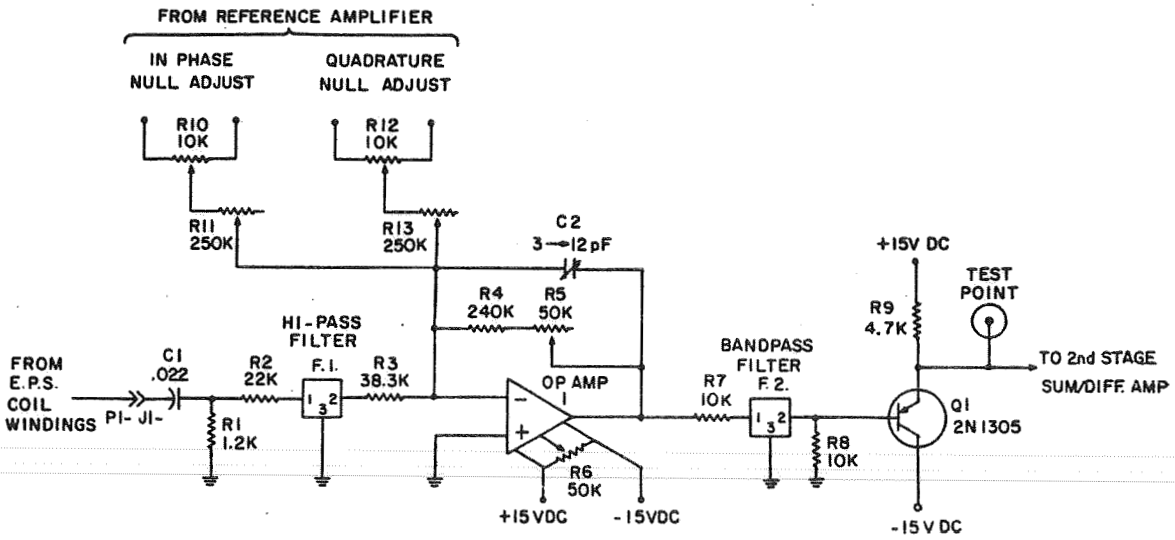

Notes:
1. High-pass filter F.1.: 3db freq = 10 khz
25k/25k impedance
60db down at 5 khz
2. Bandpass filter F.2.: F_C = 20 khz
10k/10k impedance
Bandwidth = 12 khz
3. Resistors:
(a) All fixed resistors ±1%, 20 ppm/°C T.C. 1/4 w
(b) R10, R12 10-turn, precision type with locks
(c) R11, R13 1-turn, precision type with locks
4. Seven (7) of these circuits are required, (axial, HORIZ 1,2,3, VERT 1,2,3)

Figure B.4. Input nulling and preamplifier circuit (E.P.S. system)

feedback resistance can be adjusted over a small range, thereby providing gain trim, and a small variable capacitor in parallel provides phase trimming. The operational amplifier output is further filtered with a bandpass filter and the output impedance of the stage is reduced by means of a transistor emitter-follower stage. Nulling of the 20 khz is provided by controlled addition of "in-phase" and "quadrature" signals from the reference amplifiers, at the summing point of the operational amplifier. Nulling is controlled by the 10k "in-phase" and "quadrature" potentiometers bridging the balanced reference signal lines, and the range of adjustment of each control is varied with the 250k input potentiometers. A phone jack test point is provided at the output of the preamplifier stage, to allow monitoring of the nulling operation.

B:6 SECOND STAGE AMPLIFIER-AXIAL CHANNEL

The nulled and preamplified 20 khz axial pickup coil signal voltage is amplified further in a second stage variable gain amplifier shown in Fig. B.5. An output test point is provided.

B:7 SECOND STAGE AMPLIFIERS-PITCH AND YAW CHANNELS

The preamplified 20 khz pickup coil voltages from V1,V2,V3 are added together to form an a.c. signal related to pitch angle. Similarly, voltages from H1,H2,H3 are added together to form the yaw angle a.c. signal. The summation is performed by an inverting-summing operational amplifier circuit as shown in Fig. B.6. An output test point is provided.

B:8 SECOND STAGE AMPLIFIERS-VERTICAL AND LATERAL CHANNELS

The preamplified 20 khz pickup coil voltage from V1 is subtracted from that from V3 in a variable-gain difference amplifier stage to form an a.c. signal related to vertical

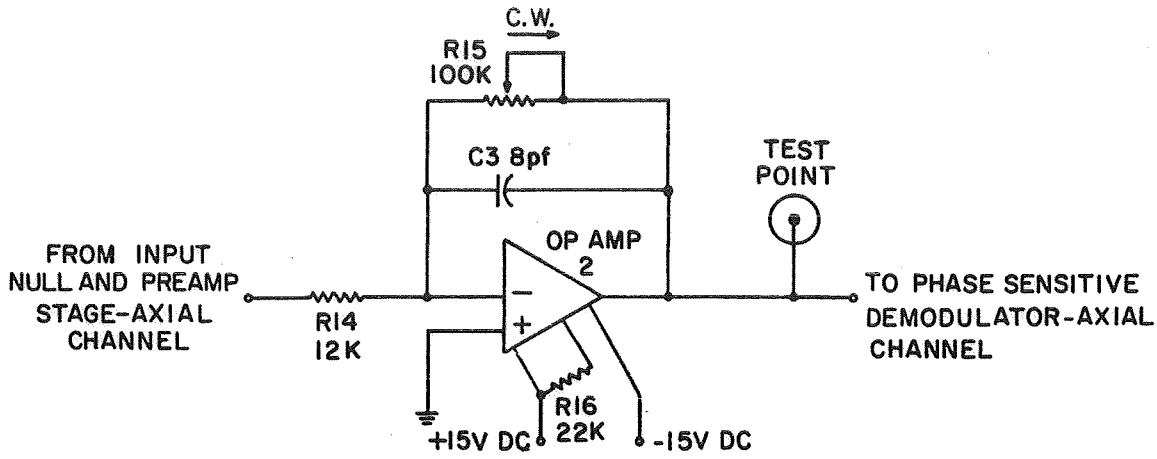

Notes: 1. Fixed resistors 1% precision, ±25 ppm/°C T.C. 1/4 w
2. R15 - single turn, precision
3. One (1) required

Figure B.5. Second stage amplifier, axial channel (E.P.S. system)

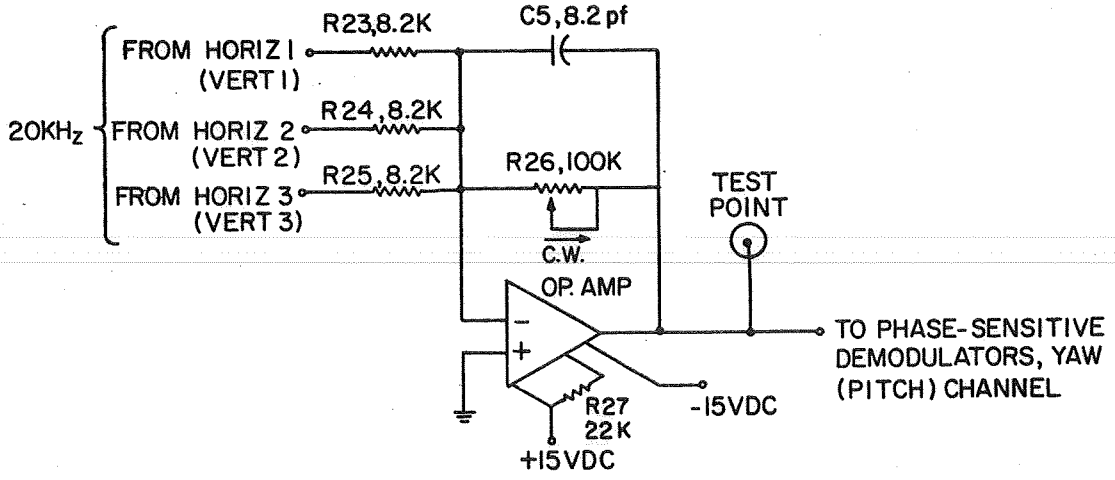

Notes: 1. Fixed resistors 1% precision, ±25 ppm T.C. 1/4 w
2. Two (2) required

Figure B.6. Second stage, summing amplifier, yaw (or pitch)

displacement. Similarly, the preamplified signal from H1 is subtracted from the signal from H3 to form an a.c. signal related to lateral displacement. The difference amplifier circuit is shown in Fig. B.7.

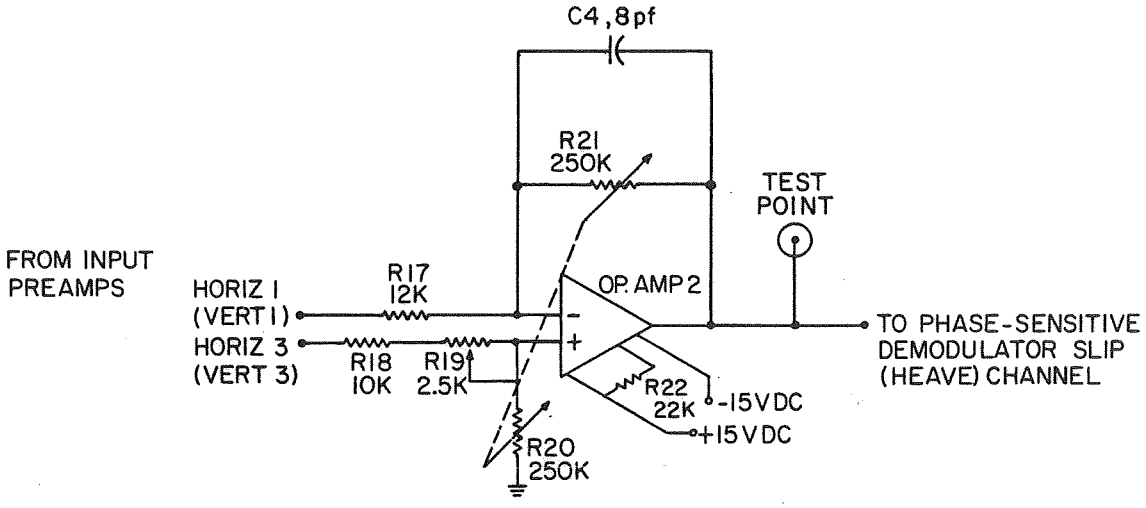

Notes: 1. Fixed resistors 1% precision, ±25 ppm/°C T.C. 1/4 w
2. R20/R21 Dual-ganged pots, single turn, precision
3. Two (2) required

Figure B.7. Second stage, difference amplifier, slip (heave) channels

B:9 DEMODULATOR STAGE[12]

The five second-stage a.c. outputs (axial, vertical, lateral, pitch, yaw) are demodulated to produce d.c. signals related to the model position. The demodulator consists of a full-wave transformer-coupled complementary-symmetry transistor switch, which is driven by a 20 khz square wave derived from the 20 khz reference signals (see B.11). The

demodulator circuit is shown in Fig. B.8.

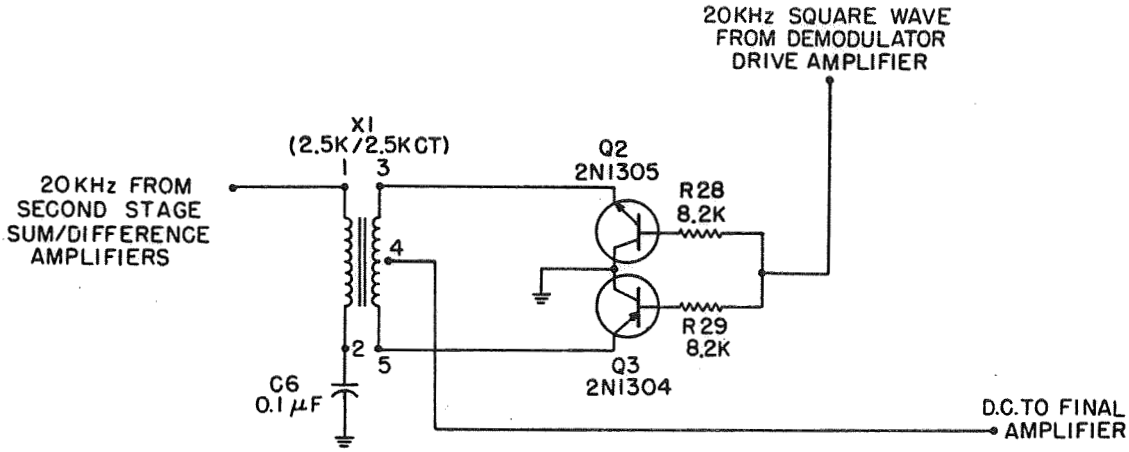

Notes: 1. X1 - Microtran PM31-M (or equiv)
2. Five (5) required

Figure B.8. Phase-sensitive demodulator circuit

B.10 OUTPUT STAGE

The demodulator output signals are low-pass filtered and amplified in a variable-gain output stage. Trimming adjustment of the output d.c. level is provided, and nulling of any residual line-frequency (60 Hz) pickup is also provided at this stage. The circuit is shown in Fig. B.9.

B.11 SQUARE-WAVE GENERATOR FOR DEMODULATOR DRIVE

High level square-wave signals at 20 khz with phase angle adjustable relative to the excitation-reference signal are required to drive the demodulators. This is accomplished by the circuit shown in Fig. B.10. A variable-phase 20 khz

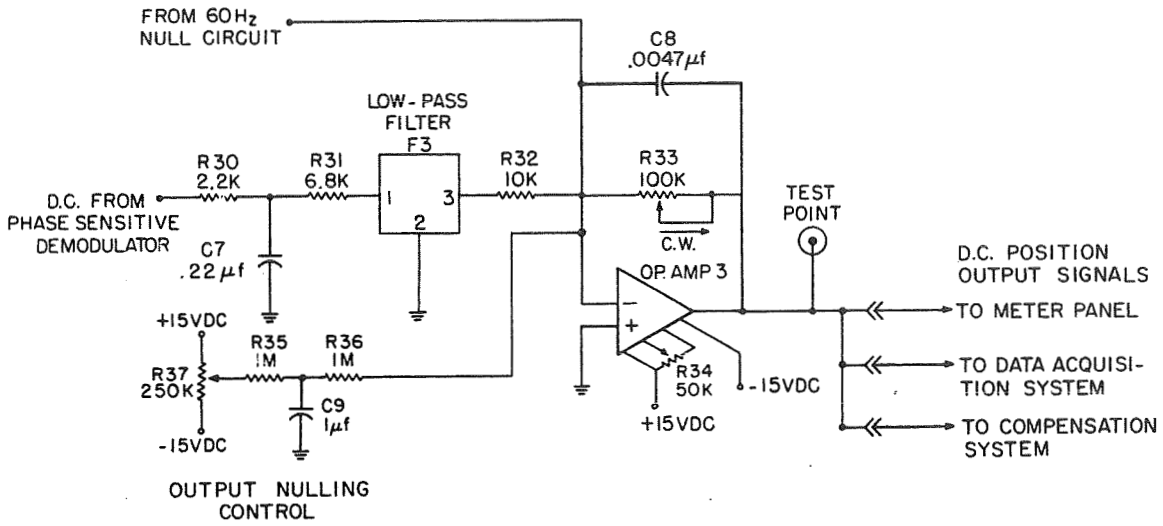

Notes: 1. Low-pass filter F.3.: 3db freq = 1 khz
10k/10k impedance
60db down at 1.6 khz
2. Fixed resistors 1% precision, ±25 ppm/°C T.C. 1/4 w
3. Five (5) required

Figure B.9. Final stage output amplifier

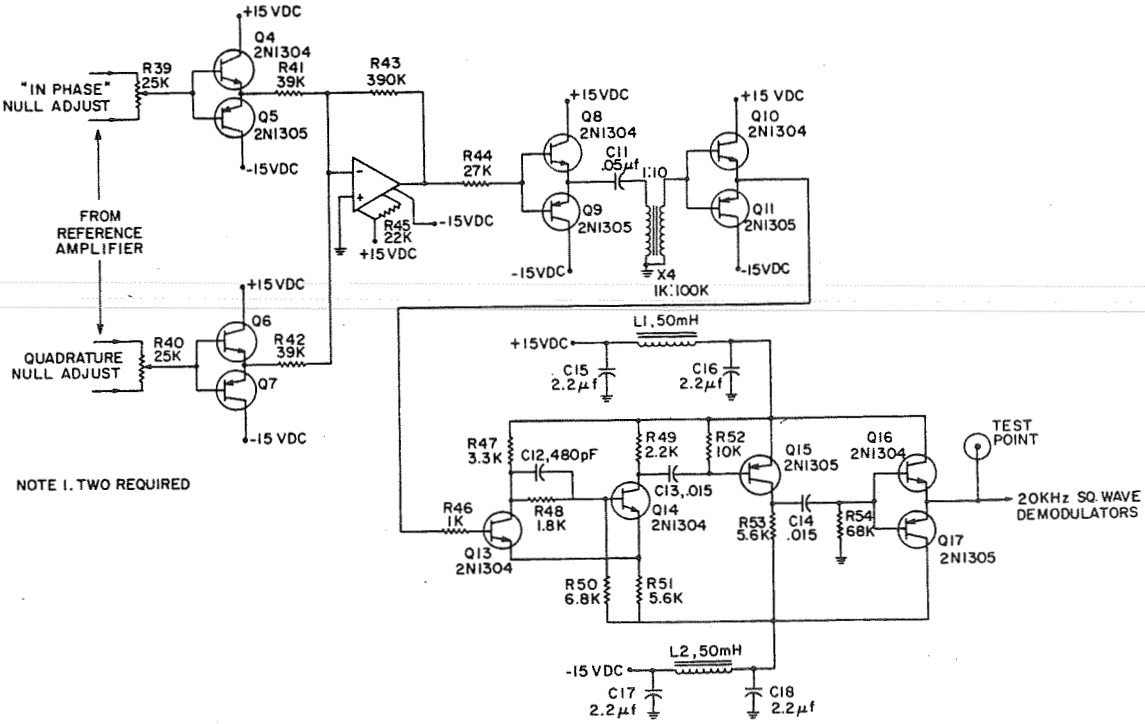

Notes: 1. Two (2) required

Figure B.10. Square wave generator for demodulator drive

signal is produced at the output of an operational amplifier by addition of two buffered signals in quadrature controlled by potentiometers bridging the balanced "in-phase" and "quadrature" reference lines. The resultant 20 khz signal is then buffered, voltage amplified by a transformer, and clipped symmetrically in a further buffer stage. The signal is then further squared in a symmetrical Schmitt trigger, amplified and buffered, to provide a low output impedance square wave at 20 khz.

Two of these circuits are required, since the required phase of the drive signal to the translational component demodulators (axial, vertical, lateral) is generally different from that required to demodulate the angular component signals (pitch, yaw).

B:12 LINE-FREQUENCY INTERFERENCE NULLING CIRCUIT

Balanced "in-phase" and "quadrature" reference signals are generated using the circuit of Fig. B.11. These signals are injected at the final amplifier stage (see Fig. B.9) and are controlled by two potentiometers for each channel in a manner similar to the input (20 khz) nulling circuit.

B:13 POSITION INDICATOR PANEL

The five d.c. output signals related to the model displacement components are displayed on an indicator panel, as shown in Fig. B.12. The meters are arranged to provide some correspondence between the direction of indicator movement and model displacement. Pitch and yaw angles are displayed on conventional meters, turned 90° such that the indicator needles imitate angular motion of the model. Translational displacements are indicated on "edgewise" meters, oriented in the direction of model movement. Selector-switch range and sensitivity controls are provided for each channel indicator.

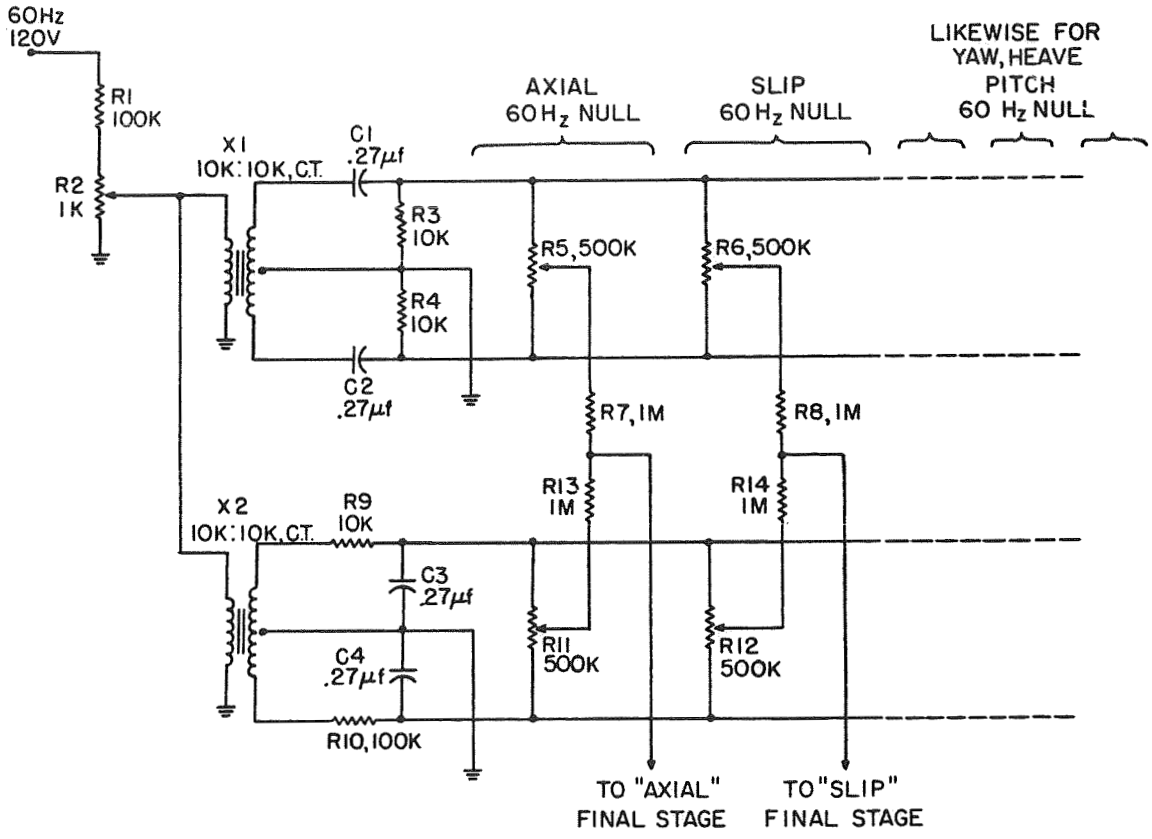

Figure B.11. Line-frequency interference nulling circuit

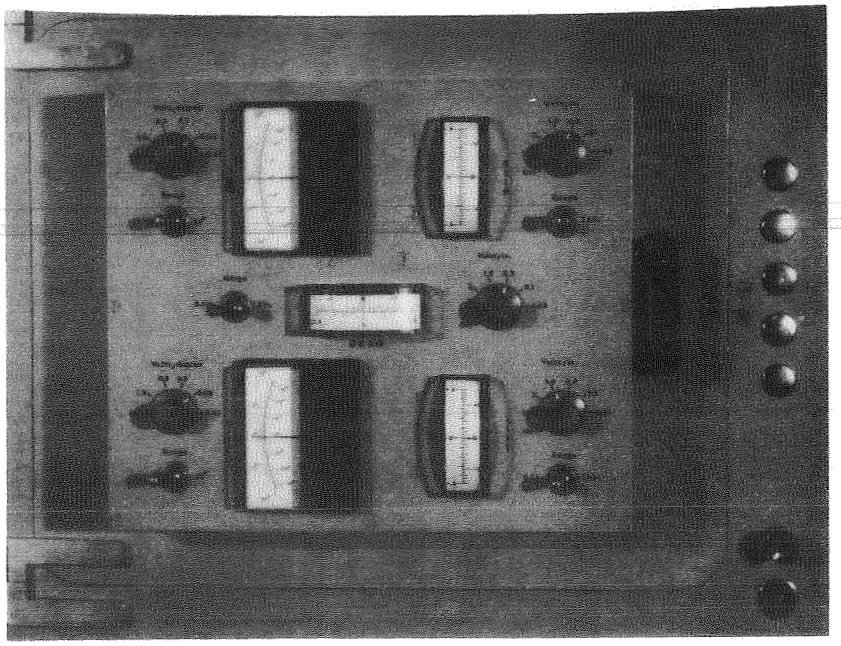

Figure B.12. Position indicator panel

B:14 PRELIMINARY ALIGNMENT PROCEDURES

Before the E.P.S. system is ready for routine operation, initial adjustments must be made. These are:

(a) Gain and Phase Adjustment of First Stages

The gain and phase shift of each of the input stages are adjusted to be equal. This is accomplished as follows:

(i) Signal input from sensor coils is disconnected.

(ii) 20 khz reference signal is disconnected from reference input; instead, is attenuated by 60 db, and split into seven common inputs to the pre-amplifier stages.

(iii) Preamplifier outputs are monitored on an oscilloscope differentially in pairs, using the axial channel as a reference. Gain and phase of each channel is trimmed to give null outputs.

(iv) Output of the second stage of the pitch and yaw channel is adjusted for null output by further trimming of the gain and phase of the VERT 3 and HORIZ 3 channel preamplifier respectively.

(b) Excitation Level

The excitation level is adjusted to 200 volts peak to peak by means of the attenuator between the 20 khz oscillator and the excitation power amplifier. This is the highest output amplitude consistent with low output distortion.

B:15 ROUTINE OPERATING PROCEDURES

Before a model is suspended in the magnetic balance system, routine adjustments must be made to the E.P.S. system electronics. All of these adjustments are made with the magnet currents turned

on and adjusted to their mean values corresponding to gravity loads, and zero angle of attack in pitch and yaw.

(a) Preamplifier Stage Nulling

The seven input preamplifier channels are nulled for 20 khz, with the model absent from the E.P.S. transducer coil, by means of the "in-phase" and "quadrature" adjustments (see Fig. B.4). The 250k range adjustment controls (R11, R13) are initially set at full resistance (Fully C.W.). The nulling adjustments are made on R10 and R12, and if necessary R11 and R13 are reduced.

(b) Second-Stage Nulling

Further nulling adjustments with model absent are made by monitoring the outputs of the second stages. The 20 khz output of the vertical position channel second stage is nulled by further adjustment of the nulling controls of the VERT 3 preamplifier. Following this, the 20 khz output of the pitch angle channel second stage is nulled by further adjustment of the nulling controls of the VERT 2 preamplifier. The same procedure is followed for nulling the lateral position and yaw angle second stage outputs, by further adjustment of the HORIZ 3 and HORIZ 2 preamplifier nulling controls.

(c) Demodulator Phase Adjustment

The model is held stationary inside the E.P.S. transducer coil, approximately one-half inch forward of the center, and at zero angle of attack. The axial position indicator controls are adjusted to bring the indicator on-scale, and the phase of the "translational" demodulator driver (see Fig. B.10) is adjusted to produce a positive maximum indication. (The demodulator phase is adjusted by the two 25 kilohm controls

R39 and R40. One or other of these controls must be set either fully counter clockwise or fully clockwise.) This adjustment will provide maximum response for axial, vertical, and lateral translational displacements of the particular model.

The model is then centered, and pitched at positive angle of attack. The phase of the "angular" demodulator driver is then adjusted to give a maximum positive pitch indication.

(d) Output Stage D.C. Nulling

Final nulling adjustments are made at the output stage (see Fig. B.9). The output d.c. nulling can be easily monitored on the position indicator panel and can be accurately monitored by setting maximum sensitivity and minimum range on the indicator controls.

(e) Output Stage Line-Frequency Interference Cancellation

Steady interference at the line-frequency and phase-locked with the line is cancelled in the output stage by adjustment of the "60-Hz NULL" controls (see Fig. B.11). This is done first with the model absent, but with the support magnets energized, and later is finally trimmed with the model suspended magnetically.

Page intentionally left blank

APPENDIX C

PROTOTYPE MAGNET SYSTEM CONSTRUCTION DETAILS

As a supplement to Chapter II, further details related to the construction of the prototype magnet system are given here. These include the coil winding details and the construction of the iron cores.

C:1 HELMHOLTZ COILS

The basic Helmholtz coil windings are shown in Fig. C.1. Each coil consists of 40 layers of twenty turns each. The conductor is .190" square - o.d., .130" round i.d. copper with double "Poly-Thermaleze" insulation. The inside diameter of the windings is double-thickness ∿25 mil fiberboard, and the sides are covered with 1/16" fiberglass board. The windings are wet-wound with epoxy resin and the terminals brought out at the sides and siamesed as shown (see Fig. 7.1 also). Overall dimensions are: inside diameter, 16",outside diameter, 32 1/2", width, 4 1/4".

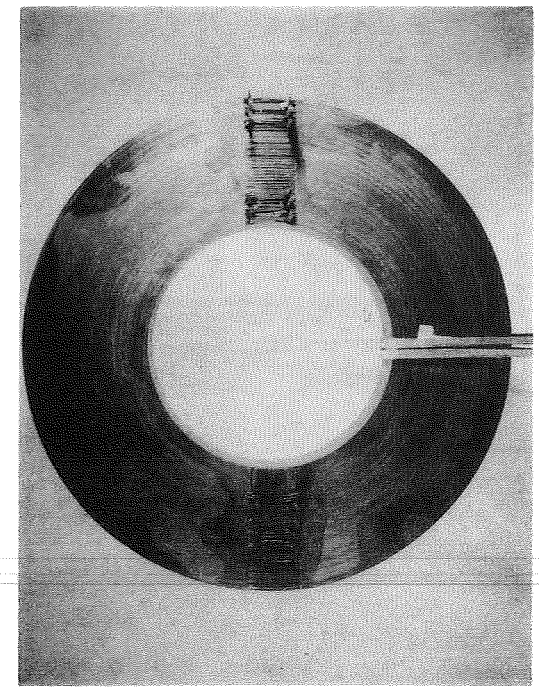

Figure C.1. Helmholtz winding before installation of cooling and electrical terminals

The "pigtail" terminals of the as-wound coil are shown in Figs. C.2 and C.3. The

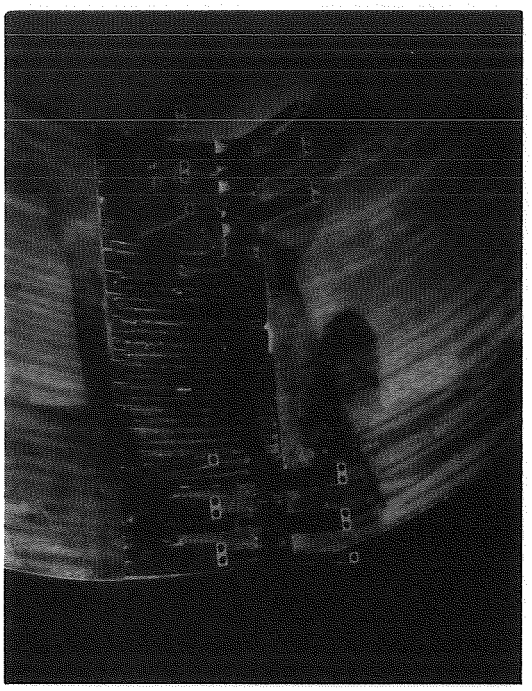

Figure C.2. "Pigtail" terminals of the Helmholtz coil magnetizing windings

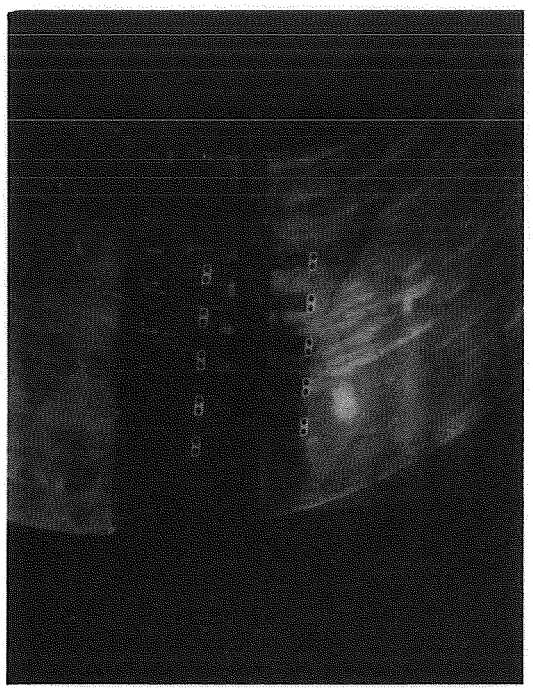

Figure C.3. "Pigtail" terminals of the Helmholtz coil drag windings

Figure C.4 shows the plumbing of the pigtail terminals to tube fittings and to the electrical connectors, for the drag windings of the Helmholtz coils. The tube fittings and connectors are secured in a fiberglass board. The front plate of a potting mold has been removed to reveal the plumbing details: the plumbing is embedded in epoxy resin after the plate is installed and the coil inverted.

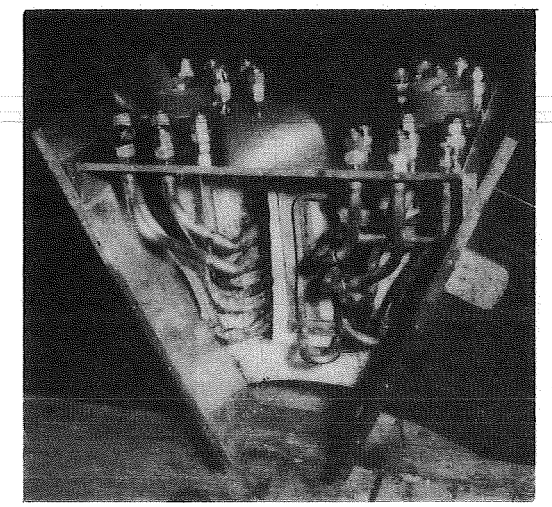

Figure C.4. Plumbing of pigtail terminals to tube fittings, and electrical connectors

C:2 SADDLE COILS

Figure C.5 shows a "Inner Saddle Coil", prior to installation of cooling and electrical terminals. The coil is wound of the same conductor as the Helmholtz coils (.190" square o.d., .130" round i.d.). It is formed from four double-layer rectangular pancakes which are bent together, jacketed with fiberglass cloth, and vacuum-potted with epoxy resin. Recessed, threaded inserts are provided at the four corners to allow connection of the saddle coils together with tie-plates. The overall dimensions and turns distribution of the saddle coils are as follows:

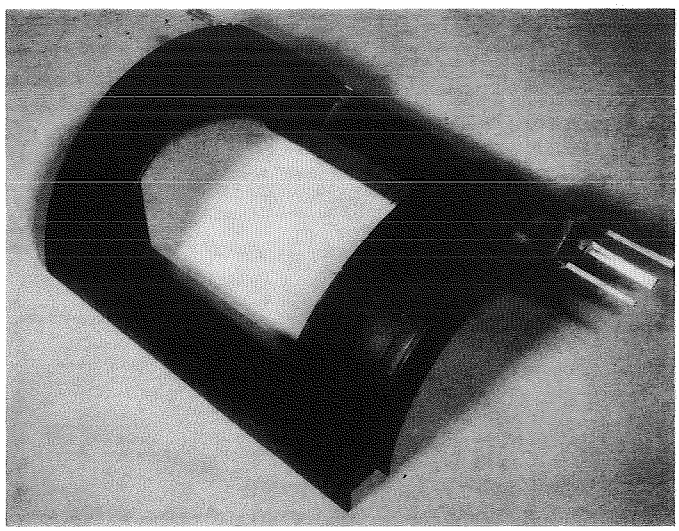

Figure C.5. Inner saddle coil before installation of cooling and electrical fittings

(a) Inner Saddle Coils

I.D. = 8.6", O.D. = 12 1/8"
Overall length = 13 1/2"

Layer 1	(inside)	Turns 8
2		9
3		10
4		11
5		11
6		12
7		13
8	(outside)	14
		88

(b) Outer Saddle Coils

I.D. = 12 1/4", O.D. = 15 3/4"
Overall length = 13 1/2"

Layer 1	(inside)	Turns 15
2		16
3		17
4		17
5		17
6		17
7		17
8	(outside)	17
		133

C:3 SIDE AND LIFT FORCE COILS

Figures C.6(a) and (b) show a side or lift force coil (one of eight), before and after installation of cooling and electrical fittings and potting with epoxy resin. The overall dimensions of these coils are: 4"x5" I.D. with 3/4" inside corner radii, 7"x8" O.D.; overall length, 6 1/4", number of turns, 290. The conductor is the same as used for the Helmholtz coils and saddle coils (.190" sq. O.D., .130" rd. I.D.).

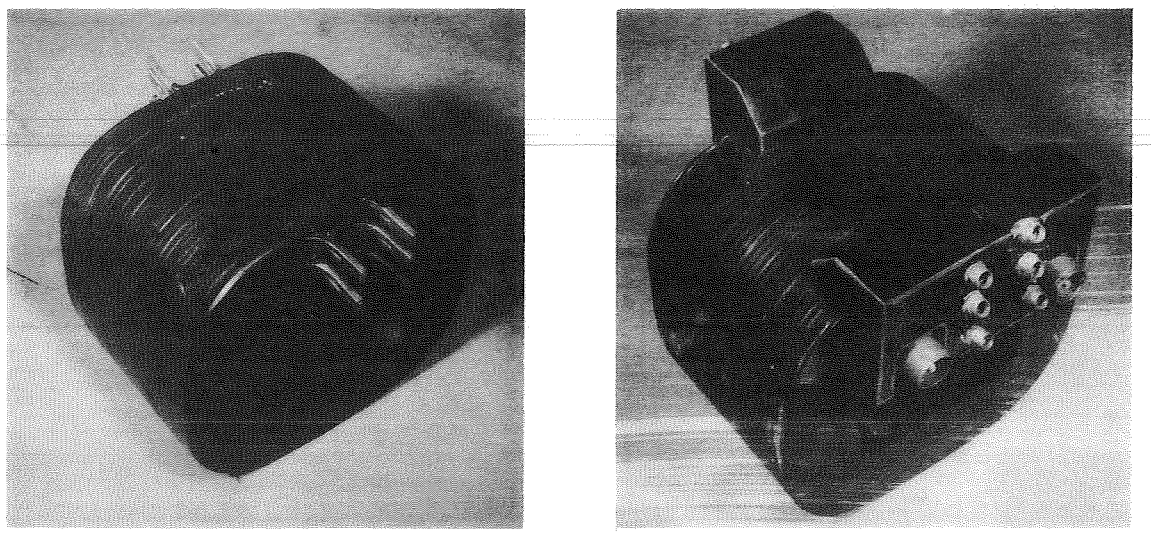

(a) (b)

Figure C.6. Side or lift force coil before and after installation of cooling and electrical fittings and epoxy potting

C:4 SIDE AND LIFT FORCE IRON CORES

The side and lift force iron core assemblies (2) are each made up of four separate laminated electrical steel pole-pieces, as shown in Fig. C.7. Each pole piece is made up of two mirror-symmetric halves, one of which is shown in Fig. C.8.

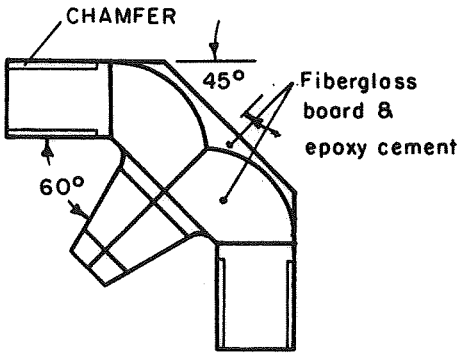

Figure C.7. Laminated side and lift force cone pole-piece subassembly

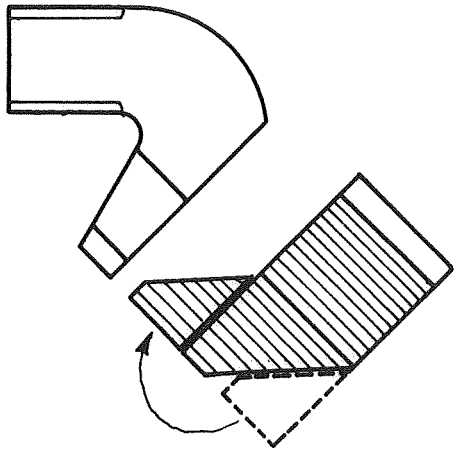

Figure C.8. Half of pole-piece

Each pole-piece half is cut from a triangular coil of steel which is wound and cemented together with epoxy resin as shown in Fig. C.9. A wedge is cut from the tapered leg of each cut-out piece, and cemented to the opposite side, to form a canted pole as shown in Fig. C.8. The parallel leg is chamfered to accommodate the inner radius of the coils. The material used is 14 mil M-6 grade silicon electrical steel.

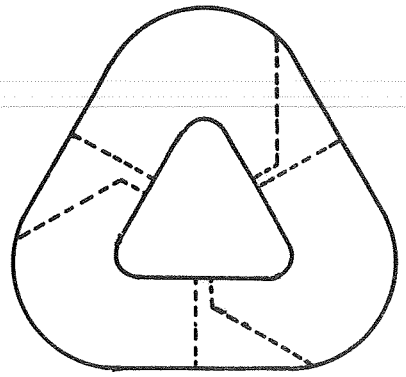

Figure C.9. Triangular steel coil showing pole-piece cuts

Each pole-piece subassembly mounts directly to the cruciform end plate. The coils are supported by the cores and located with wedges. Each side and lift force subassembly consists therefore of one end plate, four coils, and four pole-piece subassemblies.

C:5 COOLING MANIFOLDS

Figures 10(a) and (b) show the overall assembly of the suspension magnet system with coolant manifolds installed, but before installation of 1/4" nylon cooling tubes.

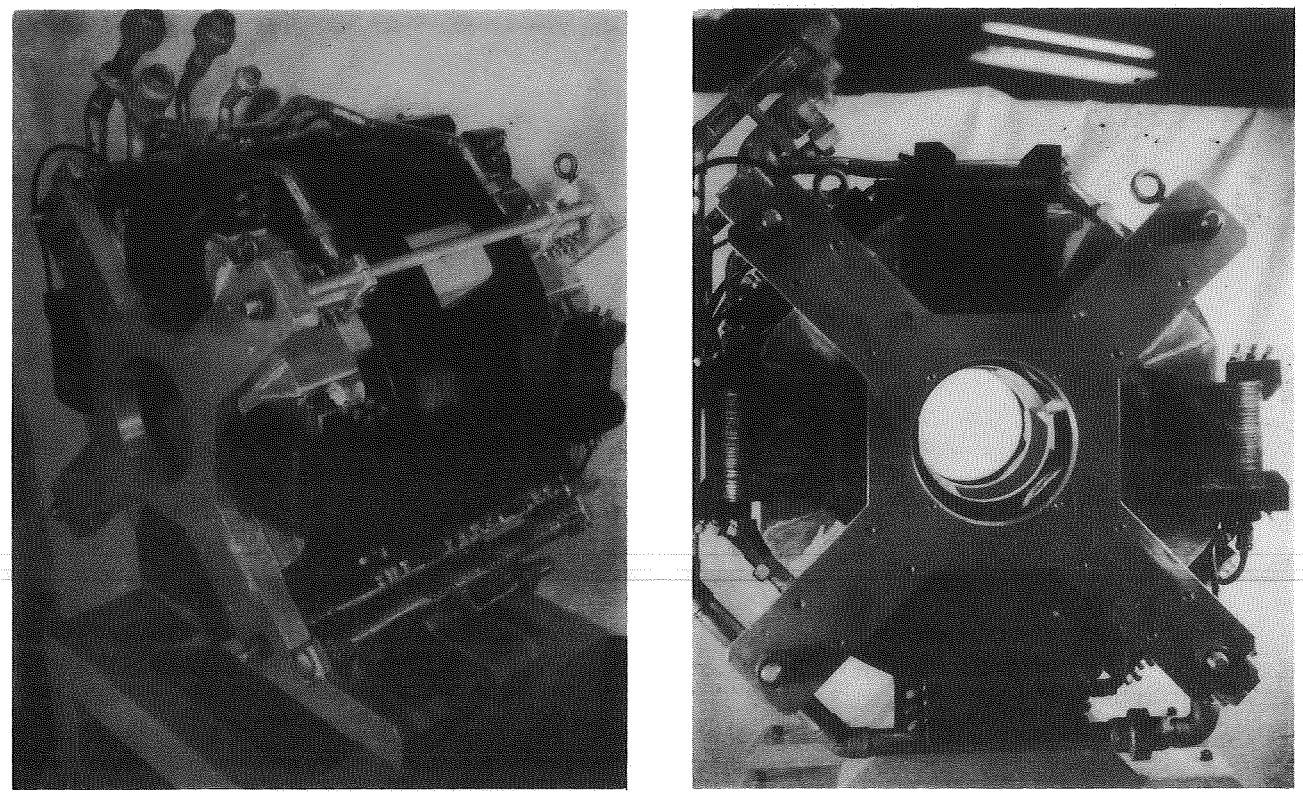

(a) (b)

Figure C.10. Magnet system assembly with cooling manifolds installed

C:6 SAFETY SHROUDS

Figure C.11 shows the completely assembled magnet system with safety shrouds installed. These shrouds are fabricated of 1/4" thick paper-phenolic board, and may be readily removed for inspection of the magnet system.

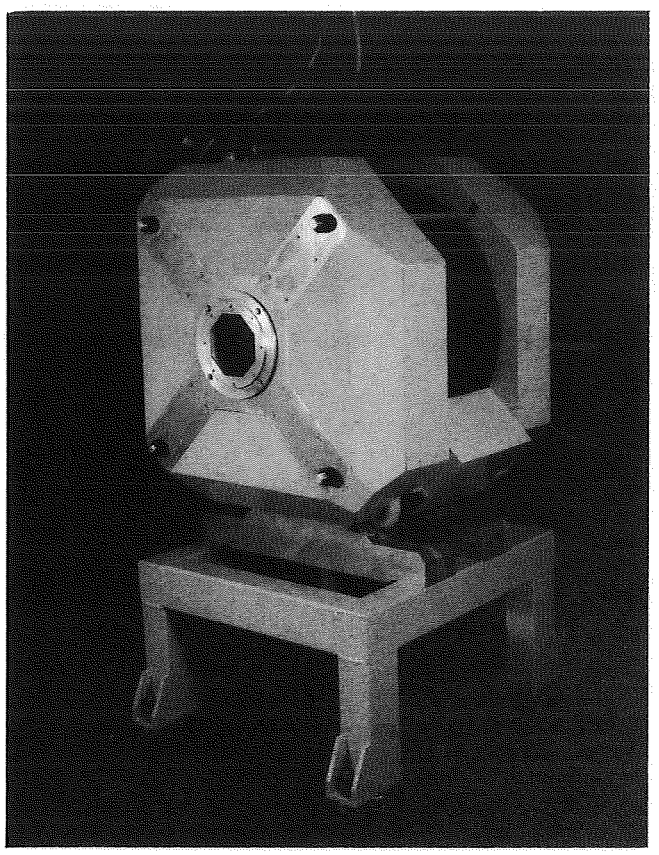

Figure C.11. Assembled magnet system with safety shrouds

C:7 SUBSONIC WIND TUNNEL INSTALLATION

Figure C.12 shows the magnetic suspension system connected to the Aerophysics Laboratory 6 1/4", M = 0 to 0.5 wind tunnel. Access is gained to the test section through the front of the system, by withdrawing the inlet nozzle section in a forward direction.

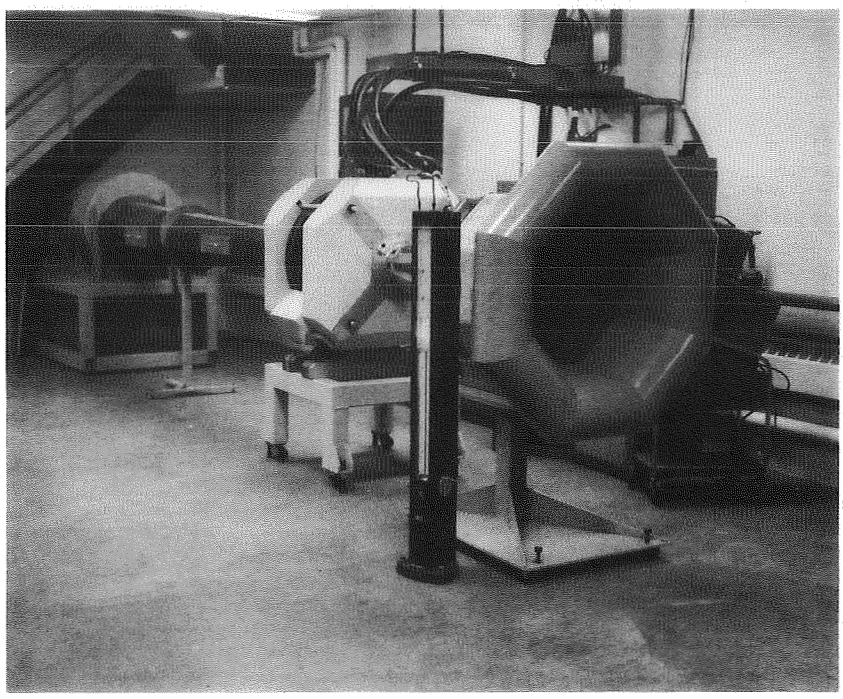

Figure C.12. Subsonic wind tunnel installation

C:8 SUPERSONIC WIND TUNNEL INSTALLATION

Figure C.13 shows the magnet system installed in the Aerophysics Laboratory Supersonic Gasdynamics Facility. Figure C.14 is a view upstream of the same facility, showing the fiberglass M = 4.3 nozzle. This nozzle is shown in Fig. C.15 in more detail. The downstream end of this nozzle (approximately 10") is made of fiberglass and epoxy layup to avoid the shielding of the E.P.S. transducer coil which would occur with an all metal nozzle. The nozzle material was chosen to withstand a tunnel stagnation temperature of 700°F.

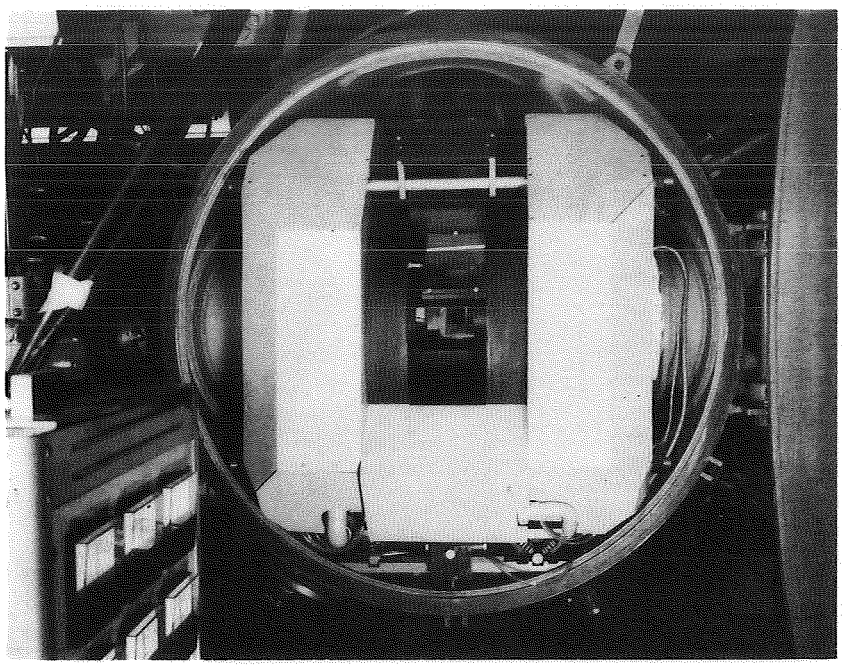

Figure C.13. Magnetic suspension installation in Aerophysics Laboratory Supersonic Gas Dynamics Facility

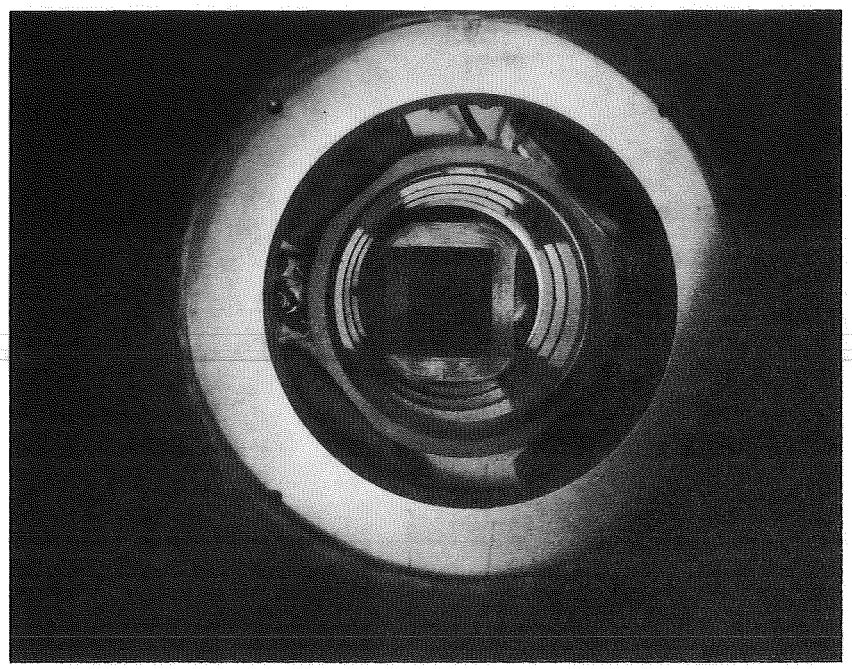

Figure C.14. Upstream view of magnetic suspension installed in Aerophysics Laboratory Gas Dynamics Facility, showing E.P.S. transducer coil and fiberglass-ended M = 4.3 nozzle

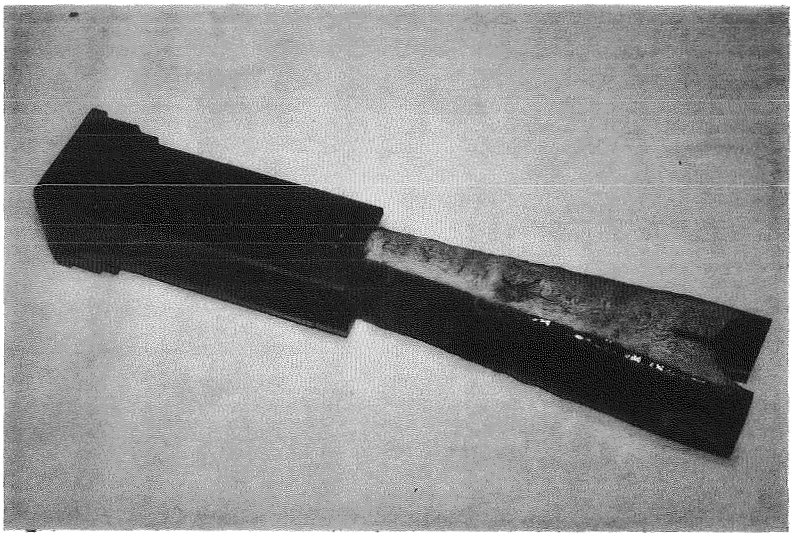

Figure C.15. Fiberglass-ended M = 4.3 nozzle

DOCUMENT CONTROL DATA - R & D

(Security classification of title, body of abstract and indexing annotation must be entered when the overall report is classified)

1. ORIGINATING ACTIVITY *(Corporate author)*
Massachusetts Institute of Technology
Department of Aeronautics and Astronautics
Cambridge, Massachusetts

2a. REPORT SECURITY CLASSIFICATION
Unclassified

2b. GROUP

3. REPORT TITLE
DESIGN, CONSTRUCTION, AND EVALUATION OF A MAGNETIC SUSPENSION AND BALANCE SYSTEM FOR WIND TUNNELS

4. DESCRIPTIVE NOTES *(Type of report and inclusive dates)*
Final Report

5. AUTHOR(S) *(First name, middle initial, last name)*
Timothy Stephens

6. REPORT DATE
November 1969

7a. TOTAL NO. OF PAGES
xx + 168

7b. NO. OF REFS
16

8a. CONTRACT OR GRANT NO.
NAS1-4421

b. PROJECT NO.

c.

d.

9a. ORIGINATOR'S REPORT NUMBER(S)
TR 136

9b. OTHER REPORT NO(S) *(Any other numbers that may be assigned this report)*
NASA CR-66903

10. DISTRIBUTION STATEMENT

11. SUPPLEMENTARY NOTES

12. SPONSORING MILITARY ACTIVITY
NASA, Langley Research Center
Hampton, Virginia

13. ABSTRACT

The basic design principles of a relatively interaction-free six component magnetic suspension and balance system are defined. The construction of a particular magnet configuration is described. The performance of the magnet configuration is evaluated. The evaluation is based upon parameters measured on the assembled and operating system. The evaluation is extended to a range of system sizes, by use of scaling laws. Design and construction of the required feedback compensation electronics system is described. Design of a five-component model position remote transducer is described. Magnet power supplies and control amplifiers are described, and the performance requirements are related to system size, model configuration, and test conditions.

14. KEY WORDS	LINK A		LINK B		LINK C	
	ROLE	WT	ROLE	WT	ROLE	WT
Magnetic suspension						
Wind tunnels						
Design						
Working model						